SCUOLA DI DOTTORATO
UNIVERSITÀ DEGLI STUDI DI MILANO-BICOCCA

Department of

EARTH AND ENVIRONMENTAL SCIENCES

PhD Executive program CHEMICAL, GEOLOGICAL AND ENVIRONMENTAL SCIENCES Cycle 37°

Curriculum in GEOLOGICAL SCIENCES

FLOODING RELATED TO CLIMATE CHANGE: RISK ASSESSMENT METHODOLOGY FOR QUANTIFYING THE IMPACT OF DEBRIS FLOW

Surname SAULLO Name STEFANO

Registration number 883925

Tutor: Giovanni Battista Crosta

Company tutor: Orsola Brasi

Supervisor: Riccardo Castellanza

Co - Supervisor: Fabio De Blasio

Coordinator: Marco Malusà

ACADEMIC YEAR 2024/2025

Summary

Figures Index

Abstract

Climate change has an increasing impact on the frequency and intensity of flooding and debris flow events, particularly in mountainous areas or regions with unstable terrain. Effective risk management for these phenomena is crucial for protecting infrastructure, people, and the environment. This research proposes a risk assessment methodology to quantify the impact of debris flows on structures in the context of climate change. The work integrates a laboratory experiment on a scaled channel representing a real-life case and numerical analysis using CFD (Computational Fluid Dynamics) software to calibrate the parameters in scale. The developed model enables the prediction of extreme events and supports decision-making in Civile Engineering and Planning of hydrogeological risk.

Chapter 1

1 Introduction

1.1 Context and Motivation

The intensification of climate change has led to a rapid shift in precipitation patterns, which now occur with greater intensity over shorter periods of time and during specific times of the hydrological year. The main effect of this is the increasing number of flooding events and debris flows, which, from a risk and hazard assessment perspective, are considered events with a low probability of occurrence, that is, rare events with a 200-year return period.

These events not only cause severe damage to infrastructure and pose risks to people's safety but also raise important scientific and technical questions about the methodologies used to predict such events. In research and infrastructure design, the use of advanced numerical models, such as Computational Fluid Dynamics (CFD) models, is emerging as one of the most promising approaches to simulating their physical behavior, enabling accurate risk assessments and more reliable and resilient infrastructure design, as well as mitigation works.

Fig. 1.1: Damage produced by debris flows and flash floods to infrastructure and buildings in the aftermath of the August 2003 event (source: Civil Protection, FVG Region, 2012)

The CFD approach, combined with laboratory-scale experiments, provides a solid foundation for improving the understanding of debris flow phenomena and refining protective intervention techniques in real-world contexts.

Risk assessment is a fundamental process for managing the impact of flooding and debris flows, as it allows the identification of vulnerable areas and the development of strategies to protect human life and infrastructure. Numerical modeling, such as CFD models, plays a crucial role in the physical behavior understanding of these phenomena, providing realistic simulations that can be used to predict the effects of extreme scenarios and their impact on the territory.

CFD models solve equations capable of physically interpreting the dynamics of fluids based on various constitutive relations, such as debris flows (water and a solid matrix), thus predicting their impact on the areas below. When coupled with mathematical and statistical predictive models, they can provide more precise forecasts of how these phenomena may evolve under future climate scenarios.

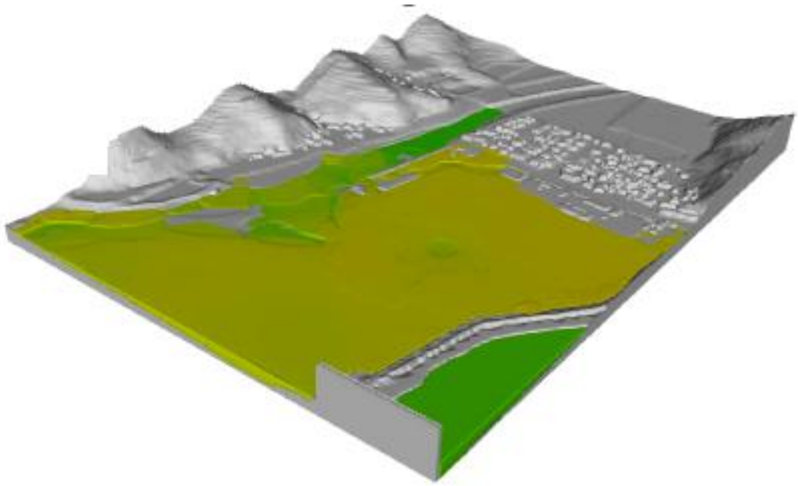

Fig. 1.2: Example of a CFD model of a large-scale debris flow event

To validate CFD models, it is essential to compare them with laboratory-scale experiments that replicate debris flow behavior in controlled conditions. These experiments allow for direct observation of the phenomena and the collection of empirical data, which can be used to calibrate and refine numerical models. Although limited in size, laboratory-scale experiments offer detailed information on flow behavior, propagation speed, travel distance, and the intensity of soil erosion.

Infrastructures exposed to the risk of flooding and debris flow must, therefore, be designed to be resilient to extreme events. Numerical models like CFD, combined with experimental data, can guide the design of more effective protective structures. Integrating mathematical models into the design phase helps optimize potential risk mitigation measures, prolonging the infrastructure's service life and improving safety conditions.

In summary, the increasing frequency and severity of flooding and debris flow events require a multidisciplinary approach that combines advanced numerical simulations, laboratory experiments, and engineering design techniques. CFD modeling, compared with laboratory-scale experiments, thus offers a powerful tool for better understanding these phenomena and developing more effective protection solutions. However, it is essential that risk assessment and infrastructure design be based on robust scientific approaches capable of adapting to the challenges posed by climate change. Only by doing so can the safety of people and the resilience of structures exposed to extreme events be ensured.

1.2 Research Objectives

The growing intensification of climate change and the increase in the frequency of extreme events, such as debris flows, pose significant challenges for the safety of people and infrastructure, particularly in mountainous and hilly regions. Debris flows are complex phenomena, characterized by the movement of mixed materials (water, mud, sand, rocks) on steep slopes, causing severe damage to structures and infrastructure located downstream. The need to predict and mitigate these risks is therefore of paramount importance.

The main objectives of this thesis are:

1. Develop a risk assessment methodology for debris flows that combines experimental and numerical approaches to quantify the impact of such events on exposed structures.
2. Simulate and analyze the behavior of debris flows using computational fluid dynamics (CFD) models, with the goal of obtaining accurate and detailed predictions on the movement and impact of debris flows.
3. Compare the results obtained from CFD numerical models with those from laboratory-scale experiments to validate the simulations and ensure the reliability of predictions.

1.2.1 Creation of a Risk Assessment Methodology

The main goal of the thesis is to create an integrated methodology to assess the risks associated with debris flows. This methodology aims to combine data from laboratory experiments, which replicate debris flow conditions at a reduced scale, with numerical simulations based on CFD models to analyze the behavior of these phenomena under different conditions. Specifically, the methodology should:

- Quantify the risk in terms of potential damage to exposed structures, based on the velocity, energy, and pressure of the simulated flows.
- Evaluate factors influencing the intensity and propagation of the flow, such as precipitation intensity, terrain characteristics, and slope angle.
- Provide predictive tools for risk management in real scenarios by simulating various climatic and geological conditions.

1.2.2 Numerical Simulations with CFD Models

The numerical analysis of debris flows will be conducted using computational fluid dynamics (CFD) models, which are a powerful tool for simulating complex flows of fluids and materials. CFD models will allow:

- Simulation of debris flow behavior under different conditions (variability in material composition, terrain slope, precipitation intensity, etc.), replicating real scenarios with high fidelity.
- Study of the propagation of debris flows, predicting flow velocity, energy transfer, distance travel, and the interaction between the flow and vulnerable surfaces.
- Analysis of the forces acting on exposed structures, such as buildings and infrastructure, to assess potential damage and the possibility of protection during the design phase.

1.2.3 Laboratory-Scale Experiments

Validating numerical models is essential for ensuring the accuracy of predictions. To this end, laboratory-scale experiments will be conducted to replicate debris flow phenomena under controlled conditions. These experiments will aim to:

- Physically reproduce debris flow conditions (materials, slope, rainfall intensity) on a reduced-scale model to directly observe and measure flow behavior.
- Collect empirical data on flow velocity, discharge, and pressure, as well as on material behavior during movement.

- Compare experimental results with CFD simulations to calibrate the numerical models and improve their reliability for real scenarios.

1.2.4 Specific Objectives and Expected Results

At the end of the research, the following results are expected:

- An operational risk assessment methodology, capable of supporting the design of safer infrastructure and the management of at-risk areas.
- Validated CFD numerical models that can be used to simulate debris flows in future scenarios, considering climate change and specific local conditions.
- Guidelines for protecting exposed structures based on simulations and experiments, which can be used by engineers and urban planners to develop effective protection solutions.

In summary, the thesis aims to develop an integrated methodology based on scale experiments and CFD numerical models for assessing the risks associated with debris flows, with the goal of contributing to the protection of infrastructure and the management of natural risks in the context of climate change.

Chapter 2

2 Theoretical Background and Literature Review

2.1 Debris Flow: Causes and Triggers

The phenomenon of debris flow is a geomorphic mass transfer process in mountain regions, consisting of a mixture of sediment and water moving through steep channels. A key feature of debris flows is that the maximum flow depth and mean velocity can significantly exceed the values observed for floods in the same channel. This phenomenon, along with high mass densities and large boulders in the flow, can modify valleys and endanger human life and infrastructure. Therefore, understanding the causes and triggers of such events is important for studying landscape evolution and for hazard assessment in alpine regions. Research on these phenomena is highly interdisciplinary, involving geoscience, hydrometeorology, hydraulics, geotechnical engineering, and granular physics.

Debris flows are defined as flows of unsorted debris and water that transit steep channels. They can range from granular flows with a high concentration of boulders to mudflows consisting of fine sediment and water. For example, the Austrian Standards (ONR 24,800, 2009) define debris flows as one of four channel processes that can occur in a creek, having specific quantitative parameters, like a volumetric sediment concentration > 0.4, that separates debris flows from floods, bedload transport and debris floods. Another example of classification is Aulitzky's classification (1982), which differentiates various types of torrents based on their expected response to extreme events:

- **Debris-flow torrents** (*Murstossfähige Wildbäche*);
- **Debris-flood torrents** (*Murfähige Wildbäche*);
- **Bedload torrents** (*Geschiebeführende Wildbäche*);
- **Flood creeks** (*Nur Hochwasser führende Wildbäche*).

An illustrative example of the approach that frames debris flows within a broader spectrum ranging from water currents to landslides is provided by the classification of Coussot and Meunier (1996).

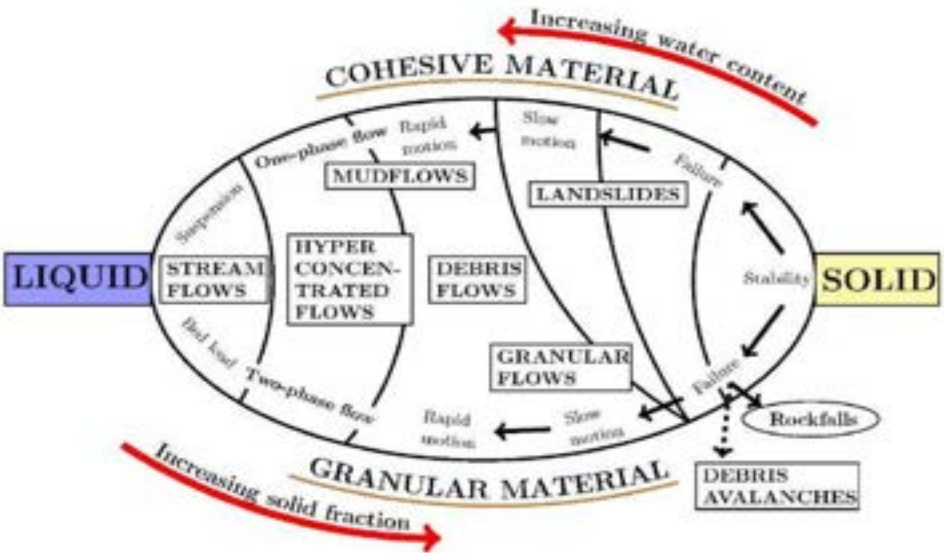

Fig. 2.1: Classification of Mass Movements on Steep Slopes (modified from Coussot and Meunier, 1996).

In this classification, in addition to the concentration of solids, the role of the granulometric characteristics of the involved materials is considered, distinguishing between cohesive and granular materials.

Their common feature is the presence of flow surges and a typical geometry: a front containing most of the coarse material, followed by a more dilute flow as it moves away from the front. Debris flow densities in motion have been recorded between 1800 and 2250 kg/m^3. The process can be seen as a saturated debris flow with strong involvement of material along the path, and a distinctive element is the presence of a confined path, typically a first or second-order drainage channel in mountain areas.

Debris flows can originate from debris floods, which are an intensive form of bedload transport, and can transform back into debris floods through the dilution of the sediment-fluid mixture while debris flows lacking coarse particles are known as mudflows.

2.2 Mechanics and Constitutive Relationships of Debris Flows

The phenomenon of debris flow represents one of the most complex and devastating geomorphological processes in sediment transport. It occurs when a mixture of water, sediment, and debris moves along slopes and valleys at high speeds, often triggered by extreme meteorological events, such as heavy rainfall or snowmelt. Understanding debris flow requires an in-depth comprehension of the physical and rheological characteristics of the fluid involved, as it does not behave like an ideal fluid but rather as a complex mixture of solids and liquids with a highly nonlinear behavior. The dynamic response of debris flow challenges traditional fluid dynamics concepts, as it is a non-Newtonian fluid, meaning its viscosity depends on the deformation rate and the concentration of solids.

From a physical standpoint, debris flow behaves as a complex mixture of solids and liquids, with a sediment concentration that can vary significantly, affecting the flow's viscosity. The viscosity in this case is not constant but depends on the concentration of the sediment and the granulometric composition of the solid material involved. Specifically, debris flows with high sediment concentrations exhibit a viscosity that increases substantially, leading to plastic or viscoplastic behavior.

Debris flows can be considered an intermediate phenomenon between landslides and floods, as they combine elements of both processes. They differ from landslides because, once initiated, their movement is highly fluid, similar to that of torrential floods, but with much higher density and destructive capacity. The speeds reached can vary from a few meters per second to over 30 m/s, depending on the terrain slope and the characteristics of the transported material.

A defining characteristic of debris flows is their selective sediment transport capacity. During movement, coarser particles tend to concentrate in the leading front of the flow, while finer particles remain in suspension in the main body. This behavior can generate a stratified structure in the flow, with a clear separation between different materials.

From a dynamic perspective, a debris flow can be divided into three main zones:

1. Initiation Zone: Typically located in steep slopes or torrential streambeds where loose debris accumulates. The initiation can occur due to water infiltration destabilizing the material, seismic events, or sudden collapses of precariously balanced material.
2. Propagation Zone: During this phase, the flow increases in volume and velocity, often incorporating new material due to erosion along the path. This self-feeding process makes debris flows unpredictable and significantly enhances their destructive potential.
3. Deposition Zone: The flow velocity gradually decreases, and the transported material settles according to its granulometry. Larger boulders stop first, while finer material can be transported over longer distances.

At a macroscopic level, a single debris flow event consists of three distinct elements:

- Debris Flow Front: Contains the coarsest materials, often including boulders and tree trunks.
- Debris Flow Body: A viscous mixture of sediments and water responsible for most of the mass transport.
- Debris Flow Tail: Characterized by a lower content of solid particles and a lower velocity compared to the main body.

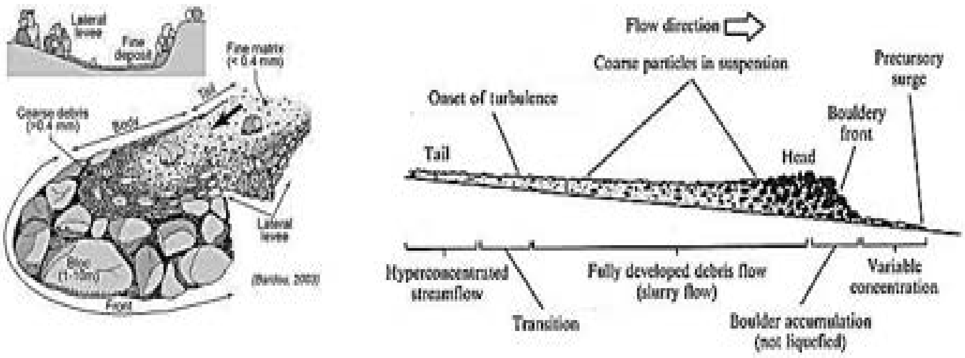

Fig. 2.2: Wave of a schematized debris flow (Pierson, 1986)

The physical properties of debris flows vary depending on the composition of the mixture and the environmental conditions. Some characteristic parameters, estimated by Iverson (1997), are presented in the following table:

Property	Symbol	Typical Values
Density of solid particles	ρs (kg/m³)	2500 – 3000
Average particle diameter	D (m)	10^{-5} – 10
Internal friction angle	φs (°)	25 – 35
Density of interstitial fluid	ρf (kg/m³)	1000 – 1200
Dynamic viscosity	μ (Pa·s)	0.001 – 0.1
Volumetric concentration of sediments	C (-)	0.4 – 0.8

Table 2.1 – Typical debris flow proprieties

To describe the behavior of this fluid, empirical laws and models based on different constitutive plasticity or viscoplasticity models are used. In these models, the fluid is considered as a material that exhibits a yield stress τ below which no flow is observed, but once this threshold is surpassed, it behaves like a viscous fluid.

Fig. 2.3: real debris flow event

Constitutive models are used to describe the rheological behavior of debris flows, i.e., the relationship between shear stress (τ) and shear rate ($\dot{\gamma}$). Due to their heterogeneous nature, debris flows are generally treated as non-Newtonian fluids, whose behavior varies according to loading conditions and mixture properties.

The main constitutive models adopted are:

1. **Bingham model**
2. **Herschel-Bulkley Model**

3. **Power Law Model**
4. **Carreau Model**

Bingham model

The Bingham Plastic model is one of the most widely used models for representing debris flows with a high concentration of solids. It assumes that the material behaves as a solid until it surpasses a yield stress threshold, beyond which it begins to flow like a fluid with constant viscosity:

$$\tau = \tau_0 + \mu\dot{\gamma}, \quad \text{if} \quad \tau \geq \tau_0$$

$$\dot{\gamma} = 0, \quad \text{if} \quad \tau < \tau_0$$

Where:

- τ_0 is the yield stress,
- μ is the plastic viscosity,
- $\dot{\gamma}$ is the shear rate

The Bingham model is widely used in engineering and geotechnical contexts to describe materials or fluids that exhibit a yield stress, such as:

- Debris flows with high solid concentration, where large amounts of sediment produce a viscoplastic behavior.
- Drilling mud in the oil industry.
- Cement paste or fresh concrete.
- Food products (certain types of dense creams or pastes).

However, this model has some limitations:

1. **Linearity Above the Threshold.** The Bingham model assumes that once the yield stress is exceeded, the relationship between shear stress and shear rate is linear. In real cases, the relationship can be non-linear (e.g., pseudo-plastic behavior).

2. **Lack of Elasticity**. The Bingham model does not account for possible elastic effects prior to flow; in reality, many materials display elastic behavior up to yield.
3. **Experimental Determination**. Parameters such as τ_y and μ_p must be determined experimentally (e.g., with rheometers or flow tests). Accurate measurement of τ_y is critical but can be challenging due to effects such as slippage, sedimentation, etc.
4. **Real Flow Conditions**. In many practical situations, flow geometry, concentration gradients, and turbulence can make behavior more complex than described by the simple Bingham model. Consequently, variants like the Herschel–Bulkley model (which introduces a non-linear flow behavior index) may be preferred.

The Bingham rheological model is a key reference for describing systems that exhibit "solid-like" behavior below a certain stress threshold and "fluid-like" behavior above it. It is straightforward to implement and interpret, yet it must be used with awareness of its limitations, especially in complex contexts such as natural debris flows, where turbulence, varying concentration, grain-size distribution, and particle interactions may require more sophisticated models or carefully calibrated parameters.

Herschel-Bulkley Model

The Herschel–Bulkley rheological model is an extension of the Bingham model that describes the behavior of viscoplastic fluids through a nonlinear relationship between shear stress and shear rate. It is particularly useful for representing materials that not only require a certain stress threshold to begin flowing but also exhibit a more complex flow behavior once in

motion one that is not simply Newtonian or linear. This model is commonly applied to various industrial, geotechnical, and natural materials such as slurries, suspensions, fresh cement, and debris flows, offering a more realistic description of their rheological behavior compared to simpler models.
The constitutive equation for the Herschel–Bulkley model is given by the relation

$$\tau = \tau_0 + k\dot{\gamma}^n$$

Where:

- k is the consistency index,
- n is the flow index.

In this equation, τ represents the applied shear stress, τy is the yield stress (the minimum stress required for the material to start flowing), k is the consistency coefficient that characterizes the material's resistance to flow once it begins moving, $\dot{\gamma}$ is the shear rate, and n is the flow behavior index. When the shear stress is below τy, the material behaves as a solid and does not flow. Once the threshold is exceeded, the behavior of the material depends on the value of n: if n=1, the fluid behaves like a Bingham fluid and exhibits linear behavior; if n<1, the fluid is shear-thinning, meaning its effective viscosity decreases as the shear rate increases; and if n>1, the fluid is shear-thickening, with viscosity increasing with the shear rate.
This model finds application in numerous complex materials that display both solid-like and fluid-like characteristics. For instance, in the case of debris flows, the concentration and grain size of sediments can significantly affect viscosity and flow behavior, necessitating a more

sophisticated model than the simple Bingham approach. Similarly, fresh cement or certain industrial slurries may exhibit a yield stress that prevents flow at low stresses but shows highly nonlinear flow behavior once the material starts moving.

A practical example can be seen in drilling muds used in the oil industry. These fluids must keep solid particles suspended when at rest, necessitating a sufficiently high yield stress to prevent sedimentation, yet they must also flow easily under the action of pumps. In such cases, the flow behavior index n is often less than 1, indicating that the effective viscosity decreases as the shear rate increases, thus facilitating pumping.

To apply the Herschel–Bulkley model correctly, it is essential to determine the parameters τy, k, and n experimentally, typically using rheometers that measure the relationship between shear stress and shear rate. Accurate calibration of these parameters is crucial, especially in materials with a wide range of particle sizes where the behavior can be unpredictable.

Despite its advantages, the Herschel–Bulkley model has limitations. While it offers an improvement over the Bingham and Newtonian models by accommodating a nonlinear flow response, it assumes that the shear stress–shear rate relationship can be described by a simple power law. This assumption may not capture more complex time-dependence or viscoelastic behaviors observed in some materials. In certain cases, more advanced models such as the Papanastasiou viscoelastic model, which introduces a regularization function for the transition from solid to fluid, or the Casson model, often used in biological contexts may be necessary to accurately describe the observed phenomena.

Overall, the Herschel–Bulkley model provides a versatile tool for describing the rheological behavior of many viscoplastic fluids that exhibit a yield stress and nonlinear response to shear. It continues to be a reference point in the analysis of complex fluids across various fields, although its correct application relies on careful experimental calibration and, in some instances, the use of more sophisticated modifications to capture the full complexity of the material behavior.

Power Law Model

The Power Law rheological model is a widely used framework for describing the flow behavior of non-Newtonian fluids that do not exhibit a yield stress. In this model, the relationship between shear stress and shear rate is expressed as a power law, and the fundamental equation is written as:

$$\tau = k\dot{\gamma}^n$$

In this equation, τ represents the shear stress, $\dot{\gamma}$ is the shear rate, k is the consistency index (which can be thought of as a measure of the fluid's viscosity), and n is the flow behavior index. The value of n determines the nature of the fluid's response to shear: if $n<1$, the fluid is shear-thinning (its apparent viscosity decreases as the shear rate increases), if $n>1$, the fluid is shear-thickening (its apparent viscosity increases with shear rate), and if $n=1$, the fluid behaves as a Newtonian fluid with constant viscosity. One of the strengths of the Power Law model is its flexibility in describing fluids that do not follow the constant-viscosity behavior of Newtonian fluids. However, it also has limitations. For instance, because the model does not incorporate a yield stress, it is not suitable for materials that require a minimum stress to initiate flow. Additionally, the power law equation can sometimes fail to accurately predict fluid behavior at very low or very high shear rates, where deviations from the power law might be observed.

Overall, the Power Law rheological model provides a useful and straightforward approach to modeling non-Newtonian fluid behavior. Its simplicity makes it a popular choice in many engineering and scientific applications, despite its limitations in capturing the full complexity of certain fluid systems.

Carreau Model

The **Carreau model** is a rheological model used to describe the viscosity behavior of non-Newtonian fluids, particularly those that exhibit **shear-thinning** properties. It is an improvement over the Power Law model because it accounts for both the Newtonian behavior at low shear rates and the shear-thinning behavior at higher shear rates, providing a continuous transition between these two regions. The Carreau model is widely used in engineering, material science, and biophysics, particularly for polymer solutions, suspensions, and biological fluids such as blood.

The fundamental equation governing the Carreau-Yasuda model is:

$$\mu(\dot{\gamma}) = \mu_\infty + (\mu_0 - \mu_\infty)\left(1 + \lambda\dot{\gamma}^2\right)^{\frac{n-1}{2}}$$

where:

- μ_0 and μ_∞ are the viscosities at low and high shear rates, respectively,
- λ is a characteristic time parameter,

- n is the power law exponent.

The Carreau model describes a smooth transition between Newtonian flow at low shear rates and shear-thinning behavior at higher shear rates. At very low shear rates ($\dot{\gamma} \rightarrow 0$), the fluid has a nearly constant viscosity equal to η_0. As the shear rate increases, the viscosity begins to decrease smoothly until it reaches η_∞ at very high shear rates ($\dot{\gamma} \rightarrow \infty$).

The parameter λ controls the transition region: larger values of λ indicate that the Newtonian plateau extends over a wider range of shear rates, while smaller values mean that the shear-thinning behavior begins at lower shear rates. The flow behavior index n determines the extent of shear-thinning, with lower values of n leading to more pronounced shear-thinning effects.

One of the key advantages of the Carreau model is its ability to smoothly transition between Newtonian and shear-thinning behaviors without requiring a sharp discontinuity. Unlike the Power Law model, which does not capture the Newtonian viscosity at low shear rates, the Carreau model correctly describes real fluids that exhibit a viscosity plateau before transitioning into shear-thinning behavior. Additionally, it is more physically realistic than purely empirical models and provides better accuracy in predicting fluid behavior across a broad range of shear rates.

However, the Carreau model has some limitations. It does not account for yield stress, meaning it cannot describe fluids that require a minimum stress to begin flowing (e.g., Bingham or Herschel–Bulkley fluids). Furthermore, for materials with complex time-dependent behavior (such as thixotropic or viscoelastic fluids), additional modifications or more advanced rheological models may be necessary.

The following graph illustrates the differences between the constitutive models, highlighting how shear stress varies as a function of shear rate.

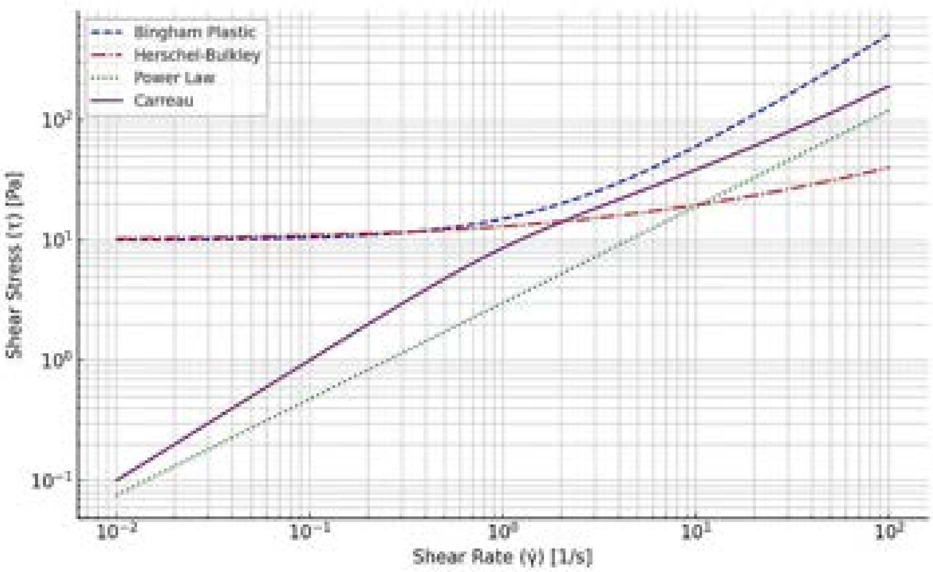

Fig. 2.4: constitutive models

This analysis demonstrates that the choice of the model depends on the physical properties of the mixture and the loading conditions. Bingham and Herschel-Bulkley models are more suitable for cohesive debris flows with yield stress, while the Power Law and Carreau models are more appropriate for describing flows where viscosity changes with shear rate.

2.3 Methods and Formulas for Calculating the Impact Forces of Debris Flow

The impact of debris flows on obstacles such as bridge piers is a key issue in hydraulic and structural engineering. The forces exerted by debris flows depend on flow properties, pier geometry, debris composition, and impact dynamics. Below, I summarize key analytical, empirical, and numerical models used to estimate impact pressures and forces.

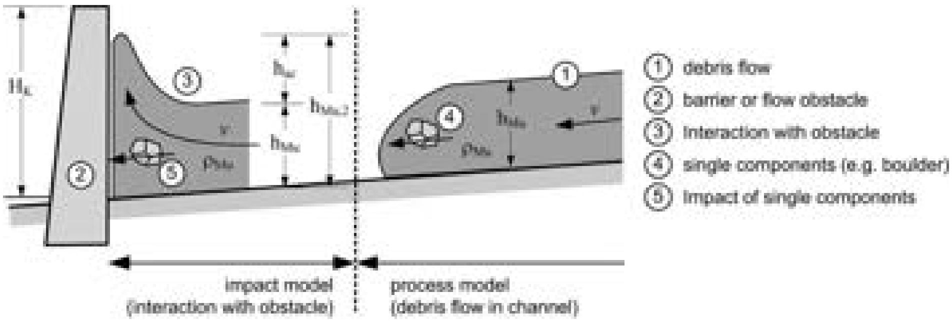

Fig. 2.5: Process and impact model for debris flow estimation on structures ***(Debris flow impact estimation for breakers - Article in Georisk Assessment and Management of Risk for Engineered Systems and Geohazards · June 2011)***

The impact force of debris flow on an obstacle is influenced by several factors:

- **Density (ρ)**: Higher sediment concentration increases impact pressure.
- **Velocity (v)**: The kinetic energy of the flow directly affects impact force.
- **Flow height (h)**: Determines the pressure distribution along the impacted structure.

- **Flow type**: Debris flows can behave as granular flows, hyperconcentrated flows, or viscous flows, affecting force calculations.
- **Stress anisotropy (j)**: Accounts for the stress distribution in granular debris flows.

The force exerted by a debris flow on a bridge pier can be classified into different impact types:

1. **Hydrostatic force** – Occurs when the debris stagnates around the pier, generating a static lateral pressure.
2. **Hydrodynamic force** – Generated when a moving debris flow impacts the structure, causing a dynamic pressure.
3. **Empirical and Experimental Formulas**

2.3.1 Hydrostatic model

A simplified approach to estimating impact force considers the hydrostatic pressure exerted by the debris mass:

$$p_d = k\rho g h$$

where:

- p_d = debris impact pressure,
- ρ = bulk density of debris flow,
- g = gravitational acceleration,
- h = flow depth,
- k = empirical coefficient (varies based on debris composition and serves as a scaling factor that adjusts the theoretical pressure

exerted by the debris flow to account for variations in composition, viscosity, and particle concentration.).

The **empirical coefficient** k in the **hydrostatic model** is a key parameter used to modify the standard hydrostatic pressure equation to account for the unique behavior of debris flows. Unlike clear water, debris flows exhibit complex rheological properties due to their high sediment concentration, particle interactions, and non-Newtonian behavior. The coefficient k effectively adjusts the calculated pressure to better match experimental or field observations.

The value of k reflects how the debris flow behaves compared to purely hydrostatic fluid. Several factors influence this parameter:

- **Particle Concentration:** Higher solid fractions increase resistance to deformation, leading to different pressure distributions.
- **Sediment Size and Distribution:** Coarse-grained debris flows exert higher normal stresses, increasing k.
- **Cohesion and Rheology:** High clay or fine sediment content alters the fluid-like behavior, affecting impact pressure.
- **Velocity and Turbulence Effects:** Even in low-velocity scenarios, some dynamic effects (such as granular collisions) can increase impact pressures, modifying k.
- **Porosity and Pore Water Pressure:** High pore pressures within a saturated debris mass can reduce normal stress and lower k.

The value of k is often determined through **experimental calibration** using laboratory flume tests and real-world debris flow observations.

Different studies have proposed varying values for k, depending on the specific characteristics of the debris flow:

Study	Debris Flow Type	Range of k
Mizuyama (1979)	High-density debris flow	1.5 - 3.0
Armanini & Scotton (1992)	Mud-rich debris flow	1.2 - 2.5
Rickenmann (1999)	Granular debris flow	2.0 - 4.0
Faug et al. (2021)	Granular-dominated impact	1.8 - 5.0

Table 2.2 – values for k depending on the specific characteristics of the debris fow

These values indicate that the impact pressure of debris flows is generally higher than pure hydrostatic pressure, requiring an adjustment using k. Several researchers have proposed empirical formulas to estimate k based on debris flow properties. Some common approaches include:

1. **Function of Volume Fraction of Solids (ϕ)**:

$$k = 1 + 2\phi$$

   where ϕ is the volume fraction of solid material in the debris flow.

2. **Dependence on Bagnold's Granular Flow Number (N_g)**:

$$k = 1 + \frac{N_g}{10}$$

   where N_g is a dimensionless number representing the balance between inertial and viscous forces.

3. **Empirical Equation from Field Data**:

$$k = 1.5 + 0.8\left(\frac{\rho_s}{\rho_w}\right)$$

   where ρs is the solid particle density, and ρw is water density.

2.3.2 Hydrodynamic model

For high-velocity debris flows, the hydrodynamic pressure component must be considered:

$$p_d = \alpha \rho v^2$$

where:

- v = velocity of the debris flow,
- α = dynamic pressure coefficient.

This model accounts for the kinetic energy of the moving debris mass and is particularly useful for estimating the force on vertical obstacles.

The dynamic pressure coefficient α is a crucial empirical parameter that adjusts the theoretical force exerted by a moving debris flow. It accounts for the non-Newtonian behavior, turbulence, and complex interactions within the debris mass, which differ significantly from clear-water flows.

In classical fluid dynamics, the impact pressure of a moving fluid is often given by:

$$p = \frac{1}{2}\rho v^2$$

where the coefficient is 1/2 for Newtonian fluids. However, debris flows are highly non-Newtonian, meaning their behavior depends on:

- **High sediment concentration** (solid fraction affects stress transmission),
- **Particle collisions** (granular effects modify impact force distribution),
- **Flow rheology** (viscoplastic, Bingham, or granular flow properties),

- **Impact surface effects** (rigid vs deformable structures).

The coefficient α\alphaα **compensates for these complexities**, making it a crucial factor for realistic impact force calculations.

Extensive **experimental and field studies** have been conducted to determine reasonable values of α for different types of debris flows. A range of values has been reported:

Study	Debris Flow Type	Range of α
Armanini & Scotton (1992)	High-density debris flow	1.5 - 3.0
Rickenmann (1999)	Granular debris flow	2.0 - 4.5
Hungr et al. (2005)	Mud-rich debris flow	1.2 - 2.8
Faug et al. (2021)	Granular-dominated impact	1.8 - 5.0

Table 2.3 – values for α depending on the specific characteristics of the debris flow

- **Higher values** ($\alpha > 2.5$) occur in granular flows with significant collisional interactions.
- **Lower values** ($\alpha < 2.0$) are found in more fluid-like, fine-grained debris flows.
- **Very high α** values (up to **5.0**) have been observed when debris flows impact rigid barriers, where kinetic energy dissipation is minimal.

Several researchers have proposed empirical and semi-theoretical formulations for estimating α.

a. **Function of the Solid Volume Fraction ϕ:**

$$\alpha = 1 + 2.5\phi$$

where ϕ is the solid volume fraction of the debris flow.

- For low-density flows ($\phi = 0.2$), $\alpha \approx 1.5$.

- For high-density flows (ϕ = 0.4), α ≈ 2.5.

b. Dependence on Froude Number Fr:

A common semi-empirical relation links α\alphaα to the Froude number:

$$\alpha = 1 + \frac{Fr}{5}$$

Where

$$Fr = \frac{v}{\sqrt{gh}}$$

- **For low-energy flows** (Fr = 1Fr), α ≈ 1.2.
- **For high-energy flows** (Fr = 5), α ≈ 2.0.

This equation reflects the increasing dynamic contribution to impact pressure with flow velocity.

c. Experimental Formula from Field Data:

Hungr et al. (2005) proposed an empirical equation for impact force:

$$p_d = (1.5 + 0.8 \cdot Fr)\rho v^2$$

which suggests that:

$$\alpha = 1.5 + 0.8 \cdot Fr$$

- For slow debris flows (Fr = 1), α = 2.3.
- For fast flows (Fr = 4) α = 4.7.

This formula is widely used in hazard assessments.

d. **Flow Type and Rheology:**
   - Granular flows: High α (2.5 - 5.0) due to particle collisions.
   - **Mudflows**: Lower α (1.2 - 2.0) as the flow behaves more like a viscous fluid.

2.3.3 Empirical and Experimental Formulas

Various empirical models have been developed based on experimental and field data:

1. **Mizuyama (1979):**

$$P = \rho_s H v^2 / g$$

where H is the flow depth and vvv is the mean velocity.

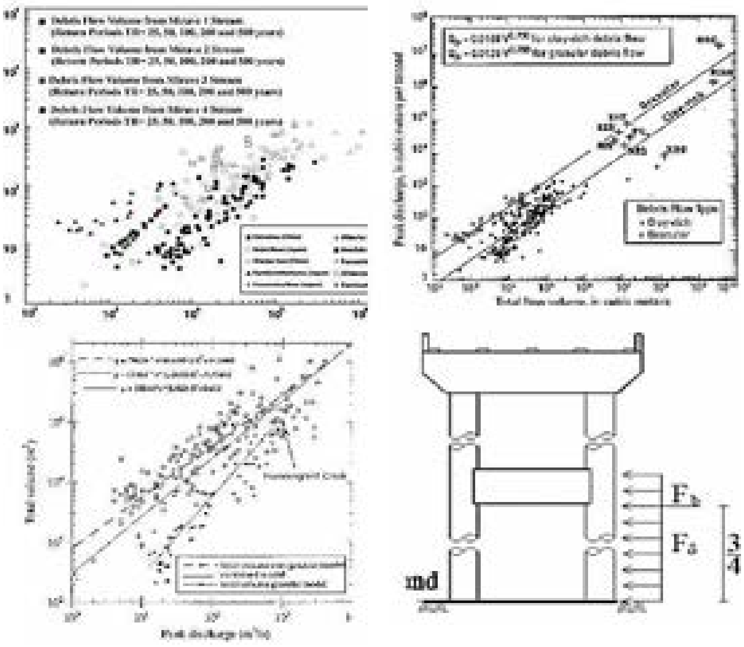

Fig. 2.6: Mizuyama Experiment results

2. **Hungr et al. (1984):**

$$P = \rho_s A v^2 \sin\beta$$

where A is the impact area and β\betaβ is the impact angle.

3. **Zheng (2014) – Froude Number-Based Model:**

$$P = 5.3 F_r^{-1.45} \rho_s v^2$$

where Fr is the Froude number, which relates velocity to gravitational acceleration.

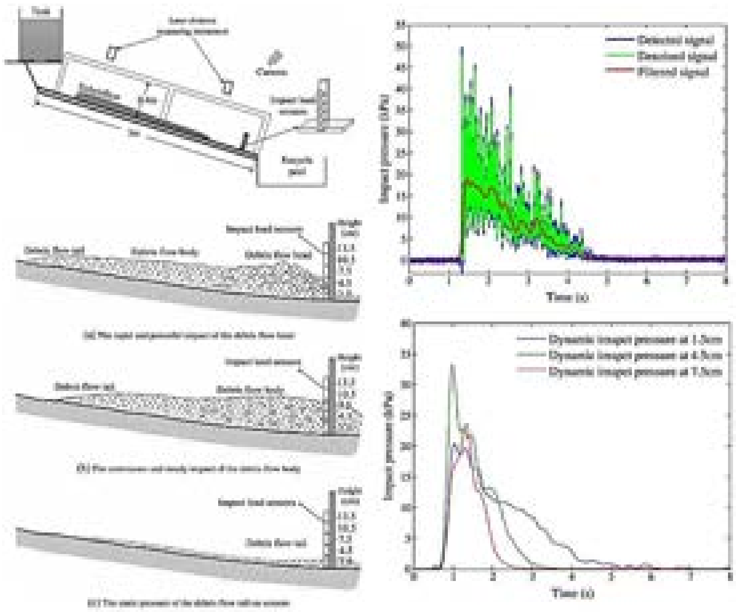

Fig. 2.7: Zheng (2014) image of experimental investigation

2.4 Numerical Models for Debris Flow Simulation

Numerical modeling of debris flows is essential to understand the dynamics of these phenomena and to assess their impact on infrastructure. Various software tools have been developed to simulate the behavior of debris flows, adopting different approaches based on specific governing equations. Numerical models can be classified into three main categories:

1. **Models based on Navier-Stokes equations** (three-dimensional CFD models);
2. **Models based on Saint-Venant equations** (shallow water models);
3. **Models with a Lagrangian approach**, such as Smoothed Particle Hydrodynamics (SPH).

Below is a detailed discussion of the different types of models and the main software tools used for debris flow simulation.

2.4.1 Models Based on Navier-Stokes Equations (CFD)

The Navier-Stokes equations describe the motion of a Newtonian fluid and can be extended to model debris flow behavior by including non-Newtonian effects, particle interactions, and sedimentation. The general conservation equations for mass and momentum are:

Continuity Equation:

$$\frac{\partial \rho}{\partial t} + \nabla \cdot (\rho \mathbf{u}) = 0$$

Momentum Equation:

$$\rho \left(\frac{\partial \mathbf{u}}{\partial t} + \mathbf{u} \cdot \nabla \mathbf{u} \right) = -\nabla p + \nabla \cdot \tau + \rho \mathbf{g} + \mathbf{F}$$

Where:

- ρ is the fluid density,
- **u** is the velocity vector,
- p is the pressure,
- τ is the viscous stress tensor,
- **g** is the gravitational acceleration.
- **F** = external forces (e.g., interaction with obstacles).

Debris flows exhibit **highly turbulent behavior** due to the interaction between fluid and solid particles. CFD models often employ turbulence models such as:

- **Reynolds-Averaged Navier-Stokes (RANS)** models (e.g., $k-\varepsilon$, $k-\omega$) for time-averaged turbulence representation.
- **Large Eddy Simulation (LES)** for resolving large-scale turbulent structures.
- **Direct Numerical Simulation (DNS)** for highly detailed flow analysis (though computationally expensive).

CFD models use different numerical techniques to solve the **Navier-Stokes equations** efficiently:

1) **Finite Volume Method (FVM)**
   - Discretizes the computational domain into control volumes.
   - Ensures mass and momentum conservation locally.
   - Used in software like FLOW-3D, OpenFOAM, and ANSYS Fluent.
2) **Finite Element Method (FEM)**
   - Uses interpolation functions over elements to solve the governing equations.

- Well-suited for complex geometries and structural interactions.
- Implemented in COMSOL Multiphysics.

3) **Lattice Boltzmann Method (LBM)**
   - Alternative approach solving the Boltzmann equation instead of Navier-Stokes.
   - Efficient for multiphase flow simulations.
   - Used in software like Palabos.

The main CFD software used for debris flow simulations are:

1) **FLOW-3D**

FLOW-3D is an advanced CFD software that uses a Volume of Fluid (VOF) approach to track the interface between fluid and air. Key features include:

- Non-Newtonian viscosity models to represent debris flow behavior;
- Fluid-structure interaction implementation;
- Adaptive computational grids to optimize resolution;
- Capability to simulate solid transport and sedimentation with advanced models.

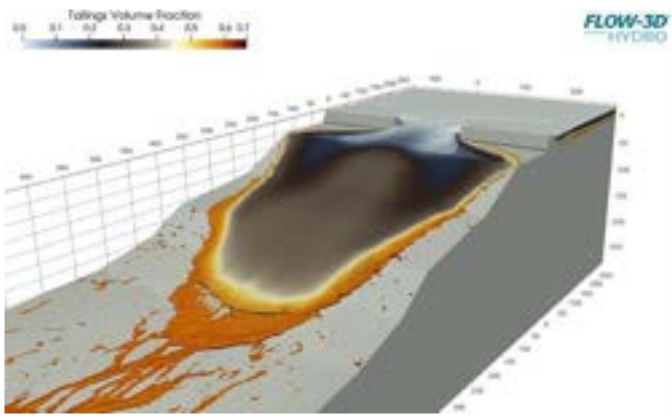

Fig. 2.8: Flow 3D tailing model example

2) **OpenFOAM**

OpenFOAM is an open-source CFD software widely used in research and industry. For debris flow modeling, OpenFOAM offers:

- Customizable solvers for Navier-Stokes equations;
- Implementation of multiphase flow models such as Volume of Fluid (VOF);
- Advanced discretization methods for stability and accuracy;
- Ability to handle complex boundary conditions, such as obstacles and infrastructure.

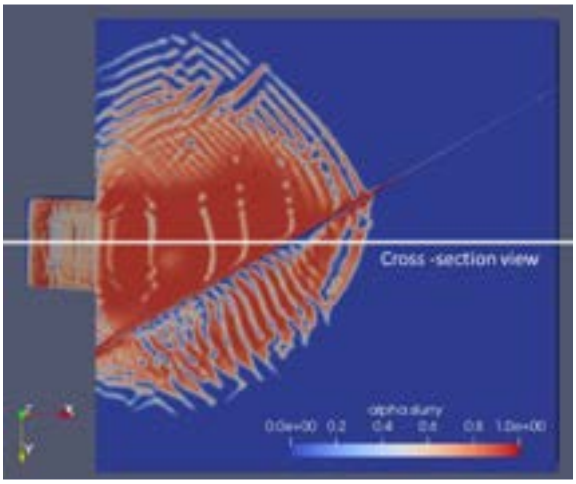

Fig. 2.9: Example of Open Foam debris flow simulation

3) **ANSYS Fluent**

ANSYS Fluent is a commercial CFD software providing powerful tools for debris flow simulation, including:

- Advanced turbulence models;
- Multiphase flow simulations and liquid-solid interaction;
- Integration with other engineering software for structural analysis;

- Intuitive graphical interfaces for visualization and result analysis.

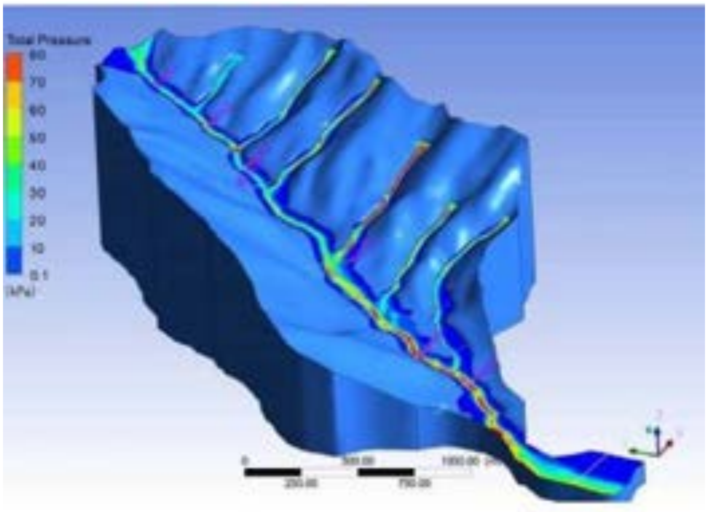

Fig. 2.10: Example of Ansys Fluent debris flow simulation

4) COMSOL Multiphysics

COMSOL Multiphysics is another CFD software that allows the simulation of multiphase flows and materials with complex rheology. Key features include:

- Coupled fluid-structure modeling;
- Customization of viscosity and sedimentation models;
- Solving multi-physics problems with coupling between solid transport and hydraulics.

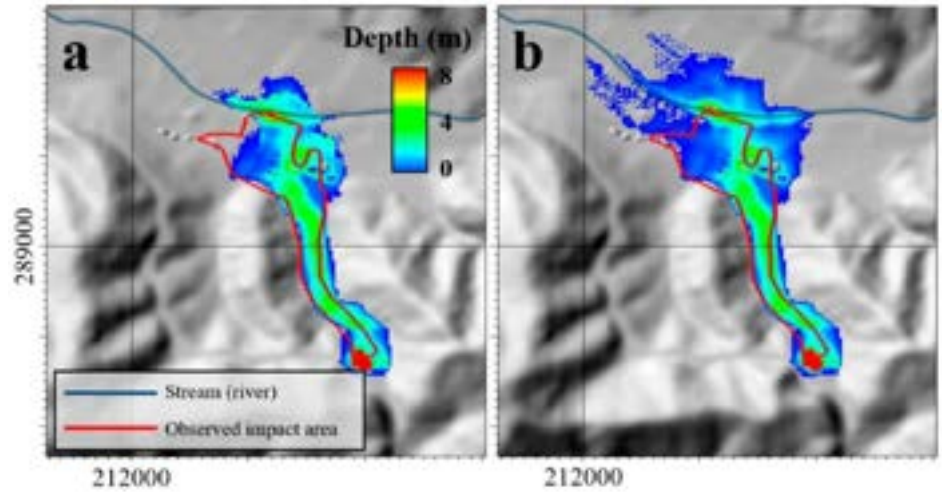

Fig. 2.11: Example of Comsol debris flow simulation

5) TELEMAC-MASCARET

TELEMAC-MASCARET is an open-source suite used for hydrodynamic and sediment transport simulations. For debris flow modeling, it offers:

- 3D hydrodynamics with Navier-Stokes solvers;
- Non-Newtonian rheological models;
- Coupled sediment transport and morphodynamic changes;
- Open-source flexibility for advanced customization.

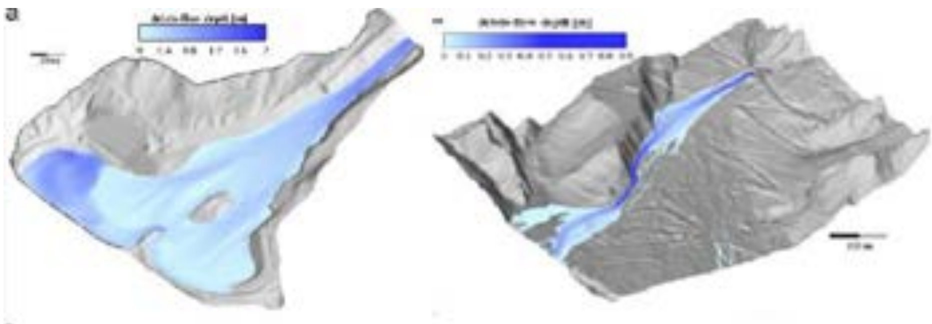

Fig. 2.12: Example of Telemac debris flow simulation

2.4.2 Models Based on Saint-Venant Equations (Shallow Water)

The Saint-Venant equations (or Shallow Water Equations, SWE) provide a simplified form of the Navier-Stokes equations under the assumption that the wavelength of the flow or the radius of curvature is much larger than the flow depth. This assumption is valid for many hydraulic phenomena, including floods, shallow debris flows, and gravity-driven flows over large surfaces.

The two-dimensional **conservative** form of the Saint-Venant equations is given by:

Continuity Equation:

$$\frac{\partial h}{\partial t} + \frac{\partial (hu)}{\partial x} + \frac{\partial (hv)}{\partial y} = 0$$

Momentum Equation:

$$\frac{\partial (hu)}{\partial t} + \frac{\partial}{\partial x}\left(hu^2 + \frac{1}{2}gh^2\right) + \frac{\partial (huv)}{\partial y} = -gh\frac{\partial z}{\partial x} - \tau_x$$

$$\frac{\partial (hv)}{\partial t} + \frac{\partial (huv)}{\partial x} + \frac{\partial}{\partial y}\left(hv^2 + \frac{1}{2}gh^2\right) = -gh\frac{\partial z}{\partial y} - \tau_y$$

where:

- h = flow depth,
- u, v = velocity components in the x and y directions,
- g = gravitational acceleration,
- z = bed elevation,
- τ_x, τ_y = bed shear stress terms.

These equations describe flow evolution considering convective acceleration, hydrostatic pressure, and bed friction but neglect three-dimensional effects and local turbulent fluctuations.

The Saint-Venant equations rely on key assumptions:

- The flow is shallow compared to its horizontal extent.
- The velocity profile is uniform along the vertical axis.
- The pressure distribution is hydrostatic.
- Bed resistance is modeled using empirical formulas (e.g., Manning's, Chezy's equations).

Despite these simplifications, shallow water models provide an excellent representation of debris flow propagation and large-scale behavior.

The main software based on these equations are:

- **RAMMS (Rapid Mass Movement Simulation)**

  RAMMS is a specialized software for simulating debris flows, avalanches, and landslides.

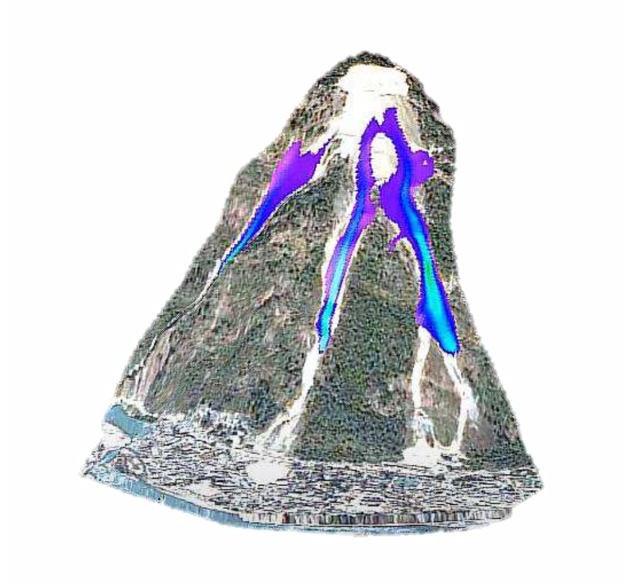

Fig. 2.13: Example of RAMMS debris flow simulation

It incorporates:

- Saint-Venant equations with enhanced formulations for granular and viscous flows.
- Non-Newtonian rheology models, including Voellmy and Bingham.
- Ability to simulate interactions between debris flow and infrastructure.
- GIS integration for terrain analysis.

- **FLO-2D**:

FLO-2D is widely used for floods and debris flow modeling.

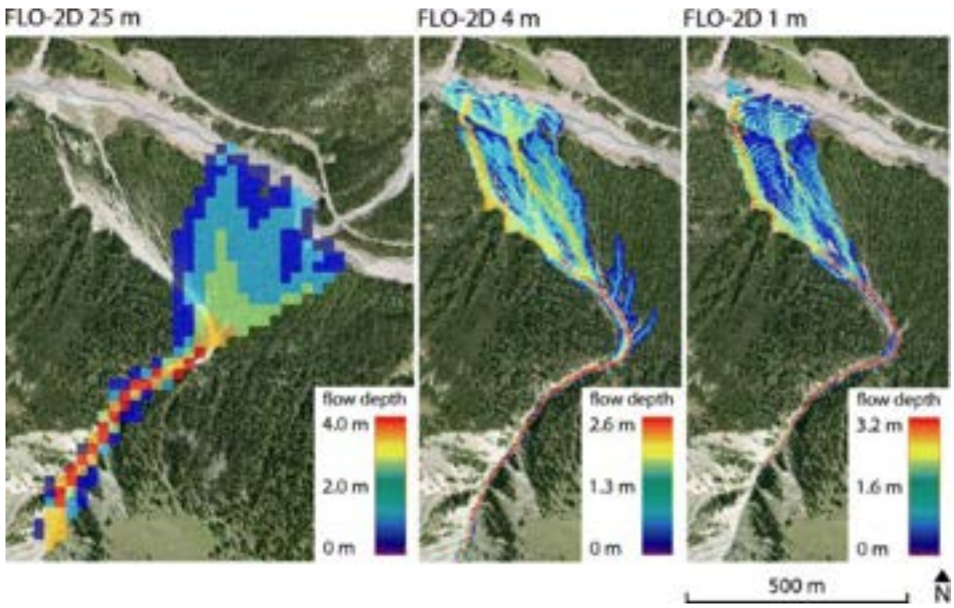

Fig. 2.14: Example of Flo 2D debris flow simulation

Its key features include:

- 2D Saint-Venant equations solved on a regular grid.
- Surface flow, infiltration, and sediment transport modeling.

- Hyperconcentrated flow models for debris-laden water flows.
- Full GIS integration for terrain processing.

- **HEC-RAS**:

  Originally designed for river and floodplain modeling, HEC-RAS has been extended to support debris flow and sediment transport.

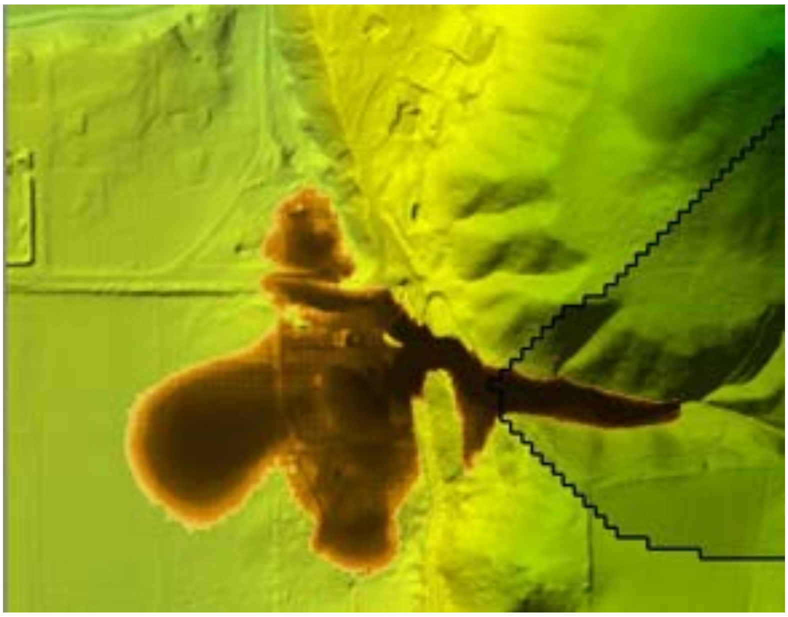

Fig. 2.15: Example of Hec RAS debris flow simulation

It features:

- 1D and 2D Saint-Venant equations for flood wave propagation.
- Sediment transport and erosion modeling.
- Debris flow modeling with different rheology model
- Ability to simulate structures like bridges, dams, and levees.
- GIS compatibility for spatial analysis.

- **TITAN-2D**:

  TITAN-2D is specifically designed for gravity-driven flows such as debris flows and pyroclastic flows.

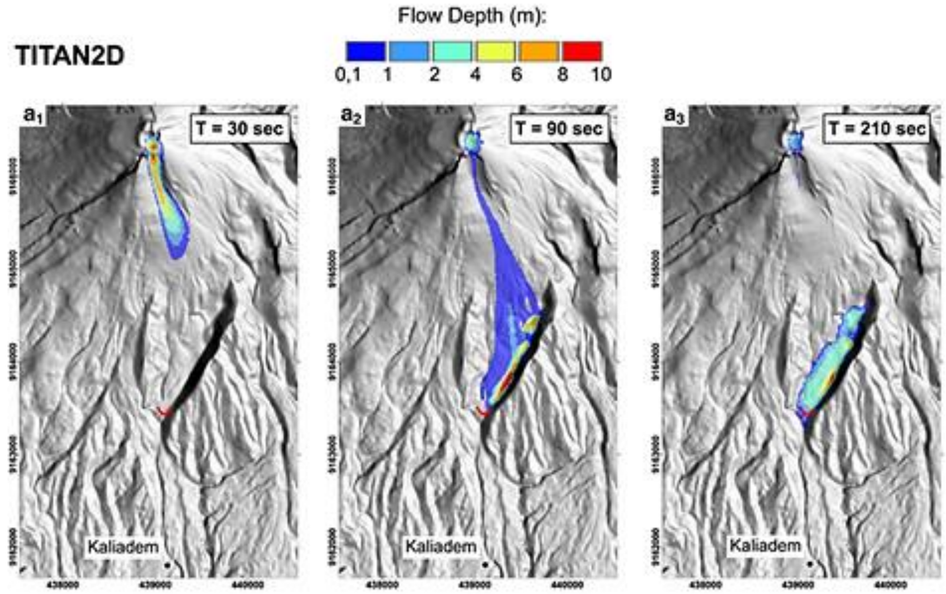

Fig. 2.16: Example of Titan 2D debris flow simulation

It utilizes:

- High-resolution Godunov methods for hyperbolic equations.
- Coulomb friction models for granular materials.
- Optimized for GPU and parallel computing, allowing large-scale simulations.

Software	Dimension	Rheology Models	GIS Integration	Applications
RAMMS	2D	Voellmy, Bingham	Yes	Debris flows, avalanches
FLO-2D	2D	Hyperconcentrated	Yes	Floods, debris flows
HEC-RAS	1D/2D	Sediment transport	Yes	River hydraulics, flood studies, debris flows
TITAN-2D	2D	Coulomb granular	No	Pyroclastic flows, debris avalanches

Table 2.4 – Comparison of Saint-Venant-Based Models

2.4.3 Models with a Lagrangian approach

Unlike Eulerian methods, which solve the governing equations on a fixed mesh, Lagrangian models track individual particles or discrete elements as they move through space. This approach is particularly well-suited for debris flows, where the interface between solid and fluid is highly dynamic, and material deformation plays a critical role.

One of the most widely used Lagrangian techniques for debris flow modeling is Smoothed Particle Hydrodynamics **(SPH)**, which represents the flow as a collection of discrete particles that interact through interpolation functions.

SPH is a mesh-free method where a set of particles represents a continuum fluid or solid. Each particle carries physical properties such as mass, velocity, pressure, and density, and their evolution is governed by the Navier-Stokes equations.

The general function and governing equation are:

1) **SPH Interpolation and Kernel Function**

The value of a function f(r) at a given position r is approximated as:

$$f(\mathbf{r}) = \sum_j m_j \frac{f_j}{\rho_j} W(\mathbf{r} - \mathbf{r}_j, h)$$

where:

- m_j = mass of neighboring particle j,
- ρ_j = density of particle j,
- W = kernel function that determines interaction strength,
- h = smoothing length defining the influence radius.

2) **SPH Discretization of Governing Equations**

Continuity Equation (Mass Conservation)

$$\frac{d\rho_i}{dt} = \sum_j m_j(\mathbf{v}_i - \mathbf{v}_j) \cdot \nabla W_{ij}$$

Momentum Equation (Navier-Stokes)

$$\frac{d\mathbf{v}_i}{dt} = -\sum_j m_j \left(\frac{P_i}{\rho_i^2} + \frac{P_j}{\rho_j^2} + \Pi_{ij} \right) \nabla W_{ij} + \mathbf{g}$$

where:

- P_i, P_j = pressures of particles i and j,
- Π_{ij} = artificial viscosity term to stabilize numerical oscillations.

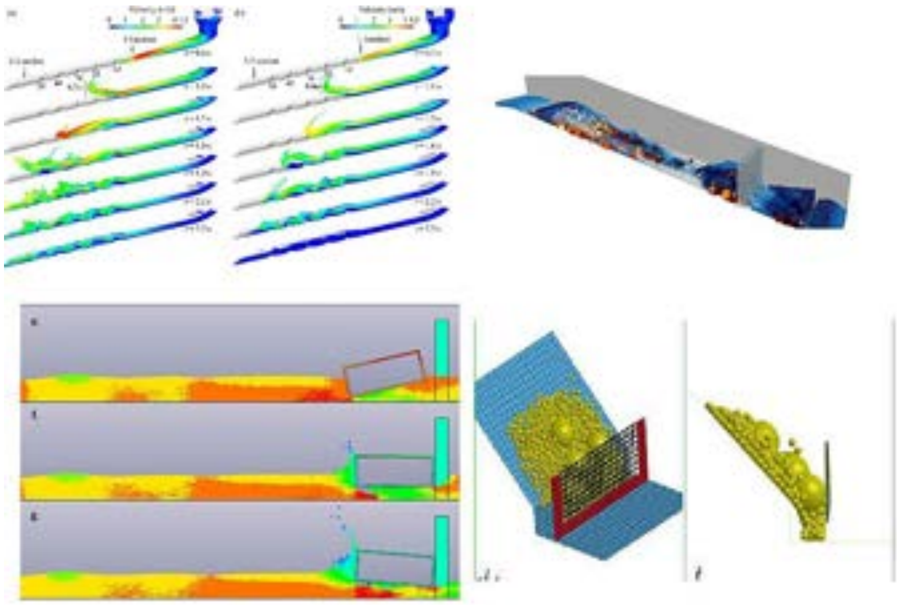

Fig. 2.17: Example of SPH models

Below, the main SPH models and their characteristics are presented in comparison.

Software	Parallel Computing	Multiphase Models	FSI Capability	Commercial/ Open-Source	Applications
DualSPHysics	GPU (CUDA)	Yes	Yes	Open-source	Hydraulic structures, debris impacts
SPHysics	CPU	Limited	No	Open-source	Tsunamis, landslide-generated waves
GPUSPH	GPU (CUDA)	Yes	Yes	Open-source	Large-scale debris flow simulations
LS-DYNA	CPU/GPU	Yes	Yes	Commercial	Structural impact, landslides
SPH-flow	CPU/GPU	Yes	Yes	Commercial	Civil engineering, FSI

Table 2.5 – Comparison of SPH Models

Chapter 3

3 Assessment of Flow-3D Model Accuracy Through Benchmark Experiments from Literature

The reliability of numerical modeling in simulating debris flow dynamics strongly depends on an accurate calibration and validation process. Before applying the model to a real-world case, it is essential to assess its capability to reproduce known physical behaviors observed in controlled laboratory experiments. In this chapter, a validation study is conducted using the experimental setup and results presented by **Zhao et al. (2018)**, which provide a detailed investigation of debris flow impact on rigid barriers under different flow conditions.

The experiment by Zhao et al. involved a dambreak-style release of a dense fluid mixture, allowing the evaluation of dynamic impact forces generated during the collision of the debris front with a rigid wall. This configuration is particularly suitable for model calibration, as it offers:

- a well-defined geometry and initial conditions,
- precise measurements of impact forces over time,
- and a clear rheological regime applicable to Bingham-type flows.

To validate the Flow-3D model, the experimental conditions were reproduced within the simulation environment, including the flume geometry, release mechanism, fluid rheology, and boundary conditions. By iteratively adjusting the Bingham parameters—yield stress and plastic viscosity—a close match between the simulated and experimental force profiles was obtained. This calibration process ensures that the numerical tool is capable of capturing both the peak impact forces and the temporal evolution of the pressure exerted on rigid structures.

The following sections describe the laboratory setup, the numerical implementation in Flow-3D, and the quantitative comparison of simulation results with the experimental data, laying the groundwork for its application to real-case scenarios in subsequent chapters.

3.1 Benchmark Experiment from Literature for Flow-3D Model Validation - Experimental Study of the Debris Flow Slurry. Impact and Distribution

The article **"Experimental Study of the Debris Flow Slurry Impact and Distribution"** by **Haixin Zhao et al.** addresses a critical issue in the design of preventive structures against debris flows: the estimation of the impact force of muddy debris flows (slurry impact) and its spatial distribution. The authors highlight the current lack of a unified formula and the widespread practice of designing structures by assuming a uniform distribution of the maximum impact force, which may result in overestimating structural resistance or in material wastage. Existing formulas are often derived from energy-based methods, more suitable for uniform flows such as water, and empirically adjusted, which does not ensure accuracy for non-uniform debris flows.

1. **Main Characteristics of the Experiment:**

- **Objective:**

  Develop a new method to calculate the impact force and its distribution of muddy debris flows, based on experimental data.

- **Experimental Setup:** Tests were conducted in a debris flow simulation laboratory. The flume measured 400 cm in length, 30 cm in width, and 40 cm in height, with an adjustable slope from 0° to 20°. A dam model with a 63° inclined surface was placed at the downstream end.
- **Instrumentation:** Eight piezoelectric sensors (0–100 kPa range, 0.1% sensitivity, 2 kHz sampling rate) were mounted at different heights on the dam surface. Sensors 1, 2, and 3 were located near the base, where the slurry depth was greatest. Sensor 2, usually registering the highest value, was used to analyze the peak impact force.
- **Experimental Material:** The test material was collected from a real site (Gan Gully, Sichuan Province), with a maximum grain size of 20 mm.

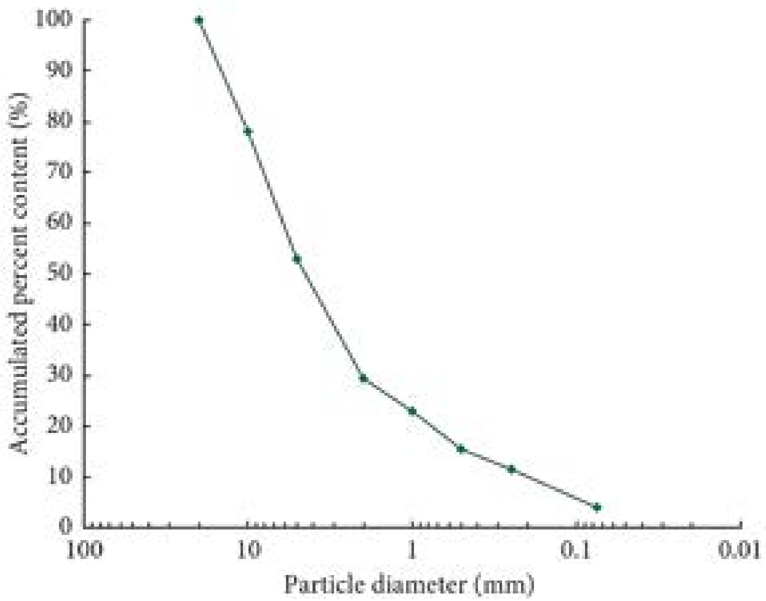

Fig. 3.1: Particle gradation of the materials used in the experiment

- **Test Variables:** A total of 33 tests were conducted, grouped to examine the effects of:
    - Debris flow density: 13, 15, 17, 19, 21 kN/m³,
    - Flume slope: 7°, 10°, 11°, 13°, 15°,
    - Debris flow volume: 60 L, 90 L, 120 L,
    - Dam front angles: 63°, 77°, 90°.
- **Preliminary Results:** The impact force distribution is non-uniform, being greatest at the center and tapering toward the sides. Impact force does not necessarily increase with density, since higher density may reduce flow velocity. Flume slope positively correlates with impact force, as it affects flow velocity. Dam angle had little effect on peak force. The debris volume has a linear

correlation with impact, as it affects slurry depth and consequently velocity.

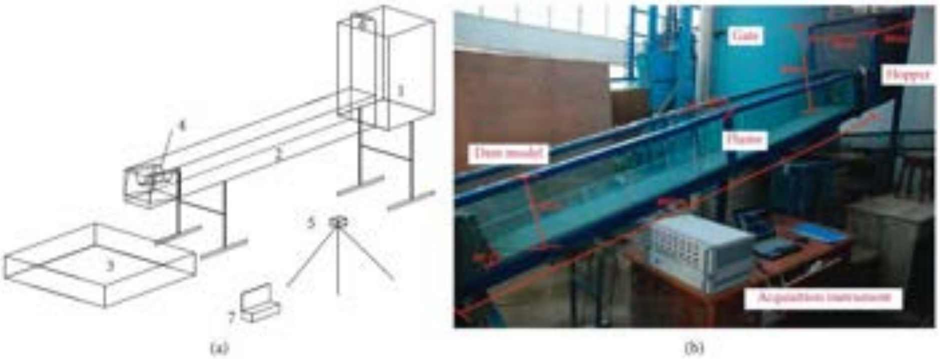

Fig. 3.2: Experimental apparatus. 1: hopper; 2: flume; 3: tasilings poll; 4: dam model; 5: camera; 6: gate; 7: acquisition instruments

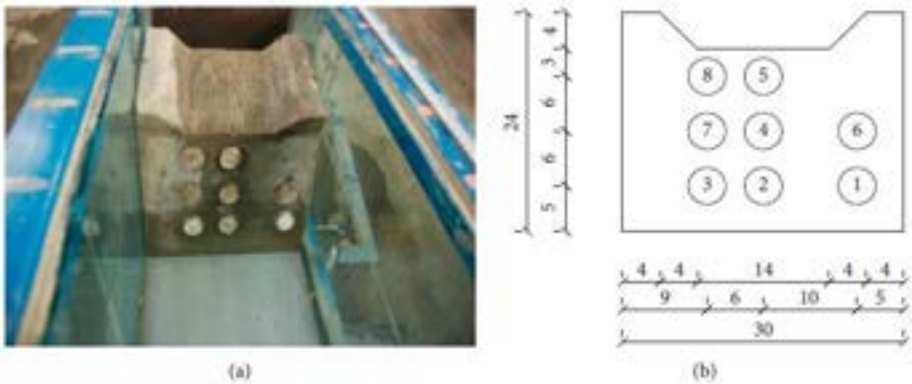

Fig. 3.3: Size of the surface of the dam, surface size of the sensor, and location of the sensor arrangement

2. Proposed Formula for Impact Force Calculation:

The authors propose a new formula derived from dimensional analysis and nonlinear regression of experimental data. It is based on three dimensionless parameters:

- **Dimensionless impact parameter:**

  $\eta_0 = P/(\rho w \cdot vs^2)$, where P is the impact pressure (kPa), ρw is the density of water (kg/m³), and vs is the surface velocity of the debris flow (m/s).

- **Froude number:**

  $Fr = v_s/gH$,

  with g being gravitational acceleration and H the flow depth.

- **Dimensionless density of debris flow:**

  c0=ρc/ρw

  where ρc is the debris flow density and ρw the water density.

The empirical equation linking these is:

$$\eta_0 = 0.18 \cdot Fr^{0.0052} \cdot c_0^{1.8142}$$

Combining this with the definition of η_0, the dimensional formula for impact pressure becomes:

$$P = (0.18 \cdot Fr^{0.0052} \cdot c_0^{1.8142}) \cdot \rho_w \cdot v^2$$

where v is the local velocity at the impact point.

For spatial distribution of impact, this expression is applied using local velocity v(x,y) calculated through a rheological model such as Bingham. The low exponent of Fr (0.0052) indicates weak dependence on Froude number.

3. **Method for Impact Distribution:**

The proposed method calculates spatial impact distribution over the dam surface by accounting for both vertical velocity variation (via

Bingham model) and lateral reduction. The lateral reduction is described using a logarithmic coefficient:

$$k_F = \frac{P_x}{P_m} = \kappa_1 \ln(a) + \kappa_2$$

with κ1 and κ2 depending on Fr, c_0, and the ratio between flow depth and unit width. The local velocity v(x,y) is computed by combining vertical (Bingham) and lateral distributions, and then used in the impact formula to calculate the spatial force distribution.

4. **Strengths of the Experiment and Proposed Method:**

a) **Novelty and Relevance:** The study addresses the limits of uniform impact assumptions and proposes a method tailored to debris flow characteristics.

b) **Strong Experimental Basis:** The method is supported by 33 laboratory tests systematically varying density, slope, volume, and dam angle, using real field material.

c) **Quantification of Impact Distribution:** Unlike earlier models, this study quantifies lateral and vertical impact force distribution.

d) **Correlation with Flow Characteristics:** The proposed formula links impact force directly to intrinsic flow properties like density and velocity.

e) **High Experimental Correlation:** Empirical equations correlate well with measured data (e.g., R^2=0.87 for η_0, R^2=0.94 for k_F, R2=0.91 for predicted vs measured impact).

f) **Practical Benefits:** Allows more accurate design of protective structures and potentially reduces material waste.

5. **Weaknesses of the Experiment and Method:**

a) **Peak Impact Measurement Uncertainty:** Due to fixed sensor placement, measurements may not always capture maximum velocity regions; bottom sensors provide only approximate maximum impact values.

b) **Limited Applicability:** The method is based on the Bingham rheological model, suitable for viscous debris flows but less applicable to dilute flows, which require different modeling approaches.

6. **Future Work:**

The authors plan to adopt advanced sensing (e.g., plate-type impact collectors) to obtain more accurate spatial and temporal impact data, and to compare lab results with field measurements to further optimize the method.

3.2 Flow-3D Model Setup Based on "Experimental Study of the Debris Flow Slurry. Impact and Distribution"

The Flow-3D numerical model was configured to replicate the experimental setup described by Zhao et al. (2018), aiming to assess its ability to predict debris flow impact dynamics. The simulation domain was designed as a flume measuring 4.0 m in length, 0.3 m in width, and 0.4 m in height, matching the laboratory geometry. A dam-like obstacle with an inclined surface of 63° was placed at the downstream end, mirroring the experimental structure.

A Cartesian mesh was employed, with uniform grid spacing of 0.02 m in all directions to ensure high spatial resolution for the flume and 0.04 m for the pool. Volumetric measurement regions were embedded at the dam front to emulate the function of the piezoelectric sensors used in the experiments. This setup enabled the numerical recording of pressure and force data directly comparable with experimental observations.

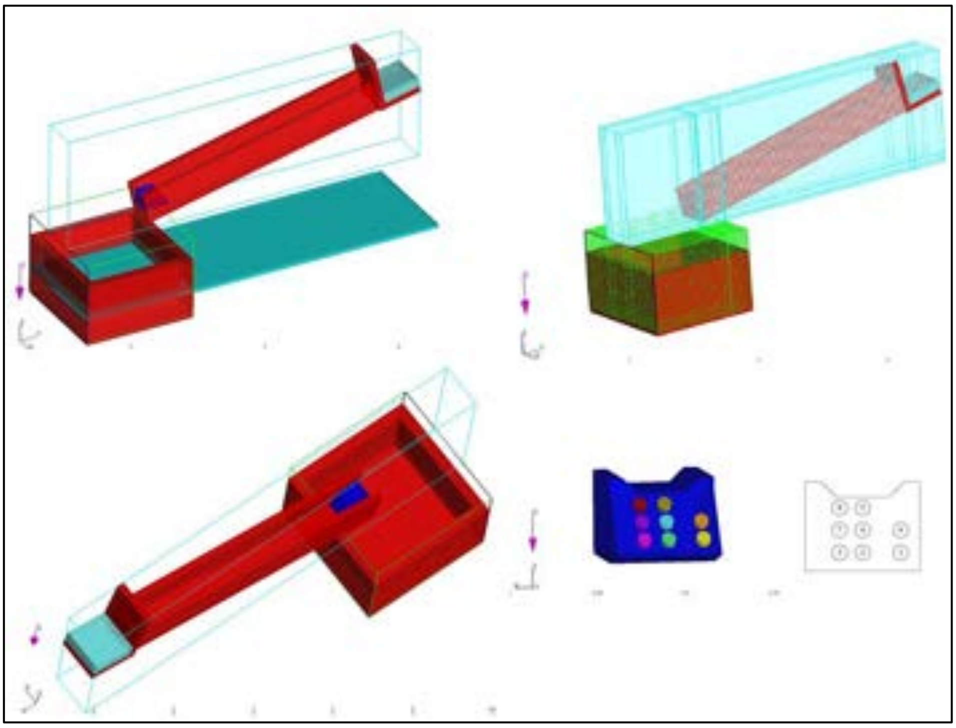

Fig. 3.4: Geometry and mesh Flow 3D model based on experimental installation

Boundary conditions were assigned as follows:

- Free outflow conditions were imposed at the flume outlet and top surface.
- All remaining boundaries were treated as rigid walls (no-slip condition).

- The debris flow was initialized as a compact volume located upstream of the gate, then released instantaneously to simulate a dam-break scenario.

The fluid was modeled using a Bingham rheological law, characterized by a yield stress and a plastic viscosity. Initial values for these parameters were estimated from literature based on similar materials (fine sand and silt) and iteratively calibrated to match the observed force peaks. A minimum strain rate threshold of 0.01 s^{-1} was imposed to ensure numerical stability, preventing excessive viscosity at low deformation rates.

3.3 Validation of Flow-3D Model Results Against Experimental Observations

The results of the Flow-3D simulation were compared to the experimental force records provided by Zhao et al., with a particular focus on Sensor 2, which recorded the highest impact forces. Time histories of impact pressure were extracted from the virtual sensors in the model and juxtaposed with those from the physical sensors.

A quantitative comparison revealed that the calibrated model closely reproduced both the timing and magnitude of the peak impact forces. The calibrated rheological parameters that provided the best fit were:

- Yield stress (τy): 120 Pa
- Plastic viscosity (μp): 1.2 Pa·s (equivalent to 1.2 kg/m/s)

The peak impact force predicted by Flow-3D differed by less than 10% from the experimental maximum, while the shape of the pressure curve during the impact phase showed good agreement in terms of rise time, duration, and attenuation.

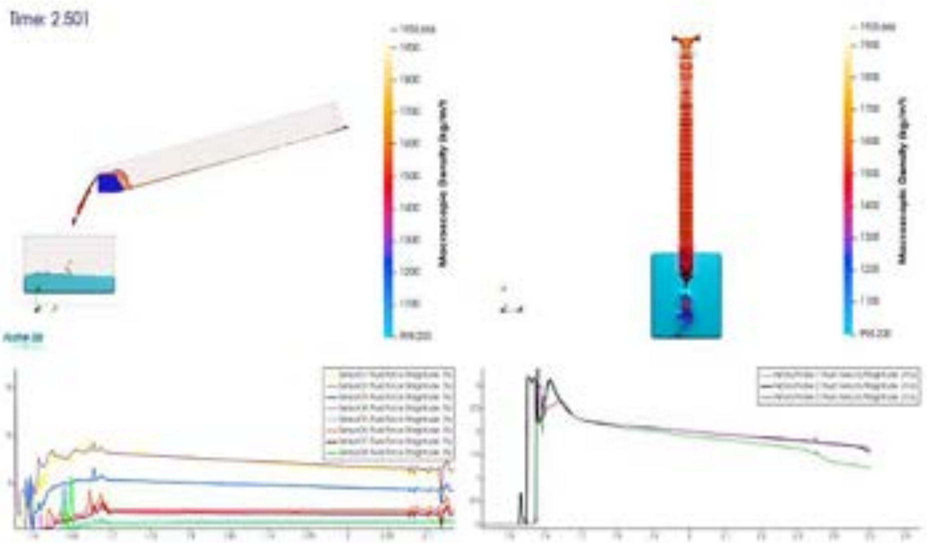

Fig. 3.5: Result after the impact – Density mapping with velocity and impact force trends.

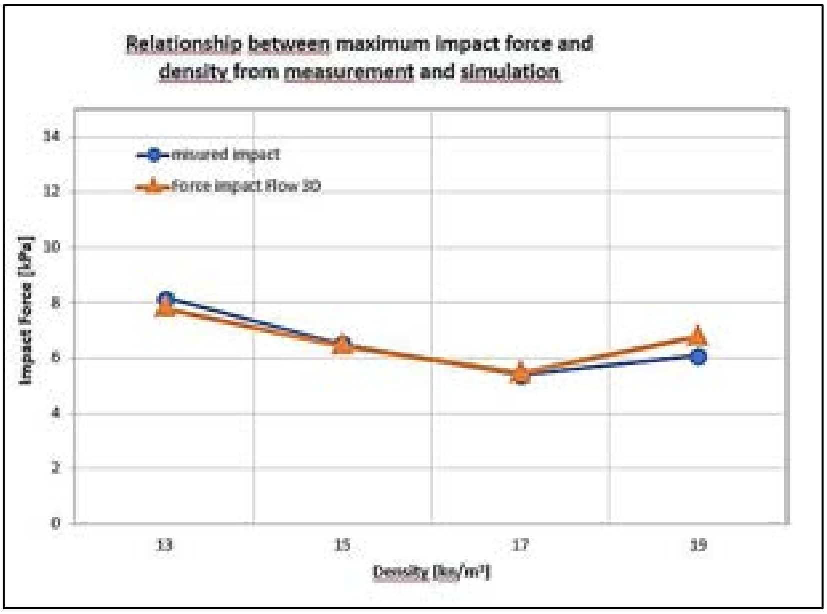

Fig. 3.6: Density – Impact Force Graph: Comparison between experimental results and Flow 3D model

To achieve these results it was necessary to calibrate the debris flow equation's parameters:

- ρ_{dbflow} = **13 kN/m^3 Bingham fluid (Cv=30%, n=1)**
- ρ_{dbflow} = **15 kN/m^3 Bingham fluid (Cv=33%, n=1)**
- ρ_{dbflow} = **17 kN/m^3 Bingham fluid (Cv=38%, n=1)**
- ρ_{dbflow} = **19 kN/m^3 Bingham fluid (Cv=42%, n=1)**

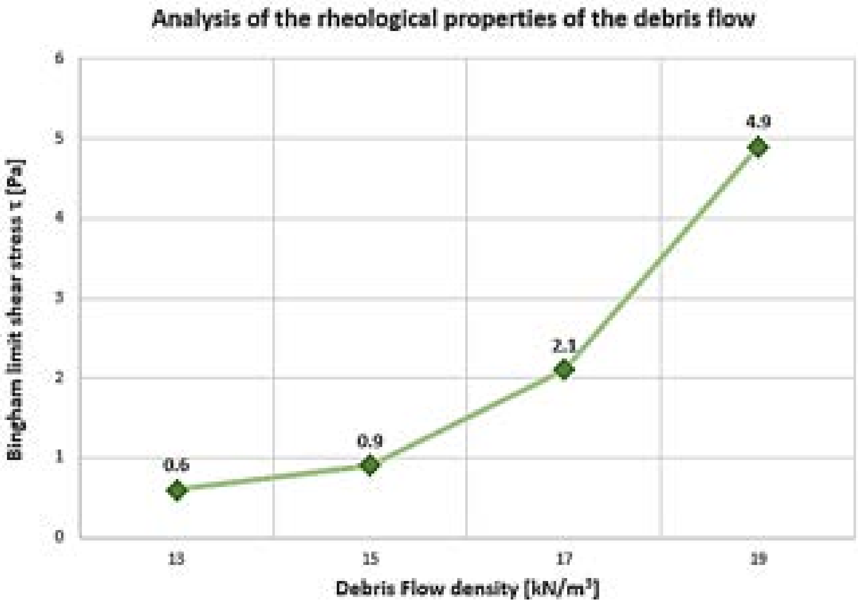

Fig. 3.7: Density – Bingham limit shear stress Graph – calibration value

This validation confirmed that the Flow-3D model, when supplied with appropriate rheological parameters and boundary conditions, is capable of accurately replicating the dynamic behavior of debris flows observed in laboratory conditions. The model's ability to resolve 3D flow structures and local pressure fluctuations represents a significant advantage over empirical or 2D approximations, particularly when assessing complex interactions with protective infrastructure.

Chapter 4

4 Real Case Study – Debris Flow Impact Analysis in the “La Valletta” Basin – Valle d’Aosta

The present chapter focuses on the numerical simulation of a real debris flow event in the “La Valletta” basin, a right-bank tributary of the Savara stream in the Aosta Valley, where repeated flow events have historically caused the blockage of the road at the basin outlet. The objective of the study is to estimate the **impact force exerted by the debris flow on a protection barrier** using the **Flow-3D computational fluid dynamics (CFD) model**, which has been previously validated against laboratory experiments published by Zhao et al. (2018). In their work, Zhao et al. developed a semi-empirical formula to predict debris flow impact pressures based on controlled flume experiments. Their results serve as a crucial benchmark to interpret numerical simulations in real-scale conditions.

In the case under investigation, a mitigation scenario was hypothesized, involving a re-profiling of the channel and the installation of a barrier designed to **dissipate the kinetic energy of the debris flow**. This structure was placed at the outlet of the basin and constitutes the critical section for evaluating the impact force.

To account for the different sedimentological configurations and rheological behaviors that cannot be fully reproduced in a laboratory flume, **three simulation scenarios were developed**:

1. **Scenario A – Tailings with coarse blocks** ($D_{max} \approx 30$ cm): represents a worst-case condition with high inertial effects and strong intergranular locking.
2. **Scenario B – Tailings without large clasts** ($D_{max} \leq 1.5$ cm): reflects a debris flow dominated by sand, silt, and fine gravel, consistent with viscous plastic behavior.
3. **Scenario C – No Tailings / Constant-density model**: assumes a homogeneous Bingham fluid with fixed density and bulk rheology, providing a simplified but conservative estimate of impact force.

This approach allows for a comparative evaluation between the **laboratory-derived impact force models** and the **real-case behavior**, highlighting the influence of sediment concentration, grain-size distribution, and rheological properties on the spatial and temporal evolution of impact pressures. The chapter also discusses the **limitations of upscaling laboratory findings** to field conditions, addressing critical aspects such as scale effects, heterogeneity in debris structure, and interaction with engineered defenses.

4.1 Geological Framework and Hydrological Analysis of the La Valletta Basin

4.1.1 Geology

The *La Valletta* catchment basin is located in the Aosta Valley and is a tributary of the Savara stream. The general geological study area covers approximately 50 km². The La Valletta drainage basin is situated within the Fenille area, on the right-hand side of the Savara stream, in the central Aosta Valley.

Regional Geological Context and Lithologies

The study area lies within the geological framework of the Western Alps, characterized by the superposition of several major tectonostratigraphic units, including the Piemontese Zone and the Briançonnais Zone. These units are separated by major shear zones, such as the Feluma Tectonic Mélange. The rocks in these zones have undergone Alpine metamorphism with various metamorphic facies.

The predominant lithologies in the wider Savara basin and surrounding slopes, including the Fenille area, consist of gneiss and micaschists (interpreted as pre-Alpine metasediments), metagranodiorites and orthogneiss (metamorphosed intrusive rocks), carbonate micaschists, calcareous schists and phyllitic schists (attributed to the Piemontese Zone or shear zones), prasinites, micaceous marbles, and carniole (sedimentary cover remnants or fault-related lenses).

Quaternary Deposits and Local Geomorphology

The morphology of the area has been heavily influenced by glacial activity. The surface deposits, dating from the Pleistocene to Holocene, are mainly of glacial (till or fluvioglacial) and colluvial origin.

The Fenille area, where the La Valletta basin is located, is characterized by a continuous strip of talus deposits extending from the upper rocky slopes down to the alluvial belt of the Savara stream. These deposits are described as composed of angular, monolithological clasts (mainly gneiss and micaschists) with a limited gravel-sand matrix. At lower elevations, these colluvial deposits may interdigitate with the alluvial materials of the Savara stream.

According to the specific lithological analysis for the La Valletta catchment (based on the parent material data layer), the predominant surface cover is *talus deposits*, accounting for approximately 98.24% of the area. Small proportions of bedrock (granites, metagranites, orthogneiss, etc. – 0.53%) and alluvial deposits (1.23%) are also present. This dominance of talus material is a distinctive feature of the La Valletta basin's surficial geology.

The geomorphology of the La Valletta basin is characterized by a very steep average slope on the valley sides (159%) and an overall basin slope of 62%. The mean elevation is 2018 m a.s.l., ranging from 1475 m to 2489 m a.s.l. These steep slopes, combined with the abundance of unconsolidated talus material, predispose the area to gravitational processes.

Relevant Geological and Hydrogeological Processes

In addition to glacial erosion and deposition, the area is subject to post-glacial reshaping processes caused by runoff, freeze-thaw cycles, and gravitational movement. Deep-seated gravitational slope deformations (DSGSDs) and landslides are present in adjacent areas. Detrital and colluvial fans are widespread along the slopes.

In the smaller channels of the Fenille area, including La Valletta, debris flow events are a significant concern. The combination of steep slopes, abundant unconsolidated detrital material, and water input can trigger such flows.

From a hydrogeological perspective, conditions depend on the permeability of deposits and bedrock. The detrital cover may be heterogeneous with poor geotechnical characteristics and the presence of perched or confined aquifers. The bedrock may be fractured. In carbonate lithologies such as marbles and carniole, karst features are theoretically possible, although observations in nearby areas have not revealed widespread karstification. Groundwater flow may also be influenced by structural features and fracture zones.

4.1.2 Hydrological Analysis

The drainage basin of the *La Valletta* catchment, delimited at the apex section of the depositional fan, and the perimeter of the depositional fan itself are shown in Figure below, overlaid on the corresponding hydrographic network and the path of the main collector within the fan.

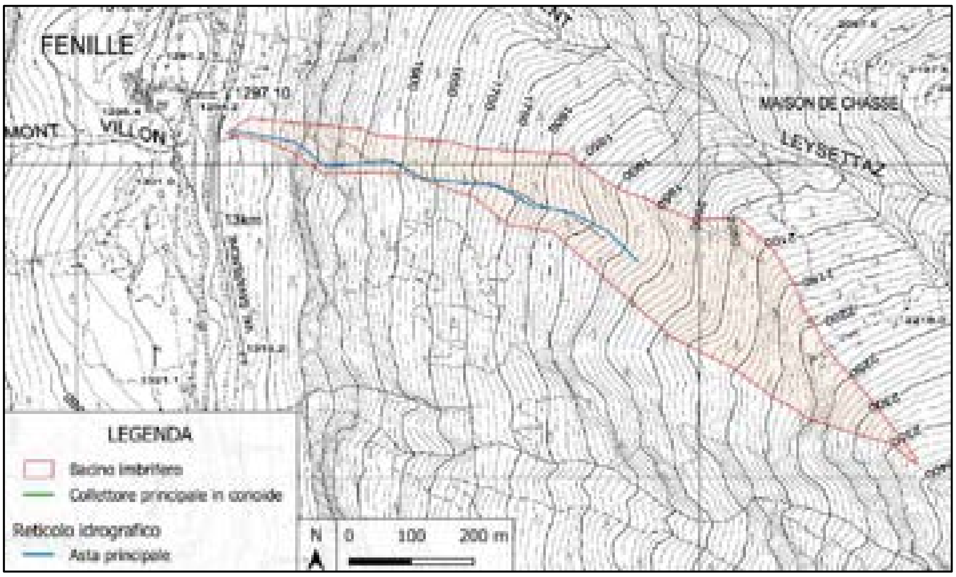

Fig. 4.1: Overview map of the La Valletta catchment basin and its hydrographic network

Based on the available cartographic data and using GIS applications, all the parameters characterizing the catchment basin, the alluvial fan, and the hydrographic network were identified and calculated. Subsequently, the slope map was produced, along with the hypsographic curve of the basin and the longitudinal profile of the main channel.

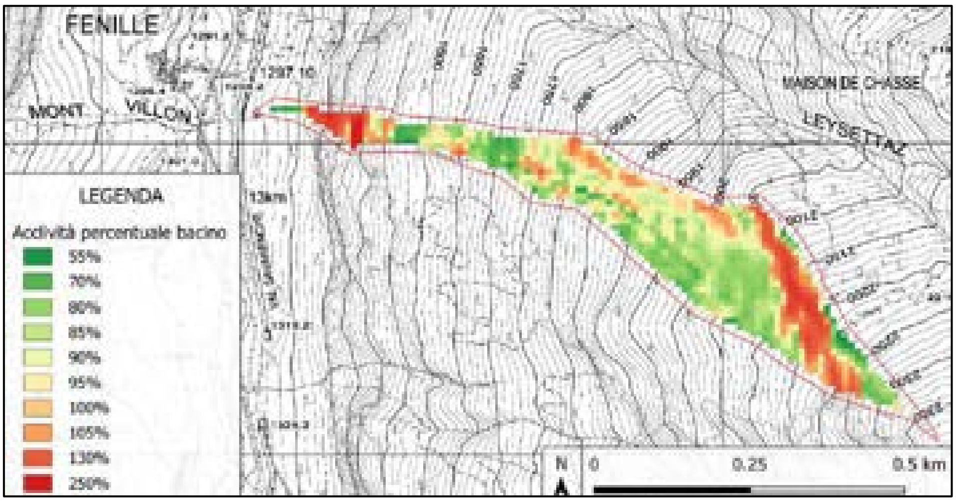

Fig. 4.2: Slope Map of the La Valletta Catchment Basin

Feeding Basin	**Value**
Total area (km²)	0.129
Forested area (km²)	0.025
Glacial area (km²)	0.000
Lacustrine area (km²)	0.000
Perimeter (km)	2.613
Minimum elevation (m a.s.l.)	1318
Maximum elevation (m a.s.l.)	2378
Form factor (Gravelius)	2.037
Mean elevation (m a.s.l.)	1928
Average slope of valley sides (%)	97
Alluvional Fan	**Value**
Area (km²)	-
Minimum elevation (m a.s.l.)	-
Maximum elevation (m a.s.l.)	-
Maximum length (m)	-

Maximum width (m)	-
Average slope (%)	-
Melton ruggedness number (-)	-
Hydrographic Network	**Value**
Main channel length (km)	0.712
Channel length up to apex of alluvial fan (km)	0.712
Slope of the main torrent channel (%)	83.93
Slope of the collector on the fan (%)	-

Table 4.1 – Main Morphometric Parameters of the La Valletta Catchment Basin

The vegetation framework and land use within the basin were subsequently analyzed and defined

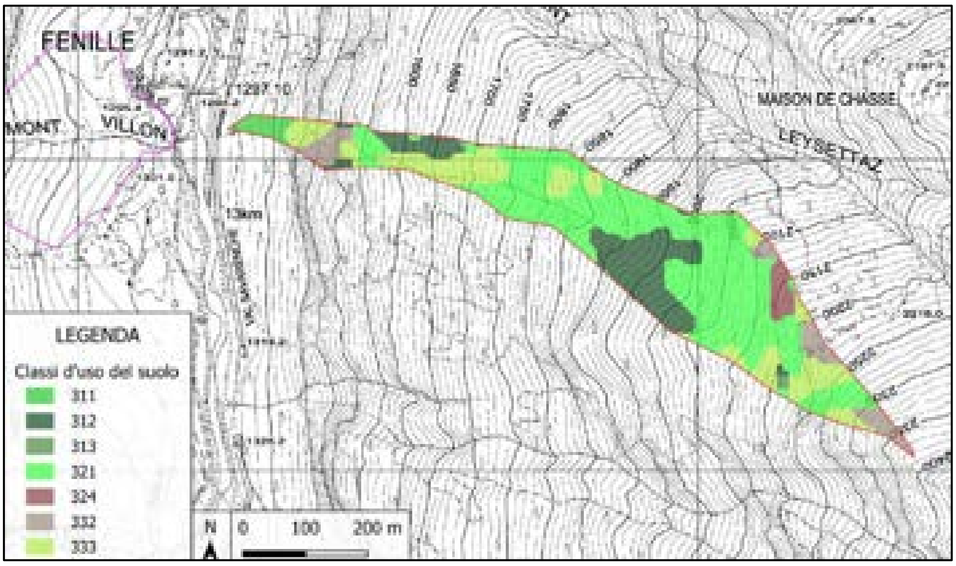

Fig. 4.3: Land Use Map of the Catchment Basin Delimited at the Proposed Culvert Location of the La Valletta Drainage Area

For the La Valletta catchment basin, a permeability map was first produced, followed by the CNII map. Based on the latter, the Curve Number for hydrologic soil group III (CN III) was determined. These values were then averaged to obtain the mean CN(III) for the entire basin, which was found to be **88.96**.

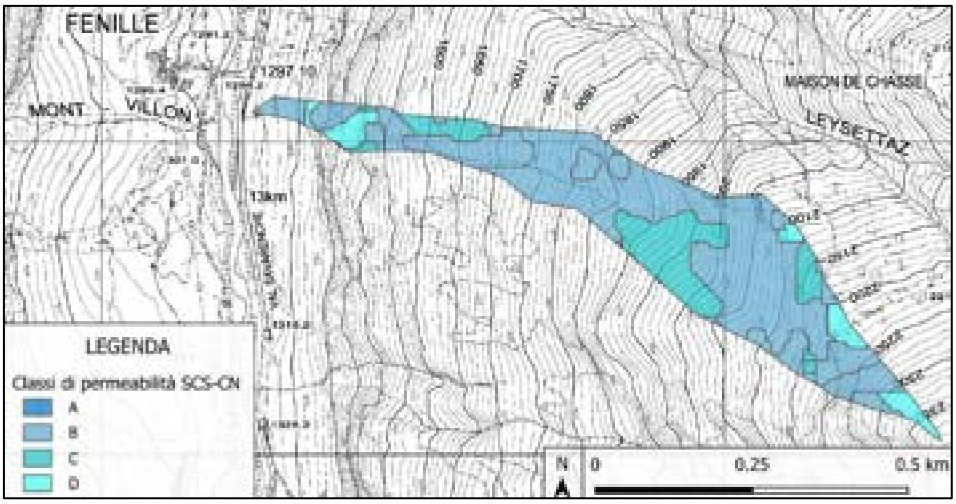

Fig. 4.4: Land Use Classes (top) and Permeability Map According to the SCS-CN Methodology (bottom) for the La Valletta Catchment Basin

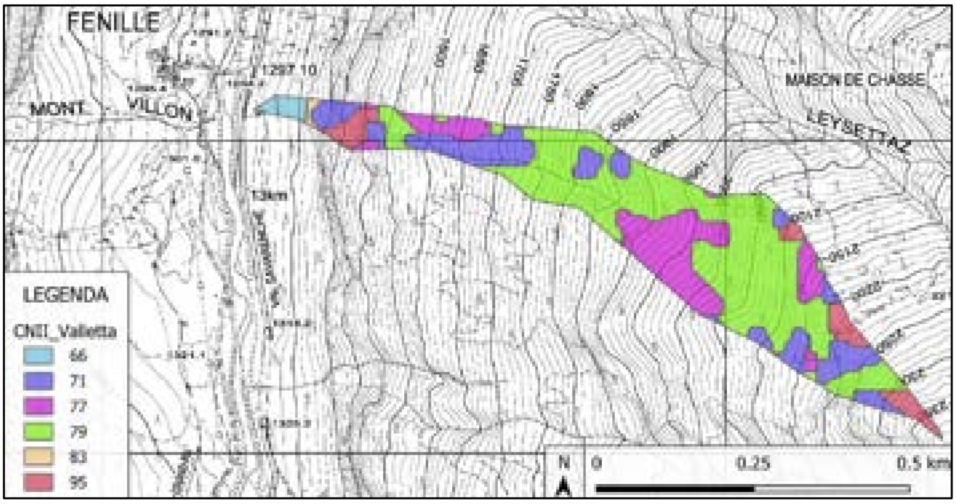

Fig. 4.5: CN(II) Map Obtained for the La Valletta Catchment Basin

By delineating the catchment area within the geoportal dedicated to the Regionalization of Precipitation Study, the **rainfall probability lines** were obtained and are shown in Figure below, along with the **growth function**. The parameters of the rainfall possibility curves (PPC) were evaluated at the coordinates of the basin's geometric centroid [x, y = 360389, 5054849], resulting in the values [a, n = 11.05, 0.465].

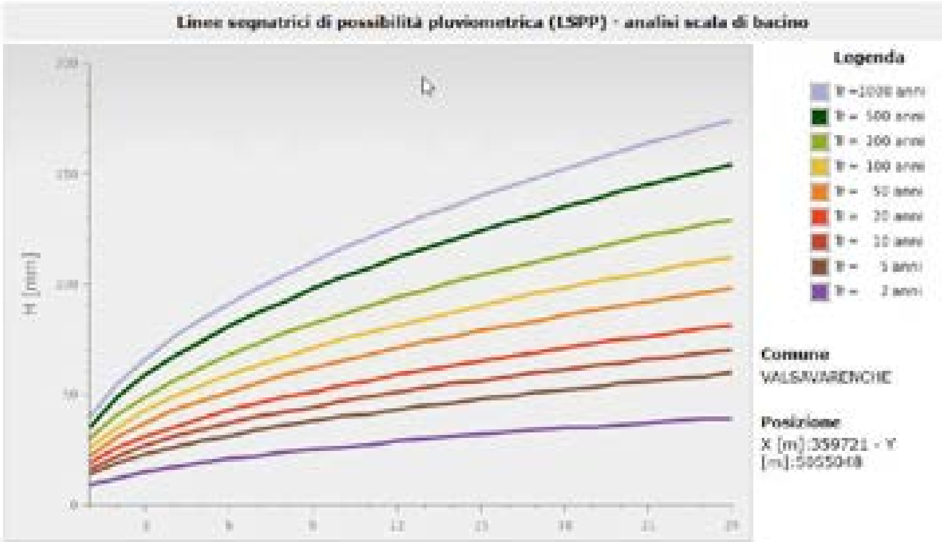

Fig. 4.6: rainfall probability lines

The formulas used to estimate the time of concentration yielded the following values:

- **Ventura's formula:** 0.05 hours
- **Pasini's formula:** 0.05 hours

As a result, a value of **0.05 hours** was adopted as the design time of concentration.

Once the **time to peak** (T_p = 0.09 hours) and the **total catchment area** (A = 0.129 km²) are known, the **peak discharge** q_p can be estimated, resulting in a value of **2.89 km²/h**. Given the time to peak and the **integration time step** (dt), it is then possible to dimension Alize the **dimensionless Mockus hydrograph**, thus obtaining the **unit hydrograph (IUH)** for the La Valletta catchment basin.

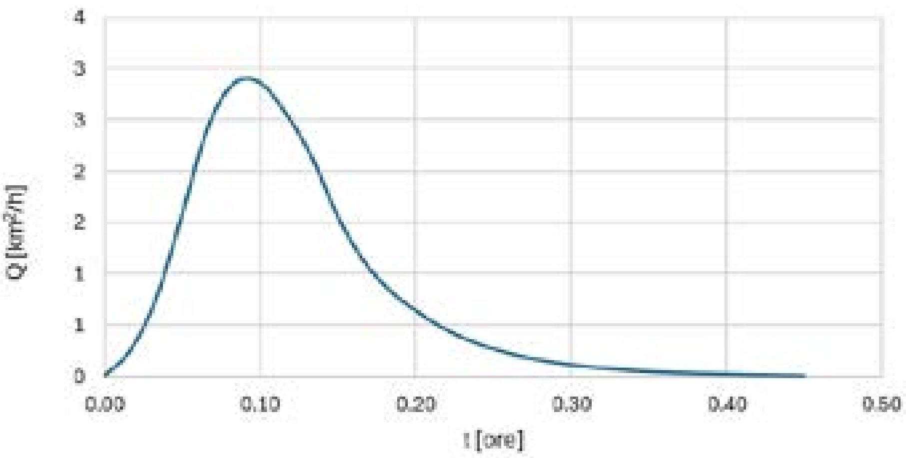

Fig. 4.7: Mockus IUH

Given the individual effective rainfall pulses and the characteristic response of the basin to each unit impulse, the **convolution integral** can be applied to determine the **design hydrograph** at the basin's closing section. This hydrograph describes how the rainfall excess over the catchment transforms into surface runoff and how this runoff is transferred over time to the **apex section of the alluvial fan**. For each analyzed **return period**, the convolution integral was solved accordingly, resulting in the **design hydrographs**.

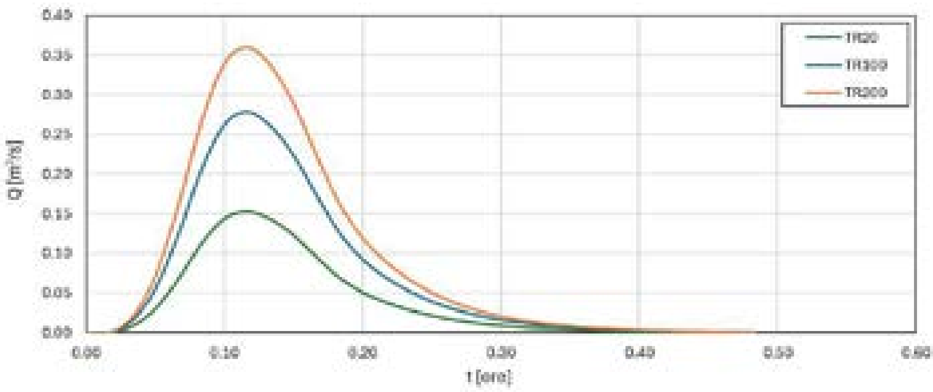

Fig. 4.8: Design Hydrographs for RP 20, RP 100, and RP 200 Obtained for the La Valletta Catchment

For the purpose of defining the **debris hydrograph (debrisgram)**, a maximum volumetric concentration of mobilizable solid material of **42%** was estimated based on the geological and lithological characteristics of the area. The resulting hydrograph was therefore derived using the **bulking factor** approach.

$$BF = \frac{1}{1 - \phi_v}$$

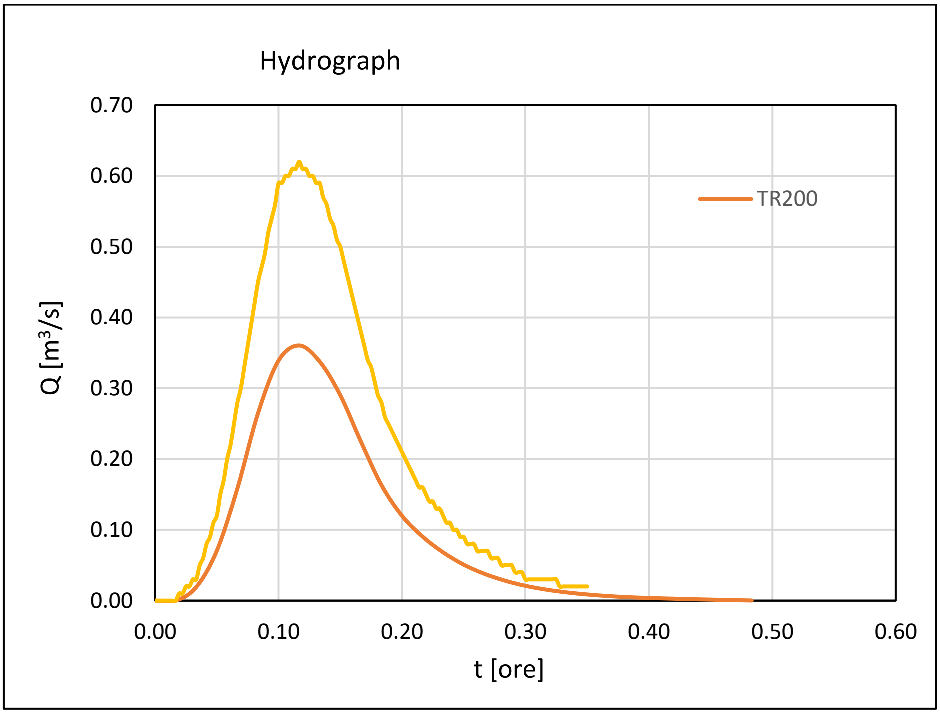

Fig. 4.9: Debris flow Design Hydrographs RP 200

This hydrograph corresponds to a **total volume of 280 m³**

Based on the values proposed by **Julien (2010)**, a **density of 1700 kg/m³** was adopted.

Volumetric Concentration (Cv %)	Concentration by Weight (Cw %)	Parts per Million (ppm)	Concentration (mg/L)	Density of Mixture (kg/m³)
0.01	0.03	265	265	1000
0.08	0.13	1324	1325	1001
0.1	0.26	2645	2660	1002
0.25	0.68	6598	6625	1004
0.5	1.31	13141	13250	1008
0.75	2	19632	19875	1012
1	2.6	26089	26500	1017
2.5	6.4	63625	66250	1041
Hyper concentration				
5	12.2	122401	132500	1083
7.5	17.7	176683	198750	1124
10	22.7	227467	265000	1155
25	46.9	469021	662500	1243
50	72.6	726027	1325000	1413
75	88.8	888266	1987500	2238
100	100	1000000	2650000	2650

Table 4.2 - Equivalent concentrations and fluid densities (after Julian 2010).

4.2 Rheological Characterization and Calibration of the Bingham Fluid Model

The rheological behavior of debris flows is a key factor in determining their velocity, runout, and the forces exerted on protective structures. In this study, the debris flow is modeled using a **Bingham plastic rheological model**, which is appropriate for highly concentrated mixtures of water, silt, sand, and fine gravel. The Bingham model is defined by two key parameters: the **plastic viscosity** μp and the **yield stress** τy, which represent the resistance of the fluid to deformation and the minimum stress required for flow initiation, respectively.

$$\tau = \tau_y + \mu_p \cdot \dot{\gamma} \quad \text{for} \quad \tau > \tau_y$$

Based on the geological and hydrological analysis of the "La Valletta" basin, a **volumetric solid concentration** of $\phi v = 0.42$ and a **debris flow density** of ρ=1700 kg/m3 were defined. These values are consistent with documented debris flow events in the region and are used as **common input parameters across all simulation scenarios** to ensure comparability and uniformity in rheological calibration.

4.2.1 Theoretical Background and Literature Models

To define these parameters, empirical relationships derived from laboratory experiments were adopted, particularly from **Sosio et al. (2006)**, who conducted rheometric tests on Alpine debris flow samples. The following exponential laws were used:

$$\mu_p = \alpha \cdot e^{\beta \phi_v}, \quad \tau_y = \gamma \cdot e^{\delta \phi_v}$$

where:

- ϕv = volumetric solid concentration,
- α=2.97×10−4, β=18.8,
- γ=0.0096, δ=24.3.

These formulas enable the estimation of rheological parameters for a range of solid concentrations typical of debris flows, considering also the sediment composition and grain size.

4.2.2 Adaptation to Simulation Scenarios

Three simulation scenarios were developed, each representing different sedimentological configurations:

- **Scenario A: Tailings with coarse blocks (D_{50} ≈ 30 cm)** This conservative configuration includes a significant proportion of coarse blocks, which are known to increase the apparent viscosity and resistance to flow due to intergranular friction and structural interlocking.
  In simulations involving coarse sediment (gravel, cobbles, or boulders with diameters > 5 cm), the plastic viscosity estimated from the fine matrix (sand, silt, clay) alone is typically underestimated. Coarse particles increase the internal resistance of the debris flow due to interparticle friction, granular blocking, and dilatancy, leading to a stiffer and less mobile rheological behavior.

  To account for these effects within the Bingham model, an empirical correction factor is applied multiplicatively to the fine-matrix viscosity:

$$\mu_{p,tot} = K_c \cdot \mu_{p,fine}$$

In this study, a factor Kc=5.5 was adopted, consistent with literature values for debris flows with coarse sediment fractions exceeding 20% by volume. This approach is supported by experimental and numerical findings from authors such as **O'Brien & Julien (1988)**, **Rickenmann (1999)**, and **Sosio et al. (2006)**.

This adjustment accounts for the enhanced internal friction and bulk stiffness of the debris mixture. Final parameters:

$\mu p = \mu_{fine} \cdot Kc = 0.798 \cdot 5.5 = 4.0$ Pa·s, $\tau y = 308$ Pa

- **Scenario B: Tailings without large clasts ($D_{max} \leq$ 1.5 cm)**
  This scenario represents a debris flow composed of **silt, sand, and fine gravel**, with a maximum grain size not exceeding 1.5 cm. Compared to Scenario A, the absence of large boulders results in reduced internal friction and structural interlocking, which affects the overall resistance to flow deformation.
  To account for this, a **reduced correction factor** Kc=1.5 was applied to the plastic viscosity μp derived from the base formulation of Sosio et al. (2006). However, since **yield stress** is more sensitive to fine matrix composition and cohesive effects rather than clast size, it was **not corrected** and retains the base theoretical value.
  $\mu p = \mu_{fine} \cdot Kc = 0.86 \cdot 1.5 = 1.29$ Pa·s, $\tau y = 260$ Pa

- **Scenario C: No Tailings – Constant density fluid**
  The debris flow is modeled as a homogeneous Bingham fluid with fixed density and rheological properties. This scenario assumes an

effective mixture behavior, without phase separation. Parameters equivalent to Scenario B were used.

Scenario	**Volumetric Concentration ϕv [-]**	**Density ρ [kg/m³]**	**Plastic Viscosity μp [Pa·s]**	**Yield Stress τy [Pa]**
A - Tailings with coarse blocks ($D_{50} \approx$ 30 cm)	0.424	1700	4	308
B - Tailings without large clasts ($D_{50} \approx$ 1.5 cm)	0.424	1700	1.29	260
C - No Tailings - Constant density fluid	0.424	1700	0.798	260

Table 4.3 – Bingham model parameters

In Flow-3D simulations with the *Tailings* module activated, the volumetric concentration must be converted into mass-based tailings concentration:

$$\textbf{Tailings Concentration} = \phi v \cdot \rho s = 0.42 \cdot 2650 = 1113 \text{ kg/m}^3$$

In Scenario A, this concentration accounts for the total solid content. In Scenario B, the same value is used, but only particles larger than 40 μm are considered as "coarse," in accordance with Flow-3D classification.

In all cases, the rheological parameters are applied uniformly to the fluid volume representing the debris mass. It is important to highlight that the **CFD models were primarily focused on the impact zone**, i.e., the region where the debris interacts with the engineered barrier. This choice reflects the main objective of the study: to estimate and compare **impact forces** across different rheological scenarios, rather than modeling the full propagation of the debris flow throughout the catchment. As such, simulation resolution and computational effort were optimized to capture detailed pressure distributions and force peaks in the vicinity of the obstacle.

4.3 Numerical Modeling Scenarios in Flow-3D

To numerically simulate debris flow behavior and evaluate its impact on a protective barrier, a set of three-dimensional simulations was carried out using **Flow-3D**, a computational fluid dynamics (CFD) software capable of simulating non-Newtonian free-surface flows. The simulations are based on realistic topographical input and replicate different rheological and geometric configurations previously defined.

4.3.1 Geometrical Setup and Boundary Condition

The computational domain was reconstructed from a detailed **Digital Terrain Model (DTM)** with a spatial resolution of **0.5 meters**. This terrain was used to define the topographic features of the "La Valletta" basin.

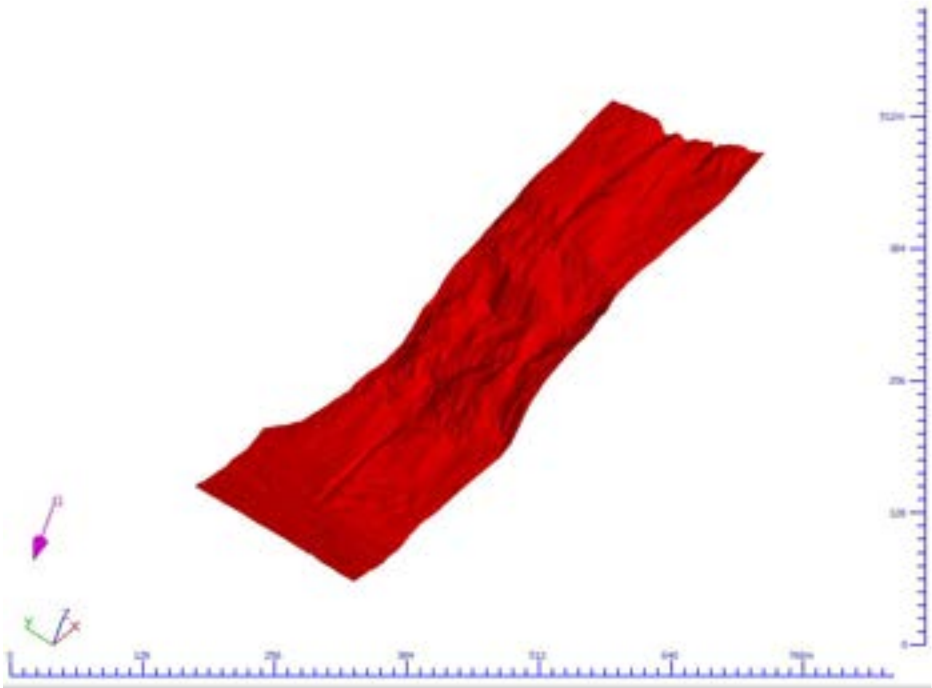

Fig. 4.10: Dtm – Flow 3d view

The simulation mesh was built using a **Cartesian grid**, with:

- uniform cell size of **0.4 m** in the **x, y, z** directions across the main domain,
- local refinement to **0.2 m** near the obstacle to improve pressure resolution.

To emulate the experimental setup of **Zhao et al. (2018)**, **volumetric monitoring regions** were embedded in the mesh at the barrier location. These regions acted as **virtual pressure sensors**, allowing the numerical model to estimate impact forces in **Newtons**, thus making the results comparable to those obtained in laboratory flume tests.

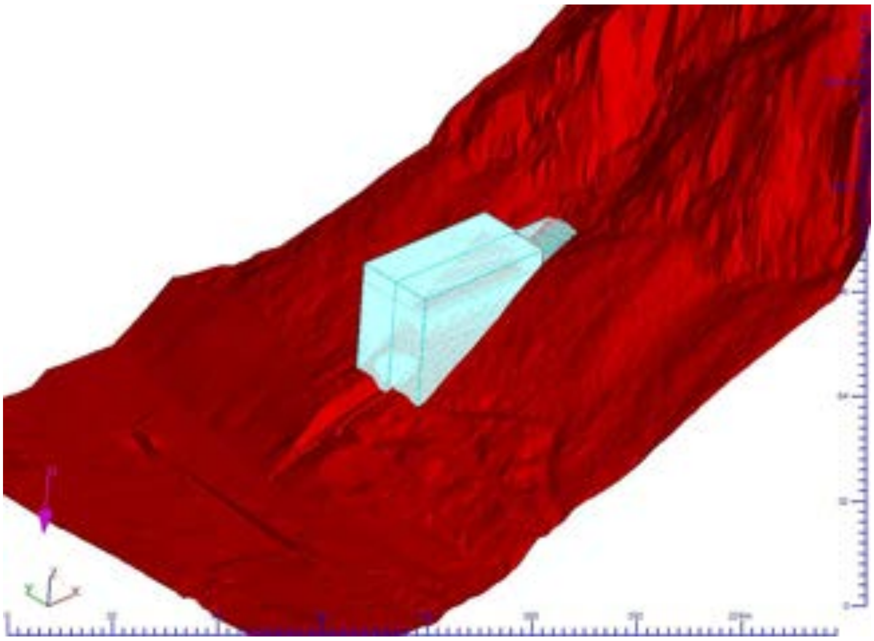

. 4.11: Terrain with cartesian mesh – Flow 3d view

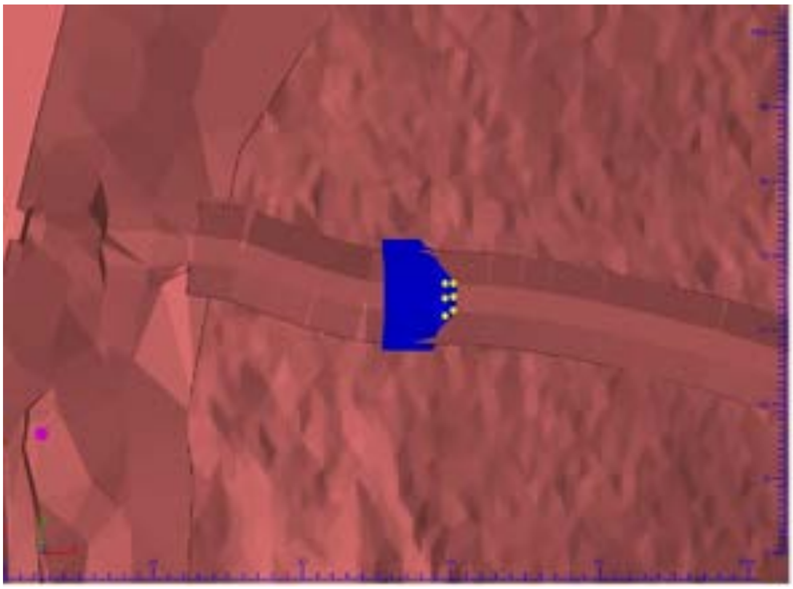

Fig. 4.12: Barrier with design terrain – Flow 3d view

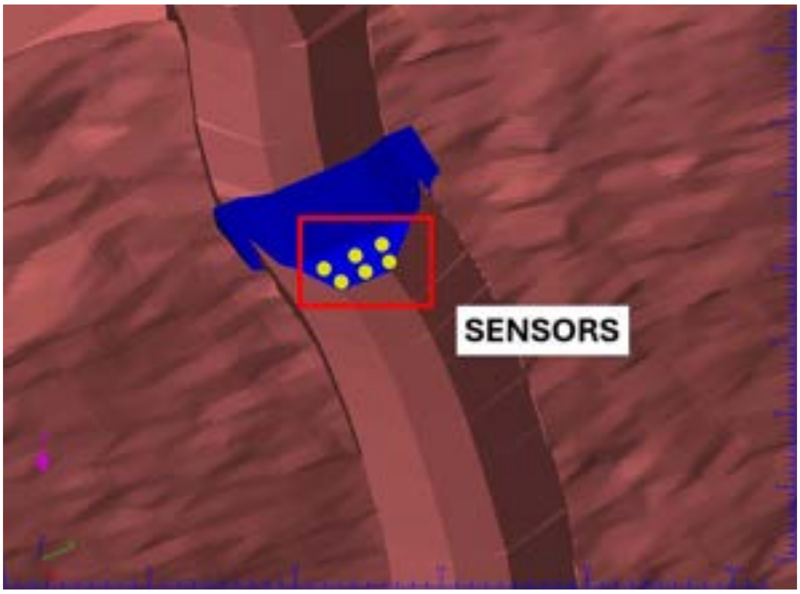

Fig. 4.13: Sensor details – Flow 3d view

The model applies **free outflow (atmospheric pressure)** conditions at the top and outlet boundaries of the domain. All remaining boundaries are considered solid and impermeable. The initial fluid condition was modeled as a **static cuboidal volume** of debris flow with a total volume of **280 m³**, corresponding to the bulking-adjusted volume derived from hydrological input. This block was released instantaneously, simulating a **dam-break-like debris flow**. The fluid volume was assigned the appropriate rheological parameters of a **Bingham fluid**, varying across scenarios.

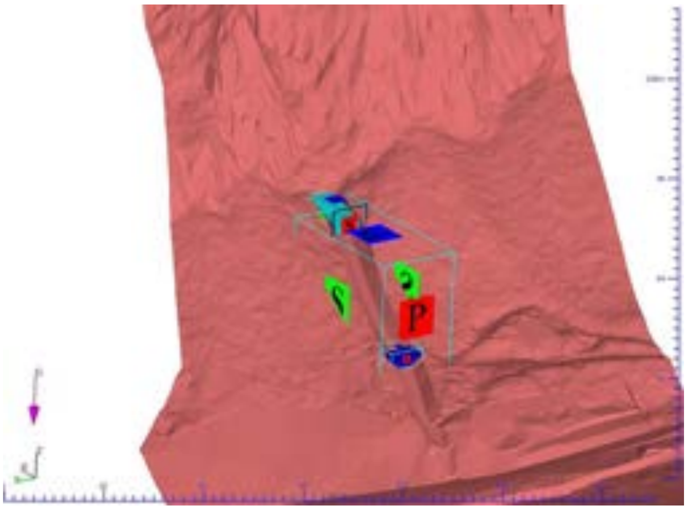

Fig. 4.14: Boundary Conditions distributed on mesh – Flow 3d view

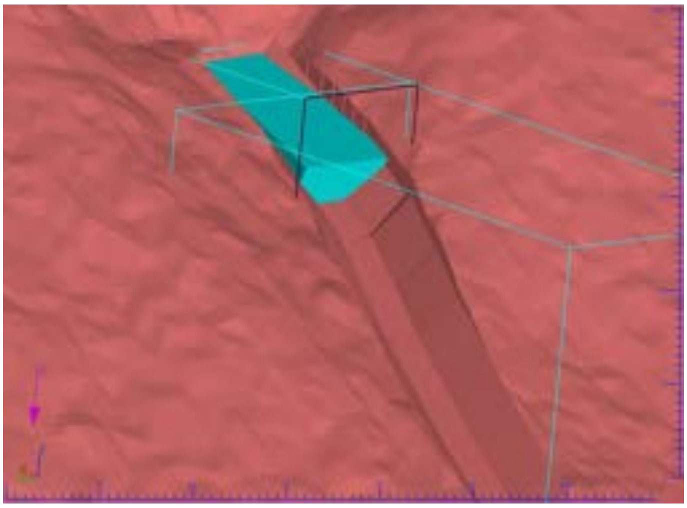

Fig. 4.15: Initial Conditions solid region for dam break mode and Tailing– Flow 3d view

4.3.2 Minimum Strain Rate and Numerical Stability

To ensure numerical stability in simulations involving Bingham-type fluids, a **minimum strain rate** must be imposed. In this study, a value of:

$$\dot{\gamma}_{\min} = 0.01 \text{ s}^{-1}$$

was adopted. This avoids singularities in the calculation of the **apparent viscosity** μapp\mu_{\text{app}}μapp, which tends to infinity as the strain rate approaches zero. The apparent viscosity of a Bingham fluid is expressed as:

$$\mu_{\text{app}} = \frac{\tau_y}{\dot{\gamma}} + \mu_p$$

As illustrated in Figure below, at low strain rates the viscosity increases rapidly due to the yield stress term. By setting a lower bound on γ˙, the simulation avoids unrealistic values and ensures consistency in flow behavior, especially in low-velocity regions.

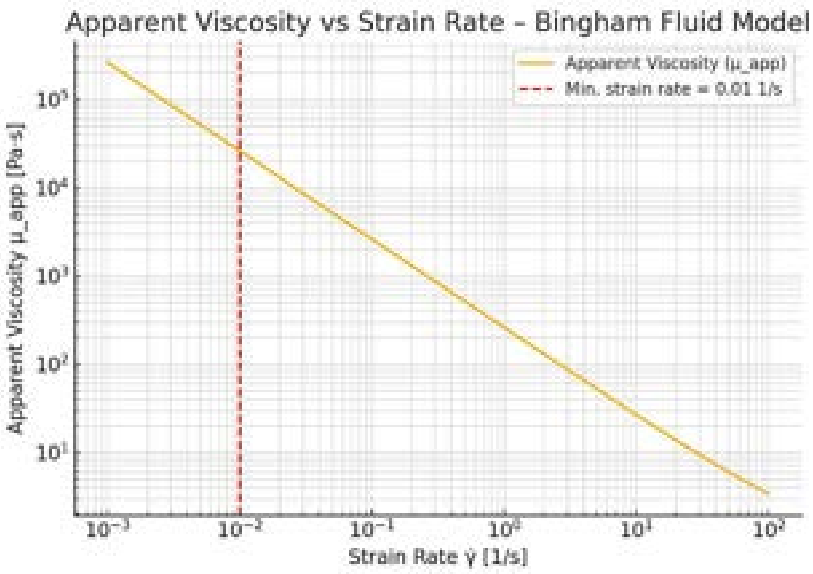

Fig. 4.16: Apparent Viscosity vs strain Rate – Bingham fluid Model

4.3.3 Preliminary Simulation: Shallow Water Model with Hybrid Mesh

Before simulating detailed impact conditions, a **preliminary simulation** was conducted using Flow-3D's **shallow water model**, which simplifies the momentum equations by assuming hydrostatic pressure distribution and negligible vertical accelerations. This approach is particularly efficient for capturing the **horizontal spreading and runout behavior** of debris flows over large topographic domains, with significantly reduced computational cost.

The mesh used for this initial run was a **hybrid configuration**, with coarser resolution in upstream areas and progressive refinement near the fan and potential impact zone. Unlike a full 3D CFD simulation, which solves the complete Navier–Stokes equations in all directions, the shallow water model relies on **depth-averaged velocity fields** and is more suitable for preliminary assessments and domain calibration.

This preliminary model helped identify the likely flow path, deposition zones, and dynamic expansion characteristics of the debris flow. Based on these results, the **location of the impact barrier** was defined.

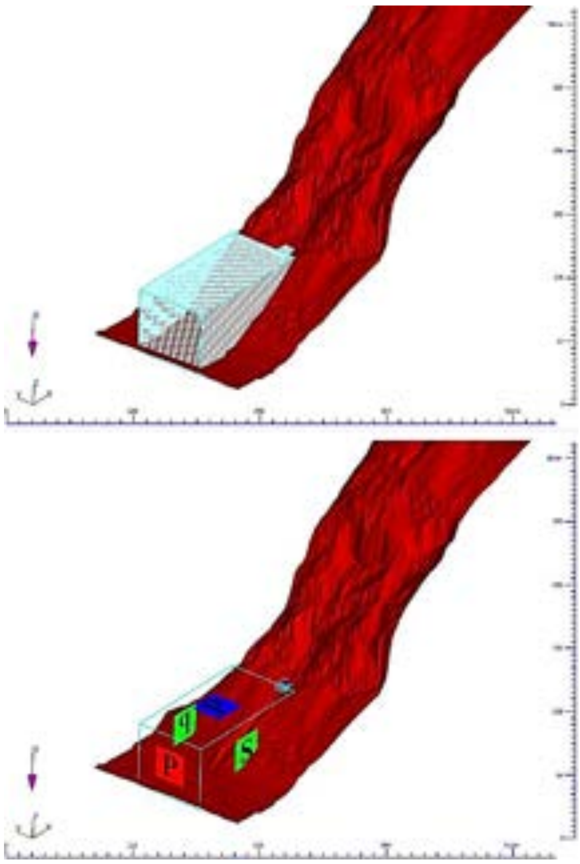

Fig. 4.17: Mesh and Boundary Conditions distributed on mesh – Flow 3d view – Preliminari shallow water model

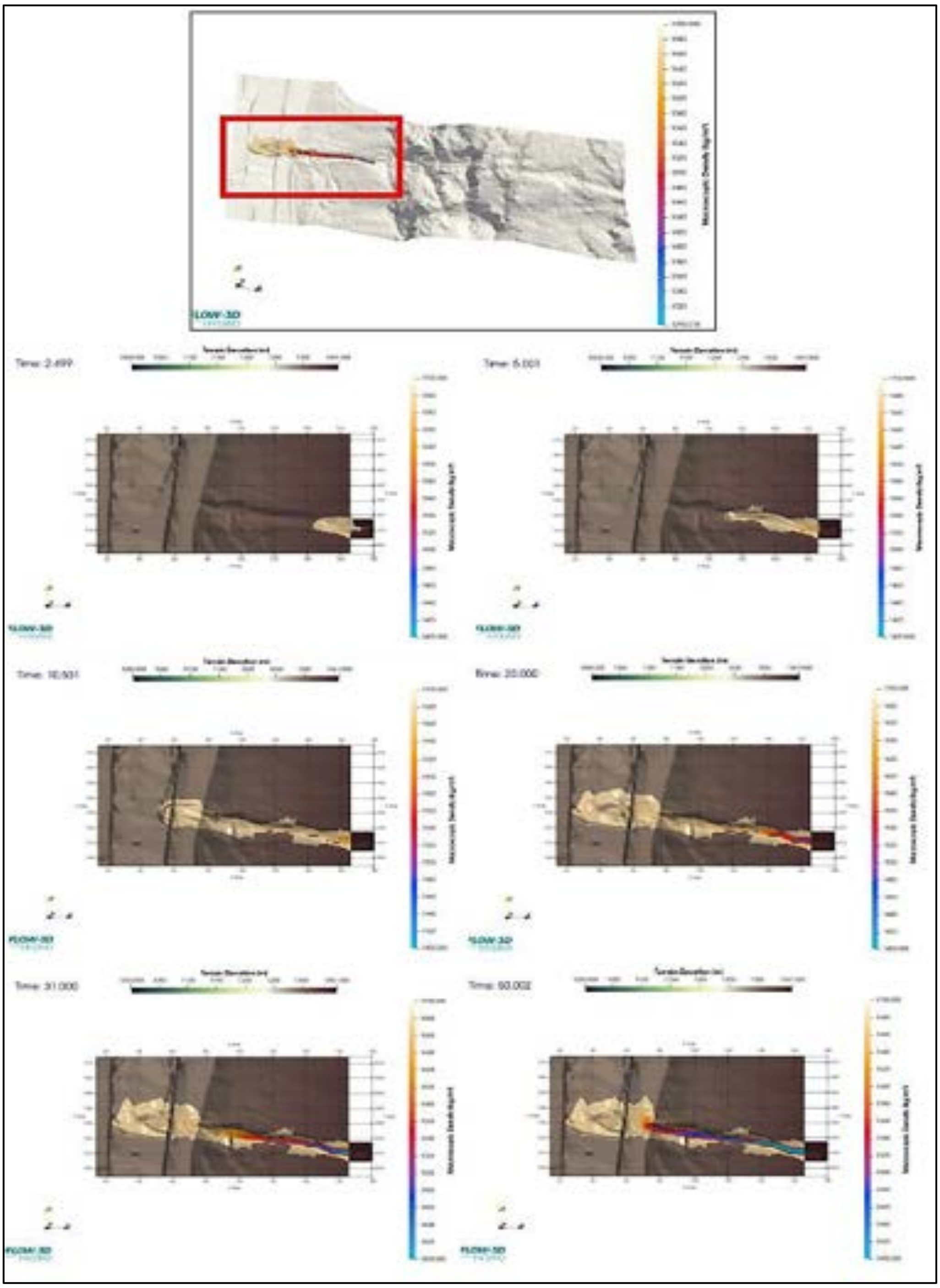

Fig. 4.18: Preliminary shallow water debris flow model

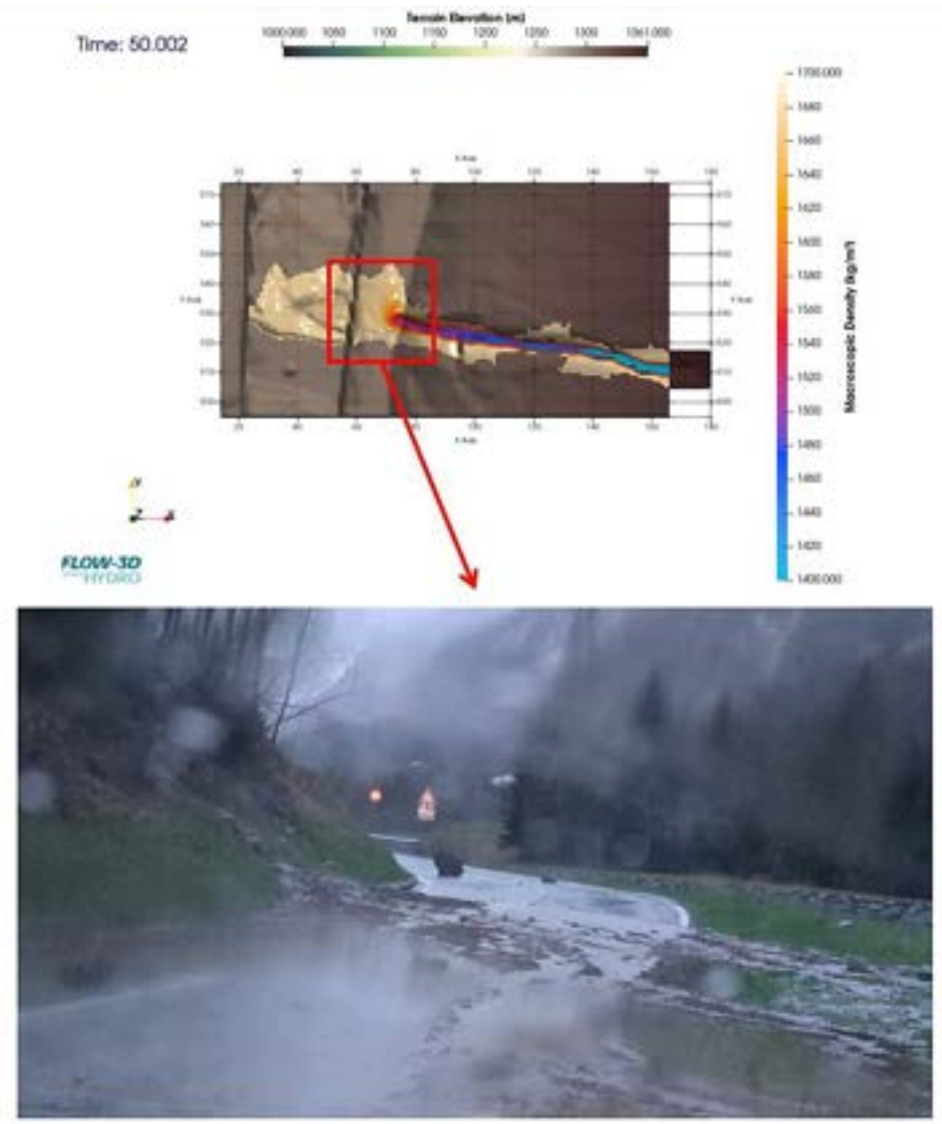

Fig. 4.19: Recent debris flow event – Aprile 2025

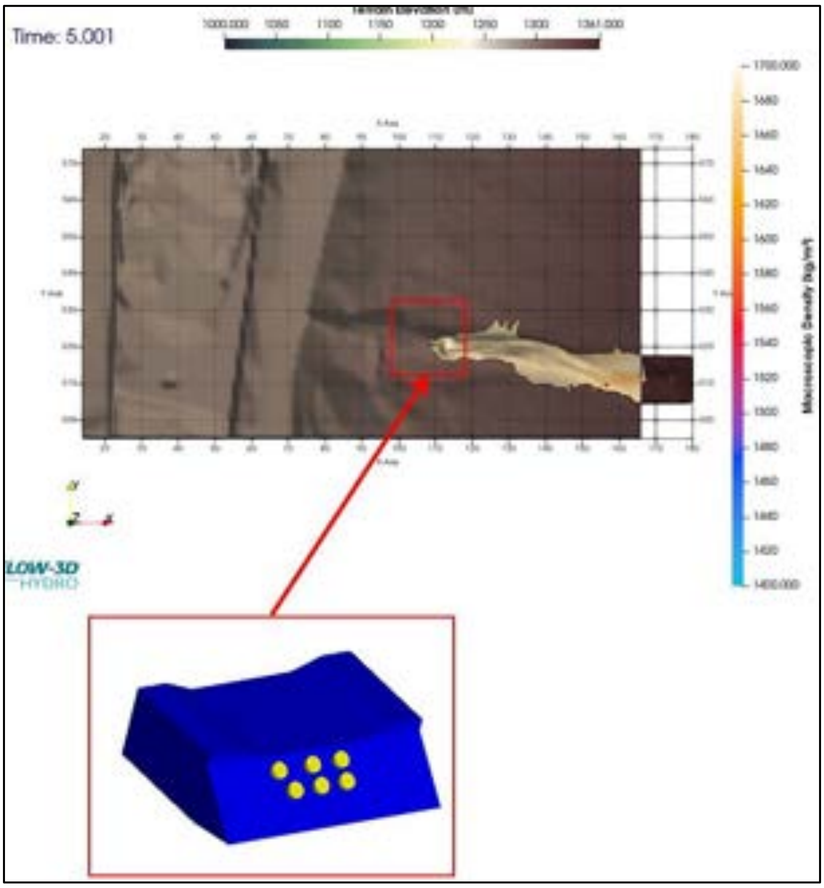

Fig. 4.20: Barrier location

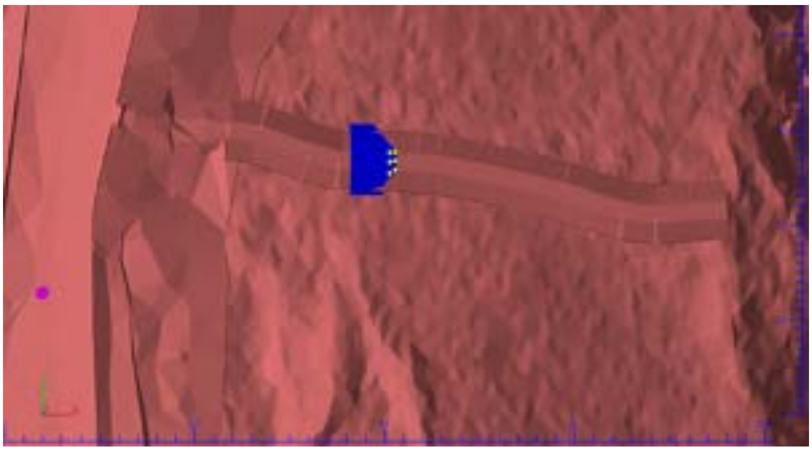

Fig. 4.21: New design flume

4.3.4 Results of Scenario A

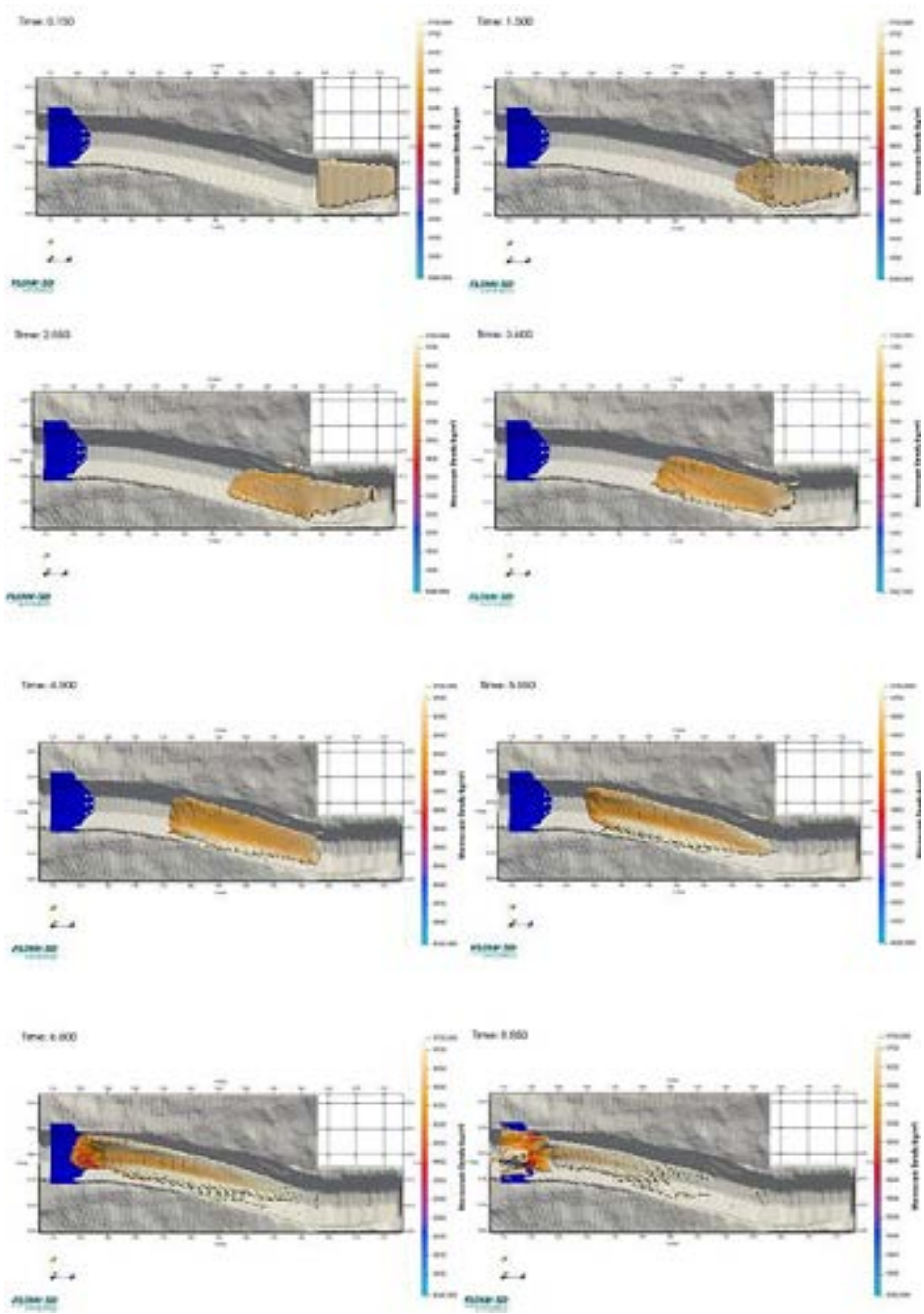

Fig. 4.22: Results Scenario A – Density mapping at different time step

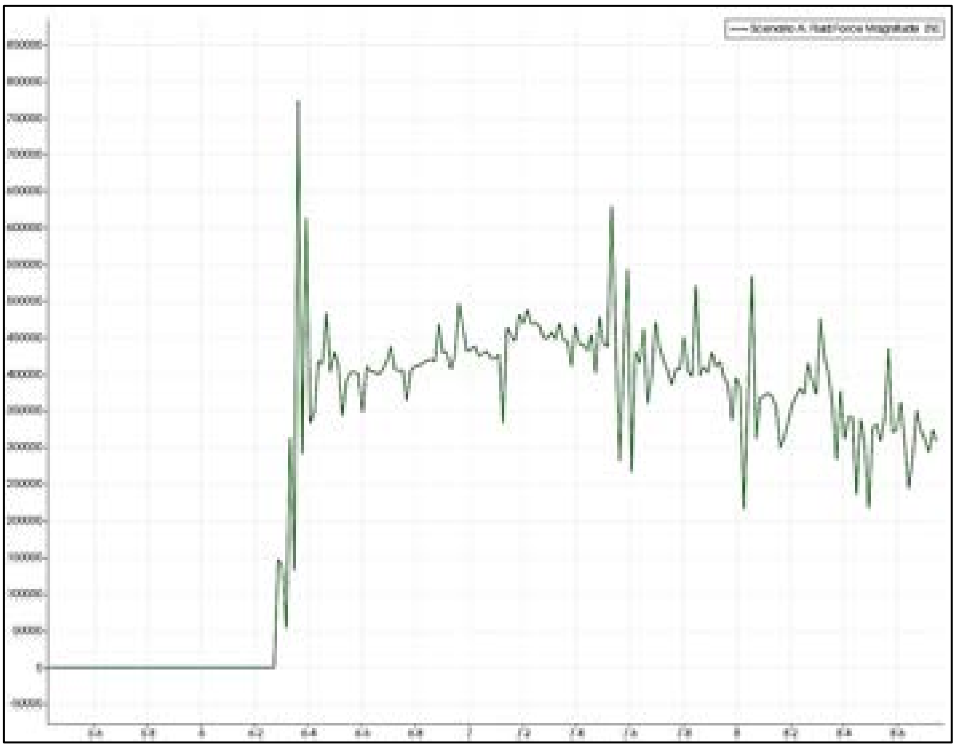

Fig. 4.23: Results Scenario A – Temporal evolution of impact forces

4.3.5 Results of Scenario B

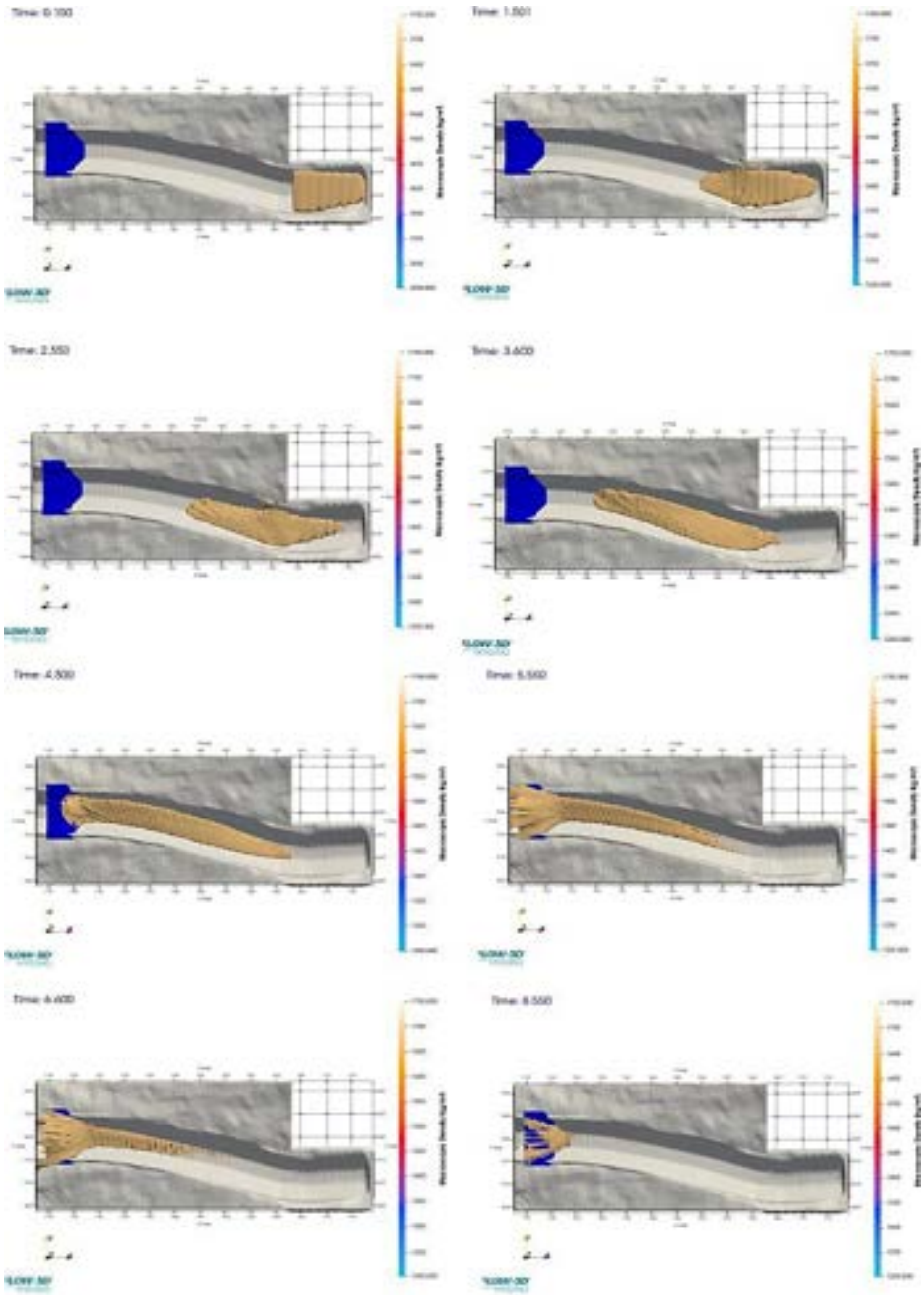

Fig. 4.24: Results Scenario B – Density mapping at different time step

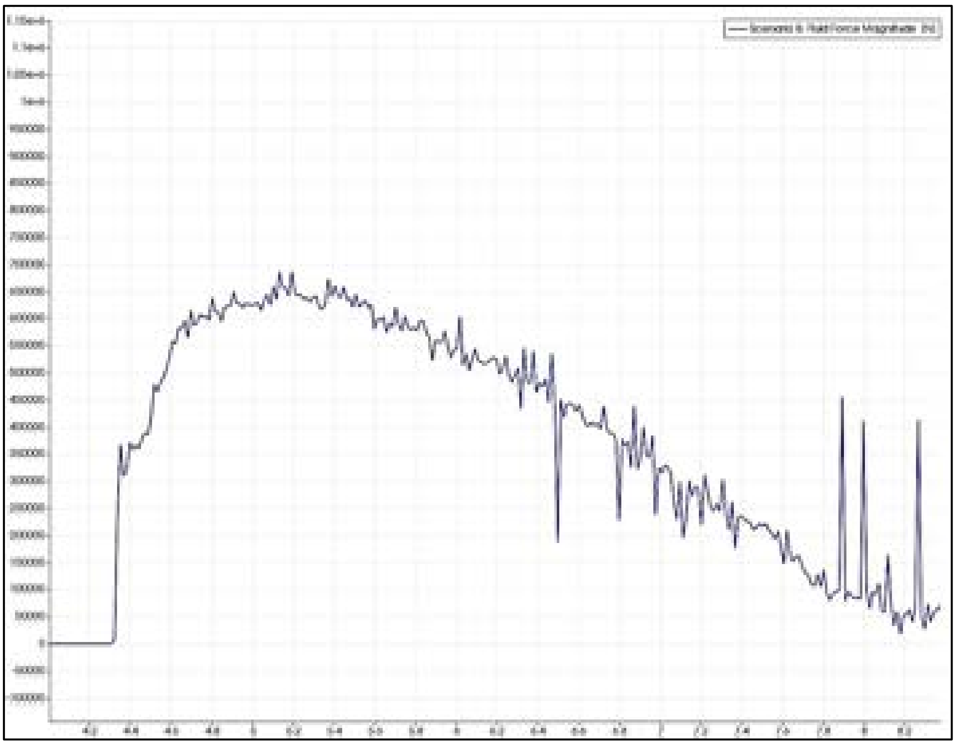

Fig. 4.25: Results Scenario B – Temporal evolution of impact forces

4.3.6 Results of Scenario C

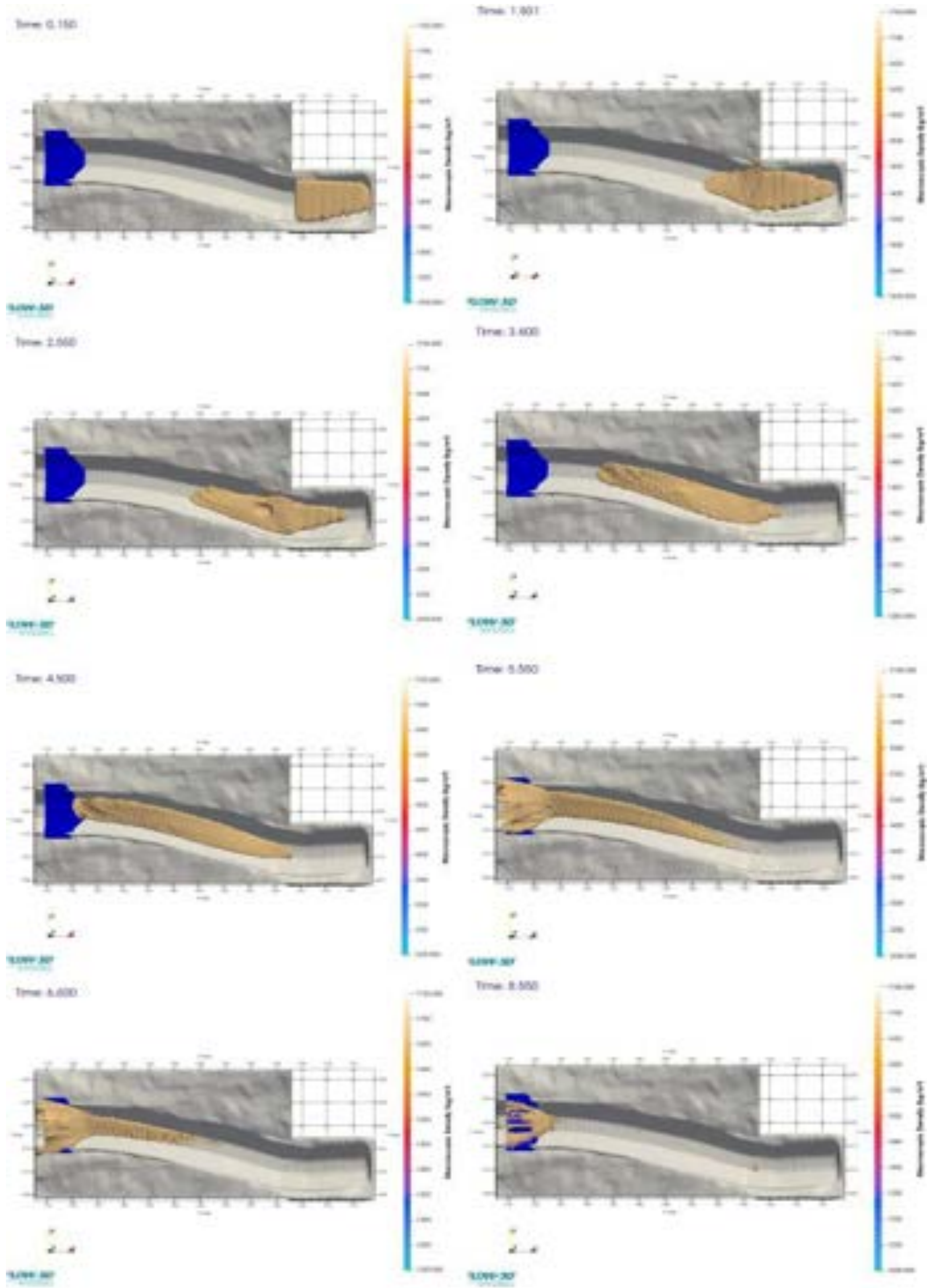

Fig. 4.26: Results Scenario C – Density mapping at different time step

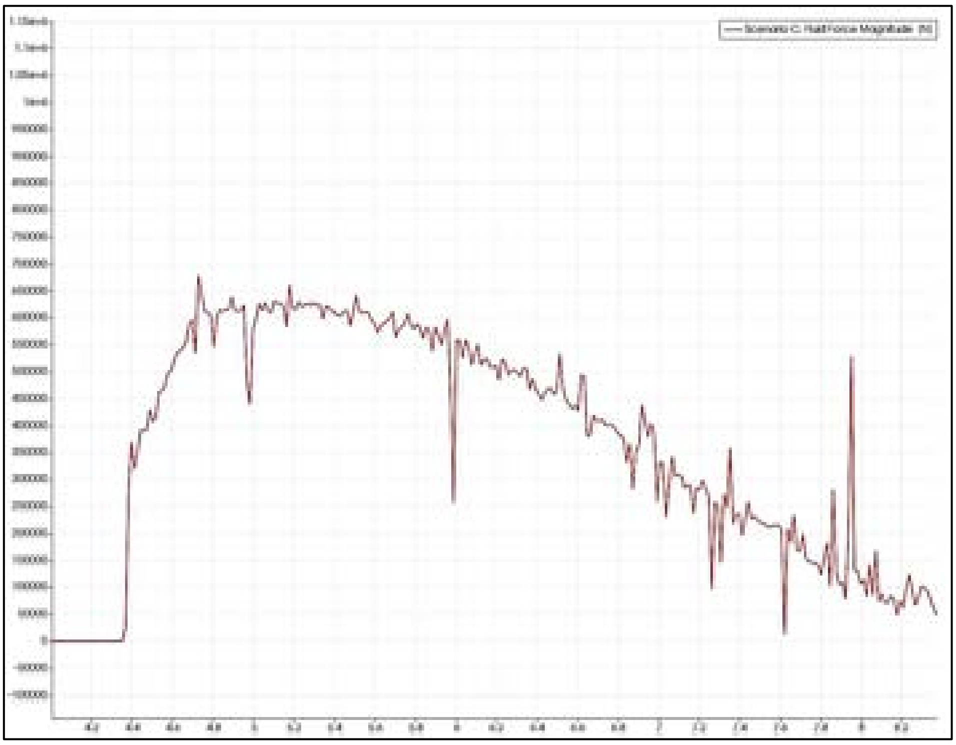

Fig. 4.27: Results Scenario C – Temporal evolution of impact forces

4.4 Comparison of Results

This chapter presents a comparative analysis of the numerical simulations performed for the three debris flow scenarios defined in the study. The objective is to evaluate how rheological assumptions, sediment composition, and fluid modeling approaches influence the impact forces exerted on a protective barrier. Special attention is given to the timing, magnitude, and variability of the forces during the impact phase.

The results from **Scenario A** (debris flow with coarse blocks), **Scenario B** (tailings composed of fine sediments), and **Scenario C** (homogeneous Bingham fluid with constant density) are analyzed in terms of their temporal evolution and peak impact forces. These are then compared both internally and against the empirical formulation proposed by **Zhao et al. (2018)**, which serves as a reference model derived from large-scale laboratory flume experiments.

In addition to quantitative comparisons of force magnitudes, the analysis also considers:

- the onset time of impact and its relation to front propagation dynamics,
- variations in macroscopic fluid density during flow evolution,
- the effect of particle size on flow resistance and energy transfer.

The following sections provide detailed interpretations of these aspects, aiming to highlight the critical role of rheological detail and physical realism in accurately predicting debris flow impact loads.

4.4.1 Comparative Evaluation of Impact Force: Scenario A Simulation vs Empirical Case Study of Zhao et al (2018)

A crucial objective of this study was to assess the peak impact force exerted by a debris flow on a protection barrier in the real-world context of the "La Valletta" basin. The results from the numerical simulation using **Flow-3D** were compared with both the empirical prediction provided by **Zhao et al. (2018)** and the reference values obtained from their large-scale experimental **case study**.

In **Scenario A**, characterized by a Bingham-type debris flow with coarse clasts ($D_{max} \approx 30$ cm), the Flow-3D simulation yielded a **maximum impact force** of approximately:

$$F_{\text{Flow-3D}} \approx 750{,}000\,\text{N}$$

This peak value was registered at the barrier location where the flow hit the structure at a mean depth of 2 m and a frontal velocity of approximately 13 m/s.

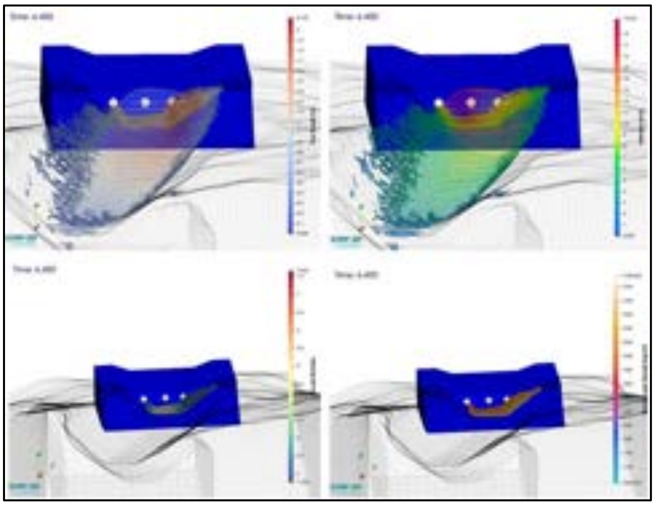

Fig. 4.28: Depth, Velocity, Froude Number and Density distribution in the fluid cross section immediately upstream of the barrier an prior to impact – Scenario A

To validate this outcome, an empirical prediction was calculated using the formula proposed by Zhao et al., developed from flume experiments with fine-grained debris material:

$$P = 0.18 \cdot Fr^{0.0052} \cdot c_0^{1.8142} \cdot \rho_w \cdot v_s^2$$

Given:

- Fr=4.8,
- c_0 = 0.42,
- ρw=1000 kg/m^3,
- vs=13 m/s,

the **impact pressure** was estimated as:

P=6356 Pa

Assuming an effective impact area of A=5.5 m^2, the total force was calculated as:

$$F_{\text{Zhao (empirical)}} = 34{,}958\ \text{N}$$

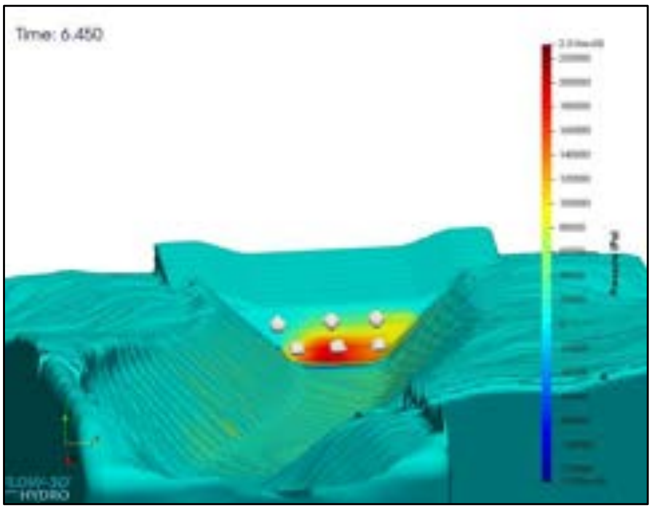

Fig. 4.29: Pressure distribution on the barrier at the moment of maximum impact

This result is approximately **22 times lower** than the peak obtained with the CFD model. The discrepancy is attributable to several factors:

- the empirical formula is based on **fine-material laboratory flows**, and does not account for the presence of **coarse blocks** or heterogeneities,
- Flow-3D captures full **3D flow dynamics**, including vertical impulses, turbulence, and direct block-structure interactions,
- the simulation includes **transient pressure surges** that are not reproducible in flume tests with rigid walls and simplified flow regimes.

Further context is provided by examining the **real-world case study** reported by Zhao et al. in Section 6 of their paper. The documented debris flow in a mountainous basin (12.2 km^2, $Q = 132\ m^3/s$) yielded **peak impact pressures** on the order of **12–15 kPa**, corresponding to total forces of about **60–75 kN** for a typical impact area of 5 m^2. These values, while higher than their laboratory experiments, remain significantly **below the impact forces observed in Scenario A** of this study, reinforcing the critical role of:

- **scale effects**,
- **coarse particle interactions**,
- and the **complex rheology** of real debris flows.

In conclusion, this comparison demonstrates that while empirical models are valuable tools for initial design, **only full CFD simulations** can capture the nuanced and amplified dynamics of impact in natural debris flow events, especially in the presence of coarse materials.

4.4.2 Comparative Analysis: Scenario B vs Scenario C

A comparative analysis of Scenarios B and C was carried out to evaluate the influence of fine sediment tailings on the impact force dynamics of debris flow. Despite the different rheological modeling approaches, the two simulations produced remarkably similar results in terms of both peak impact force and temporal evolution.

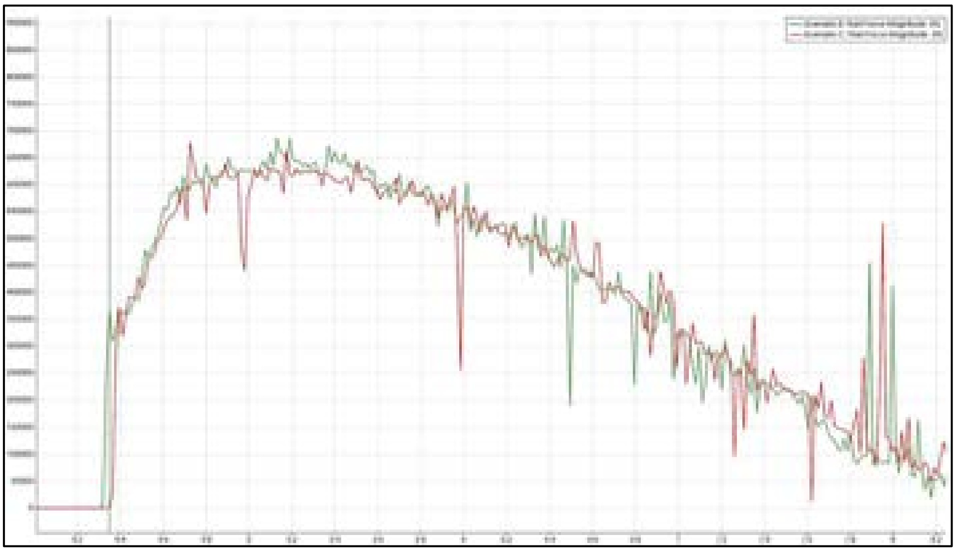

Fig. 4.30: Comparison of impact force trends, Scenario B – Scenario C

In Scenario B, the flow was modeled as a Bingham fluid with tailings composed exclusively of fine particles (maximum grain size 1.5 cm), using a plastic viscosity of $\mu p=1.29$ P Pa·s corrected by a factor Kc=1.5, and a yield stress of $\tau y=260$ Pa. The tailings concentration was set volumetrically, but the dynamic density field obtained during simulation showed negligible spatial or temporal variation. This homogeneity supports the assumption that, in the absence of large clasts, the rheological properties are predominantly governed by the cohesive matrix.

In Scenario C, the same yield stress and bulk density were applied, but the fluid was treated as homogeneous and incompressible, with constant properties throughout the domain. The plastic viscosity was slightly lower (μp=0.86 Pa·s) due to the absence of corrections for sediment concentration. However, in both cases the flow developed under similar dambreak conditions, with identical initial volumes and geometrical constraints.

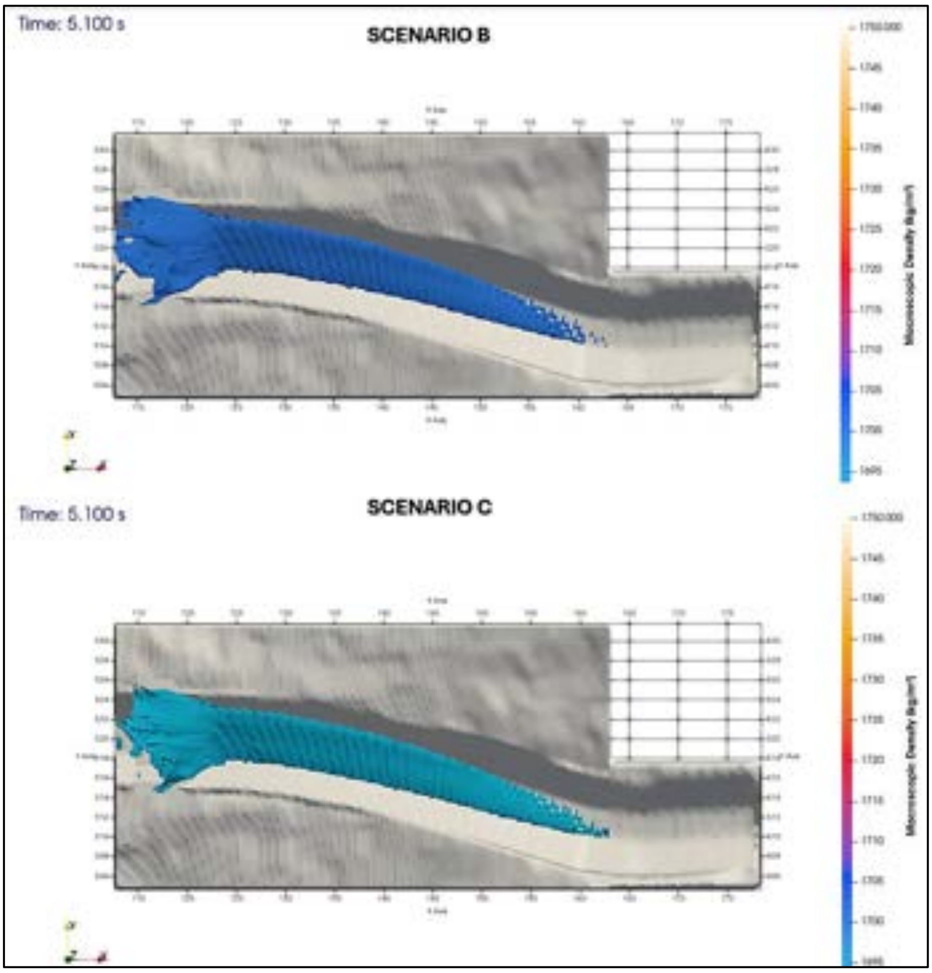

Fig. 4.31: Comparison debris at the instant of impact – Density mapping, Scenario B vs Scenario C

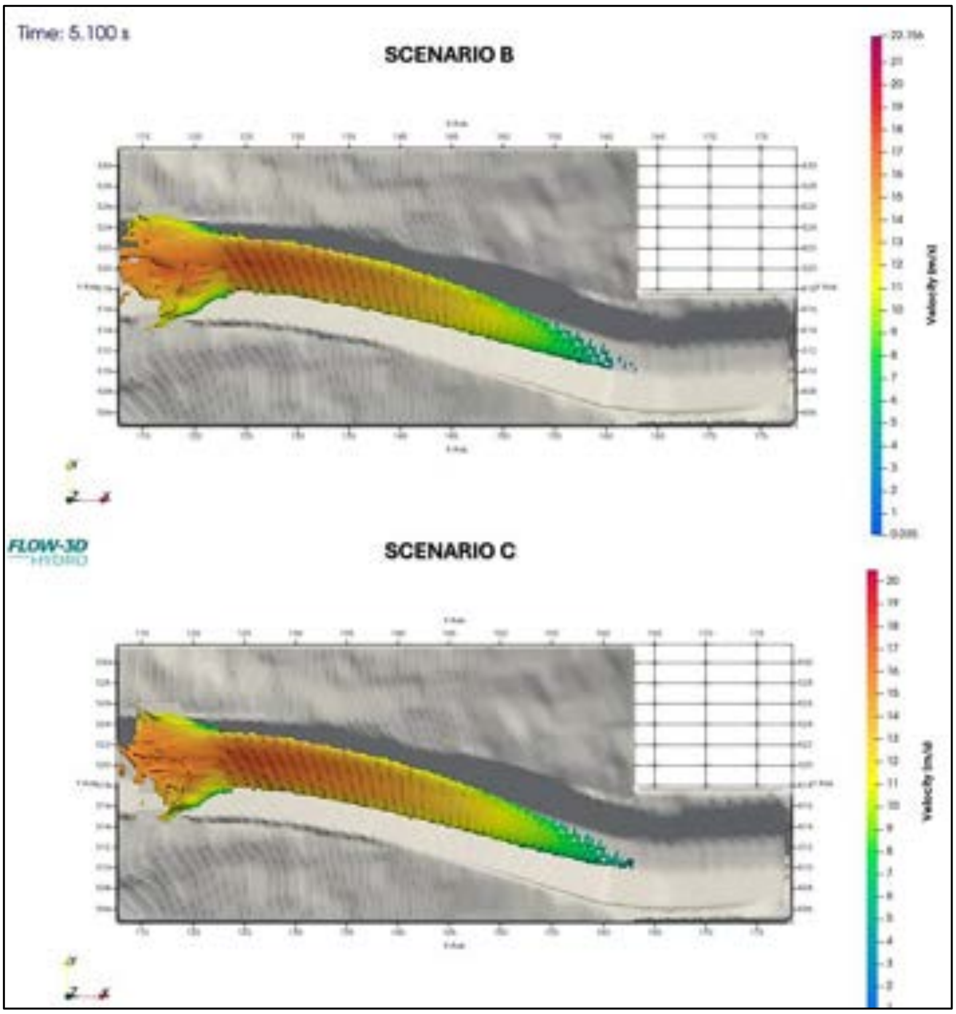

Fig. 4.32: Comparison debris at the instant of impact – Velocity mapping, Scenario B vs Scenario C

The observed impact force profiles are nearly indistinguishable in their peak amplitude and decay rate. This convergence can be explained by:

- identical yield stress and density values in both scenarios;
- minimal viscosity contrast;

- dominance of inertial forces over viscous effects in the supercritical regime (Froude number > 1);
- absence of coarse elements that could generate high-frequency local impacts.

Furthermore, the limited variation in macroscopic density observed in Scenario B reinforces the reliability of using a simplified constant-density model for impact force estimation in fine-material debris flows.

In conclusion, the results validate that under specific rheological and geometric conditions, **Scenario C can serve as a robust and computationally efficient proxy** for more detailed multiphase tailings-based models when coarse particles are absent.

4.4.3 Comparative Analysis: Scenario A vs Scenario B vs Scenario C

The comparative graph in Figure below shows the evolution of the fluid impact force magnitudes for the three simulated debris flow scenarios:

- **Scenario A** (green line): debris flow with coarse blocks (maximum particle size of 30 cm);
- **Scenario B** (blue line): flow with fine sediment tailings (maximum particle size of 1.5 cm);
- **Scenario C** (red line): homogeneous Bingham fluid with constant density.

All scenarios exhibit a similar initiation time, but distinct impact characteristics. Scenarios B and C reach their maximum impact force at approximately 4.5 s, while Scenario A peaks later at 6.5 s. Moreover, Scenario A shows a significantly more irregular force profile over time, with sustained post-peak fluctuations and higher magnitudes.

Fig. 4.33: Comparison of impact force trends, Scenario A-Scenario B–Scenario C

<u>Scenario A – Coarse Material Influence</u>

Scenario A includes coarse clasts (D_{max} = 30 cm) that significantly influence flow behavior. The rheological model was defined by:

- Density ρ=1700 kg/m^3,
- Yield stress τy=308 Pa,
- Plastic viscosity μp=3.5 Pa·s, corrected with Kc=5.5.

The **delayed arrival time (6.5 s)** is attributed to the **higher resistance to flow propagation**, resulting from both the increased viscosity and internal friction. These parameters slow down the front velocity and create a more gradual, non-uniform approach to the barrier.

Additionally, the simulation reveals that the **macroscopic density in Scenario A decreases during the flow evolution**, indicating settling or dispersal of heavier particles. This dynamic behavior contributes to the **prolonged and variable impact forces** after the initial peak, as local density and momentum transfer fluctuate due to internal rearrangement of solids and fluid phases.

Scenario B – Fine Tailings

Scenario B models debris flow using only fine sediments ($D_{max} \leq$ 1.5 cm), with:

- ρ=1700 kg/m^3,
- τy=260 Pa,
- μp=1.29 Pa·s, with Kc=1.5.

In this case, the **impact occurs earlier at 4.5 s**, reflecting **faster flow propagation** due to lower flow resistance. Moreover, the density field remains nearly constant throughout the simulation, reinforcing the assumption of homogeneous behavior. As a result, the force profile is smoother, with fewer fluctuations and a peak force around 660–680 kN

Scenario C – Homogeneous Fluid

Scenario C represents a simplified, uniform Bingham fluid:

- ρ=1700 kg/m^3,
- τy=260 Pa,
- μp=0.86 Pa·s, with no tailings correction.

Although idealized, this model produces **impact force values nearly identical to Scenario B**, thanks to similar density and stress thresholds, and the absence of coarse particles in both cases. The earlier peak at 4.5 s and the regular decay confirm that inertial forces dominate the impact process, and simplified models may suffice under fine-material conditions.

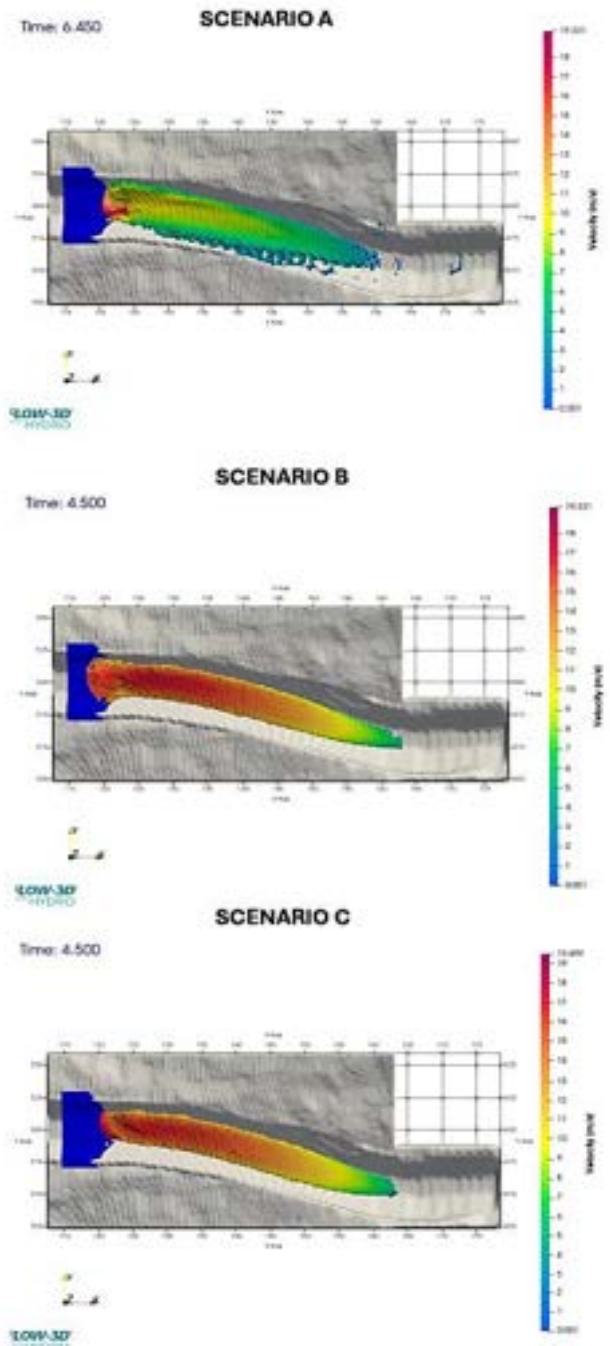

Fig. 4.34: Comparison debris at the instant of impact – Velocity mapping, Scenario A vs Scenario B vs Scenario C

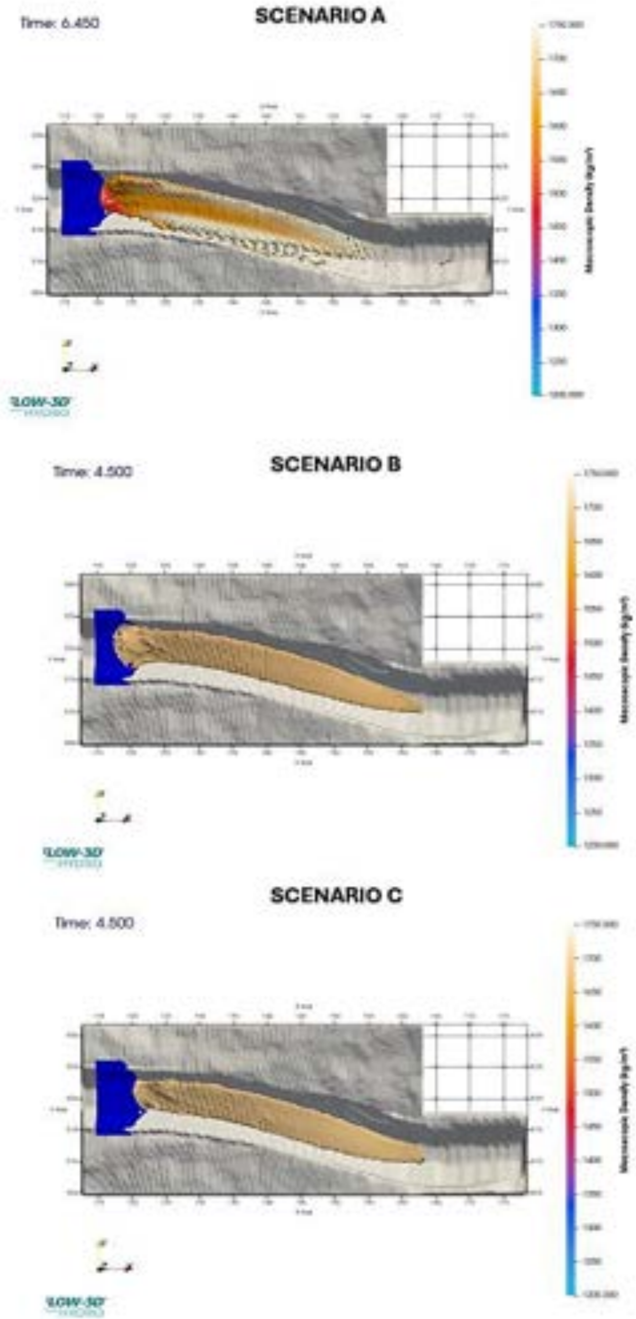

Fig. 4.35: Comparison debris at the instant of impact – Density mapping, Scenario A vs Scenario B vs Scenario C

This analysis reveals that:

- **Scenario A**, with coarse blocks, produces **delayed but stronger and less stable impact forces**, due to multiphase interactions and evolving density;
- **Scenarios B and C**, in contrast, show **faster arrival, more stable impact evolution**, and consistent density fields, validating the use of homogeneous rheology in fine-grained flows;
- The **timing of impact** and **rheological variability** have a major effect on the **distribution and peak of impact forces**, and must be considered in the design and calibration of protective structures.

4.5 Conclusions and Implications

The simulation results for the three debris flow scenarios modeled in the "La Valletta" basin have demonstrated how rheological characteristics, sediment size distribution, and modeling assumptions can significantly affect the magnitude, timing, and variability of impact forces on protective structures.

Scenario A, which includes coarse sediment ($D_{max} \approx 30$ cm), exhibited the highest impact force and the greatest temporal variability. The delayed peak (6.5 s) and fluctuating force curve were directly associated with the high plastic viscosity ($\mu p = 3.5$ Pa·s) and yield stress ($\tau y = 308$ Pa), enhanced by a corrective factor accounting for interparticle friction and structural blocking. This scenario best reflects real-world debris flows where large clasts cause intermittent high-pressure contacts and dynamic changes in density during transport.

In contrast, **Scenarios B and C**, representing fine-grained tailings and a homogeneous Bingham fluid respectively, produced nearly identical force profiles, with earlier peaks (4.5 s), smoother decay, and consistent impact magnitudes (~660–680 kN). The stability of the results in both scenarios was reinforced by the constancy of the bulk density field during the simulation, validating the use of simplified models in contexts where coarse sediment is absent.

The comparison with the empirical model by **Zhao et al. (2018)** highlighted the limitations of laboratory-derived formulas when applied to full-scale, coarse-laden flows. The empirical prediction underestimated the impact force by an order of magnitude compared to the CFD model for Scenario A, underscoring the importance of capturing 3D multiphase dynamics and the role of coarse particles in real conditions.

From an engineering perspective, these findings support the following conclusions:

- **Coarse sediment amplifies impact forces** and delays peak time due to increased resistance and density evolution;
- **Fine-grained and homogeneous debris flows** produce more stable and predictable impact behavior, suitable for simplified rheological modeling;
- **Numerical models must be adapted to the sedimentological context**, as applying laboratory-based equations to real-scale events can lead to severe underestimation of structural loads;
- **Calibration of Bingham parameters** should reflect the presence or absence of clasts using correction factors derived from literature or empirical observations.

The implications of these findings are critical for the **design and positioning of mitigation structures**, particularly in alpine basins where debris flows are recurrent. The study demonstrates that CFD tools like Flow-3D, when properly calibrated and validated, are capable of reproducing complex flow behaviors and delivering accurate estimations of forces acting on protective barriers. This knowledge directly informs risk assessment and engineering design in high-hazard geomorphic contexts.

Chapter 5

5 Scale Effects in Experimental setup of Debris Flow Impact: Class A Prediction with FLOW-3D

The laboratory flume and numerical simulations presented in this chapter were conceived with the specific goal of investigating the impact forces generated by debris flows on a real bridge pier. The reference case for the design of the experimental setup is the VI01 viaduct, part of a high-speed railway project in Southern Italy.

Fig. 5.1: Overview map of the entire Naples–Bari railway line, with detail of the Hirpinia–Orsara section

This viaduct spans the Cervaro River and crosses the Acquara stream, located in a geologically complex area of the Apennines characterized by active debris cones, frequent shallow landslides, and hyper-concentrated flood events.

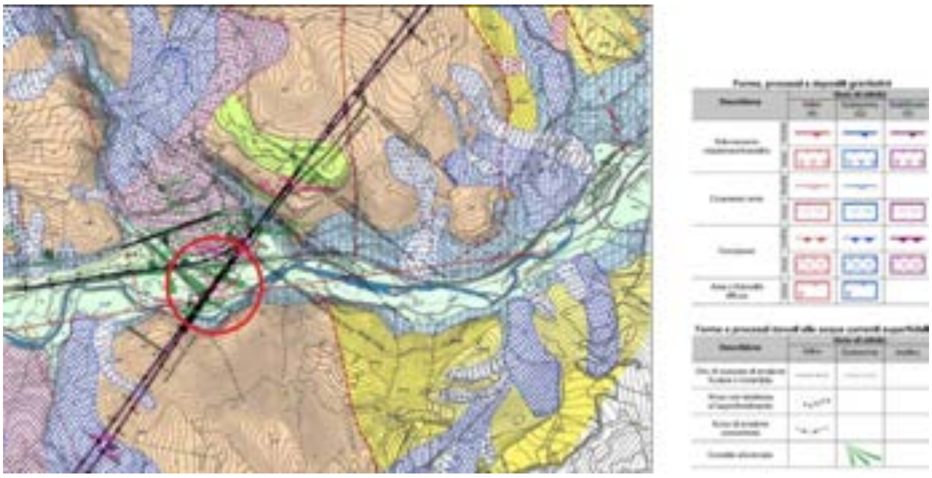

Fig. 5.2: Excerpt from the geomorphological map

The site is classified within HC2 and HC3 susceptibility classes, indicating a high to very high geomorphological hazard level, according to the guidelines of the Puglia River Basin Authority (PSAI).

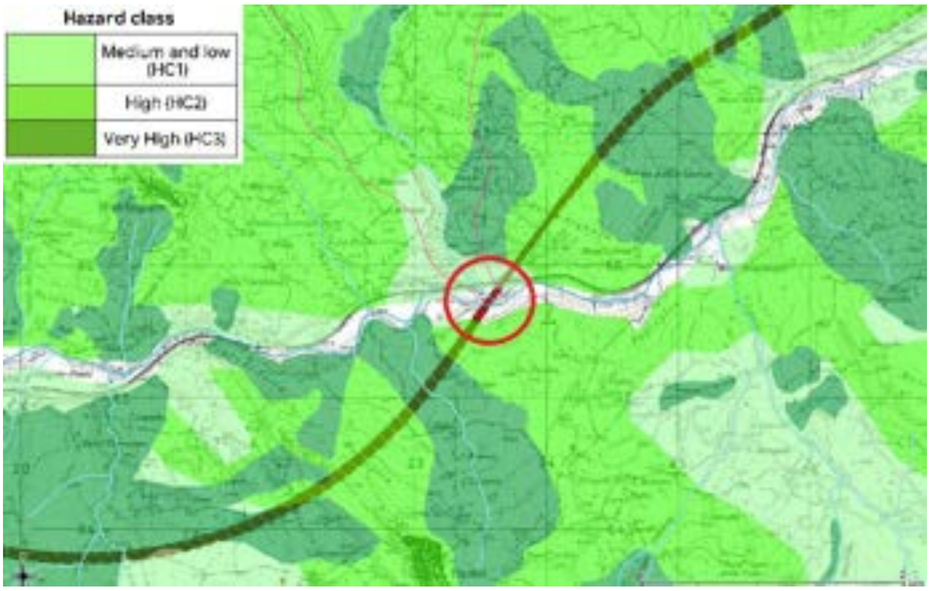

Fig. 5.3: Excerpt from the PSAI Puglia hazard map – Geomorphological hazard

The pier modeled in the flume corresponds to a 1:50 scale replica of one of the real piers of the VI01 viaduct, which is composed of several spans, including two main 60 meter spans, supported by reinforced concrete piers. The viaduct deck reaches an elevation of +356.70 m a.s.l., with foundations exposed to potential debris-laden flows from the surrounding catchments.

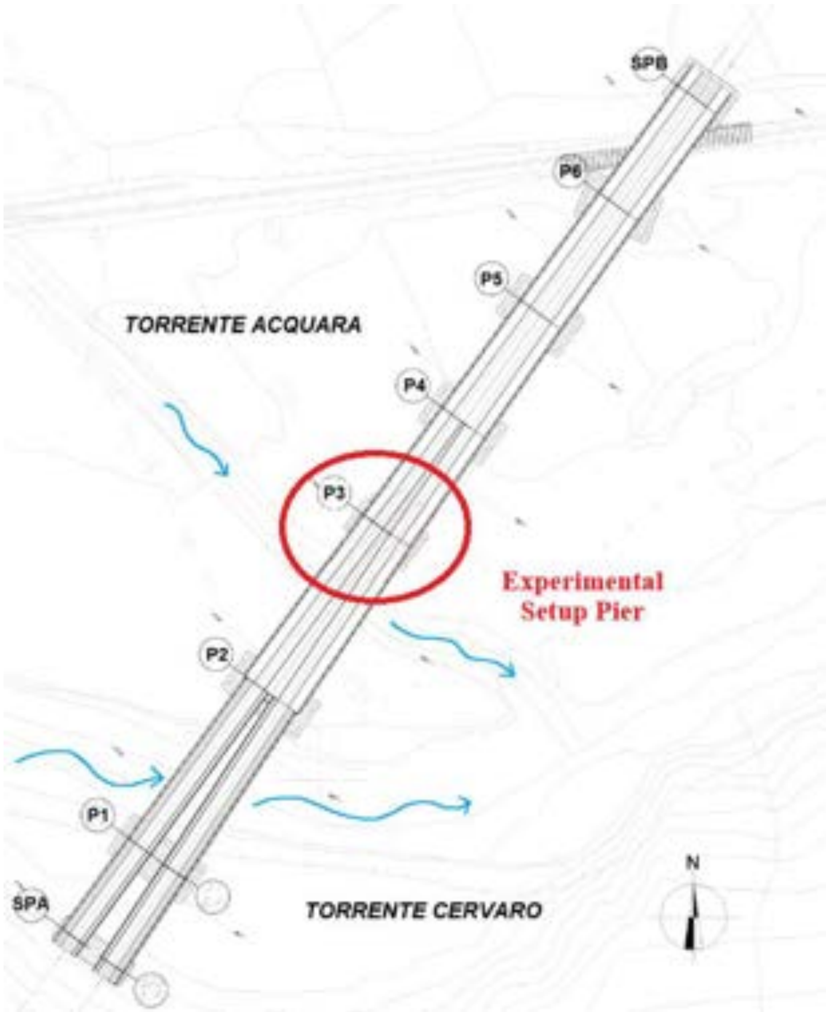

Fig. 5.4: Plan view of the designed viaduct over the Cervaro stream

Given the absence of extensive field data and the challenges of replicating such events at full scale, the laboratory installation was specifically designed starting from the real geometry of the VI01 pier, to enable a robust numerical and physical assessment of debris impact loads.

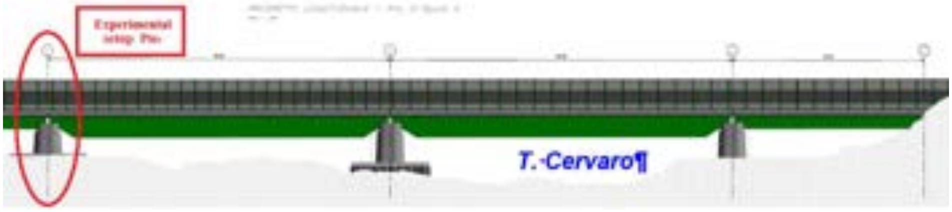

Fig. 5.5: Elevation view (Pier 3 – Abutment A) of the designed viaduct over the Cervaro River

The present study, therefore, aims to provide a Class A numerical prediction of this scenario using FLOW-3D, offering a reliable baseline for future experimental calibrations and supporting both hydraulic hazard assessments and structural design checks for critical infrastructures in debris prone environments.

The characterization of debris flow impact forces on bridge piers remains a challenging issue in hydraulic engineering, particularly in the absence of comprehensive laboratory data. This chapter aims to strengthen the predictive capability of numerical modeling in this field by presenting a Class A prediction approach, based on FLOW-3D simulations calibrated on a well-defined laboratory-scale configuration.

The study focuses on a debris flow flume designed at the University of Milano-Bicocca (UNIMIB), which represents a controlled environment for reproducing the interaction between debris flows and a simplified pier geometry. While no physical tests were conducted during this doctoral research, a fully-scaled digital replica of the flume has been developed to provide a robust numerical benchmark for future experimental work.

Class A prediction, as defined by the International Workshop on Advanced Experimental and Numerical Methods in Hydraulic Research, refers to a blind or a priori numerical prediction based solely on known input parameters, without any tuning to fit experimental outcomes. This type of prediction is crucial in demonstrating the reliability and transferability of numerical models across different scenarios and scales.

The objective of this chapter is to investigate the effects of geometric scaling on the impact forces, through simulations in which the laboratory model represents, respectively, a structure at 1:10, 1:25, and 1:50 scale. The 1:50 case corresponds to the full-scale structure (a real bridge pier), while the other two cases explore intermediate scales of application. This reverse approach allows for the assessment of how well a small-scale laboratory configuration can reproduce full-scale impact behavior.

The 1:10 and 1:25 intermediate models were introduced with the specific goal of understanding the trend of scale effects as the size of the system increases. Instead of creating new geometries, the original laboratory-scale model is numerically interpreted as if it were a reduced-scale representation of increasingly larger systems. This methodology enables a continuous and consistent framework to investigate how dynamic quantities such as impact force and velocity vary with scale. The comparison between the different scenarios enhances the understanding of nonlinearities introduced by upscaling and supports the formulation of correction factors or scaling laws..

5.1 Numerical Model Configuration

This section presents the setup of the numerical model used to simulate the debris flow impact on a simplified bridge pier, focusing on three key aspects. First, the laboratory-scale experimental flume designed at the University of Milano-Bicocca is described, as it serves as the geometrical and hydraulic basis for all simulations. Second, the rheological properties of the debris flow material are defined, including the mixture's physical characteristics and the constitutive parameters of the Bingham model. Finally, the configuration of the FLOW-3D model for the laboratory flume is detailed, with attention to geometry, meshing, and boundary conditions.

5.1.1 Experimental Flume Setup of UNIMIB Laboratory

The laboratory installation used in this study was developed at the Department of Geological and Geotechnical Sciences at the University of Milano-Bicocca (building U4). The experimental setup was specifically designed to ensure accurate measurements under controlled conditions. It consists of both the physical model constructed by Trimat S.r.l. (Viganò, LC) and the data acquisition system.

The Experimental installation used has a total length of 4455.5 mm and is divided into three main components:

- A Hopper equipped with a sluice gate mechanism,
- A mobile flume,
- A supporting aluminum frame with plexiglass panels on the sides.

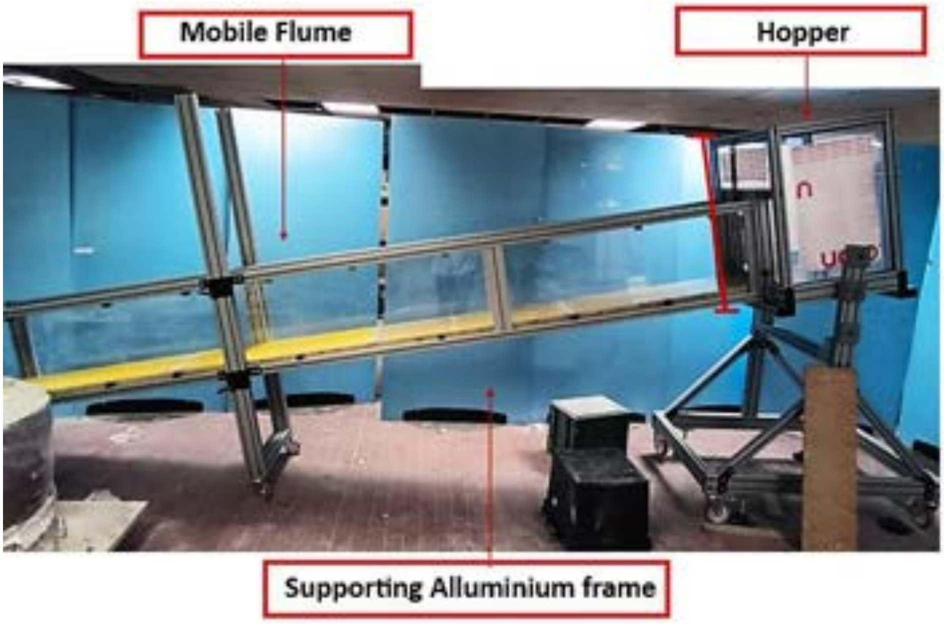

Fig. 5.6: Experimental setup - University of Milano-Bicocca

Fig. 5.7: Experimental setup – Laboratory view

The Hopper has dimensions of 605 mm (length) × 759 mm (height) × 400 mm (width), with a maximum capacity of approximately 183.68 liters. A sluice gate mechanism, secured with screws, is integrated into the front panel of the container and allows for sudden release of the debris flow.

Fig. 5.8: Experimental setup – Hopper

The mobile flume measures 3912.5 mm in length and 500 mm in width, allowing ample space for positioning the obstacle and sensors. In the test performed, the platform was inclined at an angle equal 12 degrees. The platform is mounted on wheels and guided by rails, enabling smooth and precise movement. This feature allows for repositioning of sensors and other equipment.

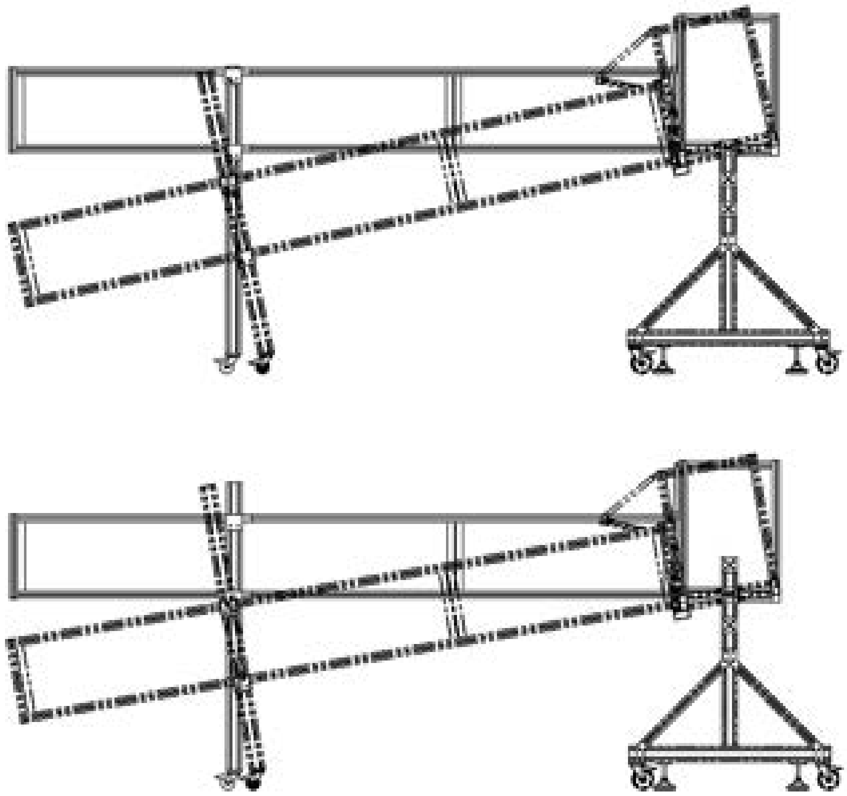

Fig. 5.9: Experimental setup – Mobile flume

The structural supports include an aluminum frame and a base with adjustable feet for stabilization. Wooden panels were secured to the base using screws, providing a solid mounting point for the obstacle and ensuring its stability during impact tests. The structure was sealed with polyethylene terephthalate (PET) sheets to ensure waterproofing.

Fig. 5.10: Experimental setup – polyethylene terephthalate (PET) sheets

A key feature of the setup is the obstacle, which represents a bridge pier scaled down at 1:50.

The pier is asymmetrical and tapers slightly from base to top: its dimensions vary from 35×10 cm at the base to 34×9 cm at the top. It was also inclined at 12° to match the slope of the flume.

The installation of the obstacle involved several critical steps to ensure stability and accuracy:

I. **Positioning:** It was placed on the mobile platform at the location where the maximum flow velocity was calculated using

Flow 3D software. The distance where the maximum impact occurs is 2 meters from the container opening. This positioning is crucial for obtaining accurate data on impact forces and pressure distribution.

II. **Fixing:** It was firmly secured to the wooden beams on the platform using high-strength bolts and brackets. This ensures that the obstacle remains stable and does not move during the experiments.

III. **Alignment:** The obstacle was carefully aligned to ensure it is perpendicular to the flow direction. This alignment is essential for the accurate measurement of impact forces and pressure distribution.

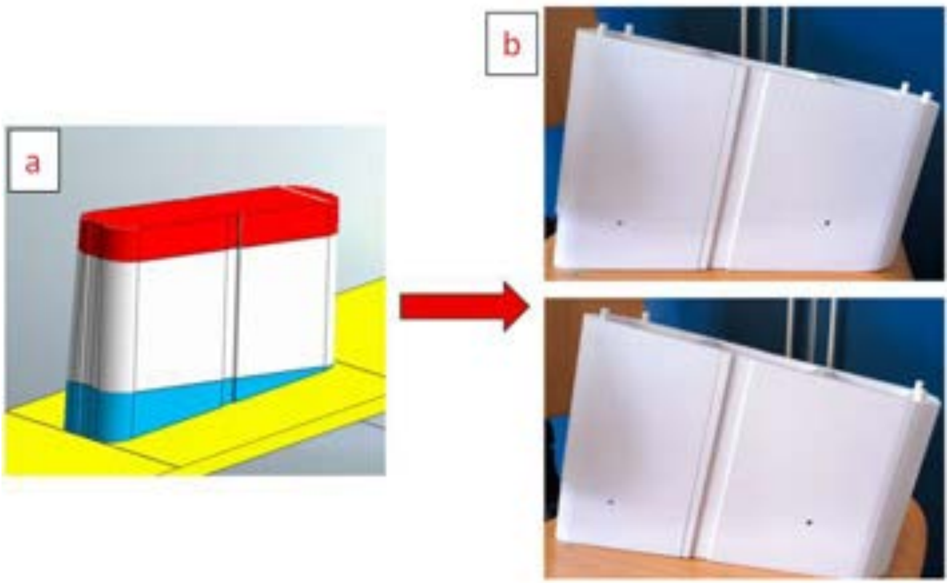

Fig. 5.11: Experimental setup – 3d model and 3d printed pier

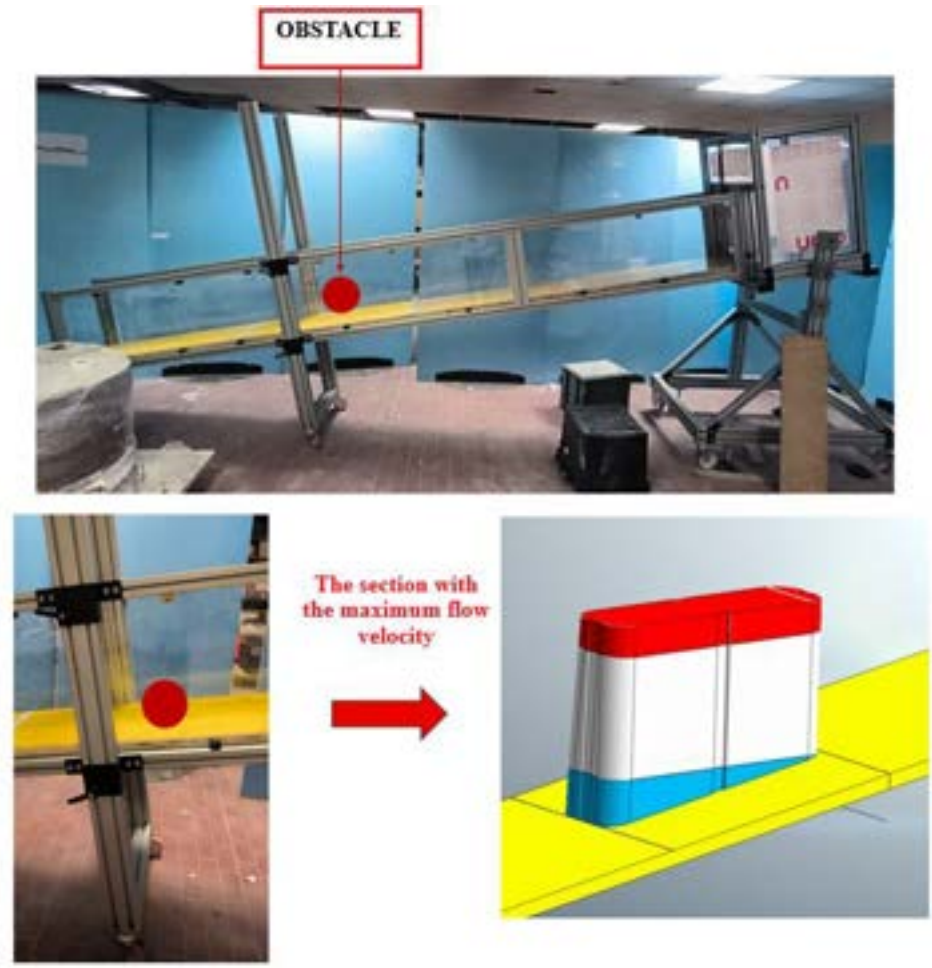

Fig. 5.12: Experimental setup – Pier cross section location

To measure impact forces, different sensor systems were adopted. Initially, a 20 kg-capacity DYHW-110 strain gauge load cell with 10 mm diameter and high sampling frequency (10 kHz) was used.

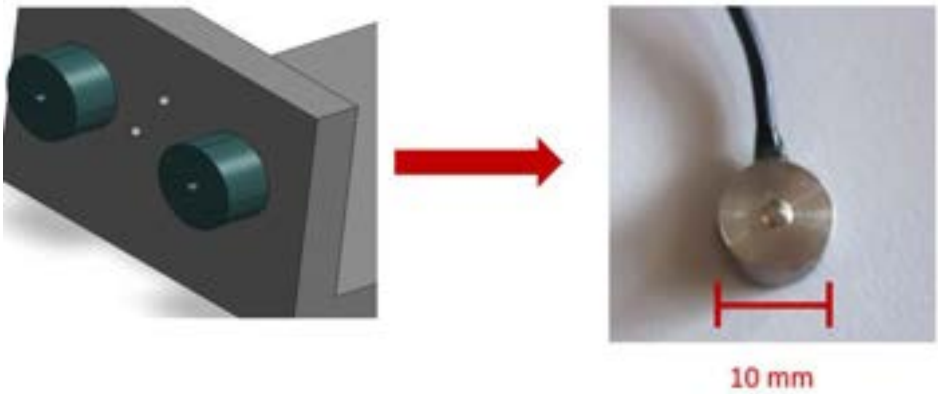

Fig. 5.13: Experimental setup – load cell

It was embedded inside the obstacle and connected to a custom data acquisition system including:

- A Raspberry Pi 5 (8 GB).
- An 8-channel ADS1256 analog-to-digital converter (ADC).
- An ICP CON SG-3016signal amplifier.
- DYHW-110. To allow some movement of the obstacle during impact, a sliding system was introduced, using two micro load cells (20 kg capacity each) mounted on a support structure. This allowed the obstacle to respond dynamically to the flow and improved the accuracy of impact force evaluation.

5.1.2 Debris Flow Material and Rheological Parameters

In the numerical simulations conducted with FLOW-3D, the debris flow material was modeled as a non-Newtonian fluid governed by the Bingham constitutive model. This section provides a detailed explanation of the adopted rheological framework, the selection of material parameters, and the methodology used to estimate them. The definition of the material and its properties was informed by experimental work conducted by Zhao et al. (2018), particularly the study titled "Experimental Study of the Debris Flow Slurry Impact and Distribution", from which particle gradation and typical concentration values were extracted (see Figure 3.1 of this thesis).

Volumetric Concentration and Mixture Properties

In this study, the debris flow slurry was considered as a non-newtonian fluid mixture with both solid and fluid phases. The fundamental quantity controlling the rheological behavior is the volumetric concentration of solids , which quantifies the fraction of the total volume occupied by solid particles. To define the input parameters in FLOW-3D, the following assumptions were made based on the reference experimental setup:

- **Total slurry volume**: 120 L
- **Solid phase density**: $\rho s = 2650$ kg/m^3
- **Mixture density**: $\rho m = 1700$ kg/m^3

From these values, we can compute the **volumetric concentration** using the following mass balance relationship:

$$\rho_m = C_v \cdot \rho_s + (1 - C_v) \cdot \rho_f$$

Assuming ρf = 1000 kg/m^3 and solving for Cv:

$$C_v = \frac{1700-1000}{1650} = \frac{700}{1650} \approx 0.424 \text{ or } 42.4\%$$

This confirms that the selected mixture has a volumetric concentration of approximately 42–45%, consistent with values used in literature.

In FLOW-3D, the solid phase concentration is introduced through the coarse particle tailing concentration, expressed in kg/m^3. This value represents the mass of solids per unit volume of slurry and is calculated as:

$$C_v \cdot \rho_s = 0.45 \cdot 2650 = 1192.5 \text{ kg/m}^3$$

This value was set as the coarse particle tailing concentration in the simulation setup, defining the solid content of the debris mixture. The parameter is applied in both the Initial Conditions and Tailings panels of FLOW-3D.

Rheological Model: Bingham Fluid

Debris flows exhibit yield stress behavior, where the material resists flow until a critical shear stress is exceeded. The Bingham model is widely used to describe such behavior and is defined by the equation:

$$\tau = \tau_y + \mu_p \cdot \dot{\gamma} \quad \text{for} \quad \tau > \tau_y$$

Where:

- τ is the shear stress [Pa],
- τ_y is the yield stress [Pa],
- μ_p is the plastic viscosity [Pa·s],
- $\dot{\tau}$ is the shear rate [1/s].

Based on the selected concentration and guided by empirical models (e.g., Coussot & Piau, 1994), the following values were adopted:

- Yield stress: $\tau_y = 6.8$ Pa
- Plastic viscosity: $\mu_p = 0.0039$ Pa·s

The plastic viscosity was estimated using the empirical relation based on concentration:

$$\mu_p = \mu_f \cdot (1 - C_v)^{-2.5}$$

Assuming $\mu_f = 0.001$ Pa·s and Cv = 45 %, $\mu_p = 0.0039$ Pa·s

These values fall within the typical range for natural debris flows and were validated against values found in Zhao et al. (2018).

To visualize the material's behavior, a theoretical rheological curve was generated for the above parameters:

$$\tau = 6.8 + 0.0039 \cdot \dot{\gamma}$$

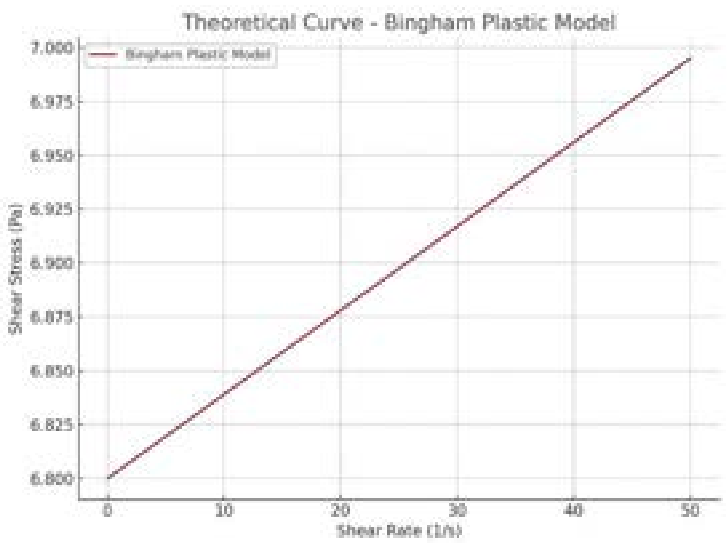

Fig. 5.14: Experimental setup – Theorical Curve – Bingham Plastic Model

This curve indicates that a minimum stress (yield) is required to initiate flow, followed by a linear increase in stress with strain rate. The figure below shows the Bingham curve computed for strain rates from 0 to $200s^{-1}$. This behavior is representative of natural debris mixtures and aligns with observations in flume experiments. It is important to note that the values adopted here were not back-calculated from experimental results, in line with the Class A prediction approach of this study.

The rheological setup also includes solid particle properties with d50 = 0.003 m.

This complete rheological definition forms the basis for the simulations presented in this work, ensuring that the debris flow dynamics are consistent with field and laboratory observations under the specified concentration conditions.

Parameter	***Symbol***	***Value***	***Unit***
Volumetric concentration	C_v	0.45	–
Solid density	ρ_s	2650	kg/m^3
Mixture density	ρ_m	1742.5	kg/m^3
Tailing concentration	–	1192.5	kg/m^3
Yield stress	τ_y	6.8	Pa
Plastic viscosity	μ_p	0.0039	Pa·s
Fluid viscosity	μ_f	0.001	Pa·s
Particle diameter	–	0.003	m

Table 5.1 – Summary of physical and rheological input parameters used for the debris flow material in the numerical simulations,

5.1.3 Numerical Flow 3D model of the Experimental Flume

The Flow 3D numerical model has been configured to replicate the experimental setup of the laboratory flume. This was achieved using the three-dimensional design model provided by Trimat Srl, the company responsible for the fabrication of the flume structure. The obstacle corresponding to the pier of viaduct VI01 was geometrically reproduced at a 1:50 scale based on the project's BIM model.

A unified 3D model was then generated and exported in STL format, which is the standard geometry input format for Flow 3D simulations.

In addition to the flume geometry, a retention tank was incorporated into the Flow 3D model to contain the outflowing debris flow. From a numerical standpoint, this feature helps reduce errors due to volume loss and allows the assignment of an initial water level as the outlet boundary condition, thereby defining a reference volume that stabilizes the numerical computation.

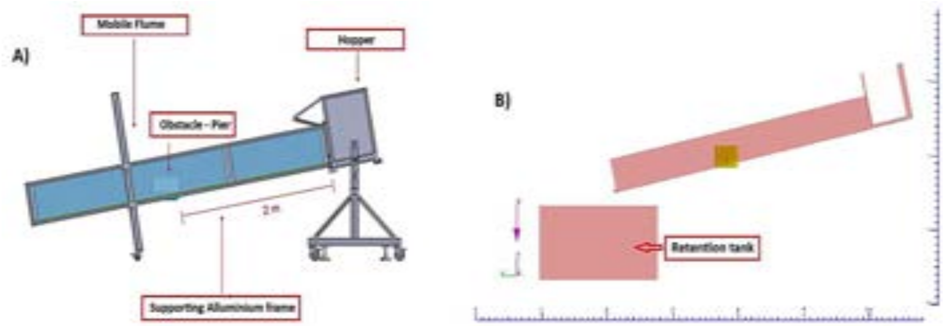

Fig. 5.15: Experimental setup – A) building 3d model, B) Flow 3D geometry model

<u>Computational mesh</u>

A key aspect in the development of the Flow 3D numerical model is the definition of the computational mesh.

Flow 3D is based on a Cartesian mesh composed of square or rectangular cells in the three spatial directions (x, y, z).

It is possible to assign different cell sizes in each direction, provided that the aspect ratio does not exceed 1:2. In the case of the flume model, five mesh blocks were defined: one for the inlet section of the flume, one for the central section including only the pier, one for the outlet section, and a final block for the retention tank. The main mesh block is the central one, where the pier is located and where the hydrodynamic force is computed. In terms of mesh resolution, a cell size of 0.01 m was used for the central block, 0.02 m for the secondary blocks of the flume, and 0.04 m for the tank. The resulting model includes a total of 1,250,000 computational cells.

This parameter plays a crucial role in the upscaling process from the laboratory-scale numerical model to the full-scale numerical model, ensuring consistency and a certain level of computational reliability. This aspect will be further detailed in the following chapter.

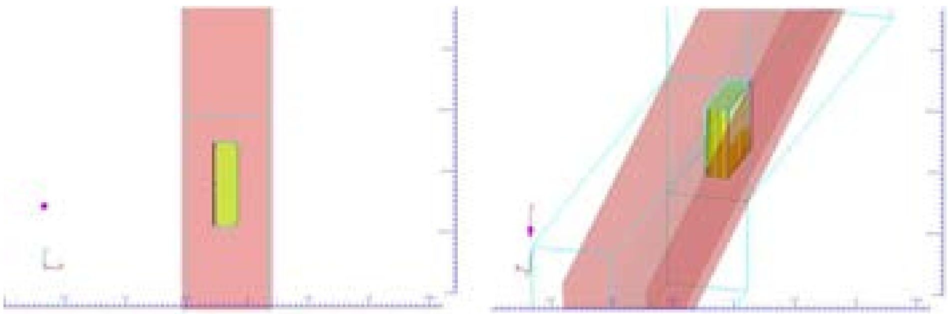

Fig. 5.16: Experimental setup – detail of pier block mesh

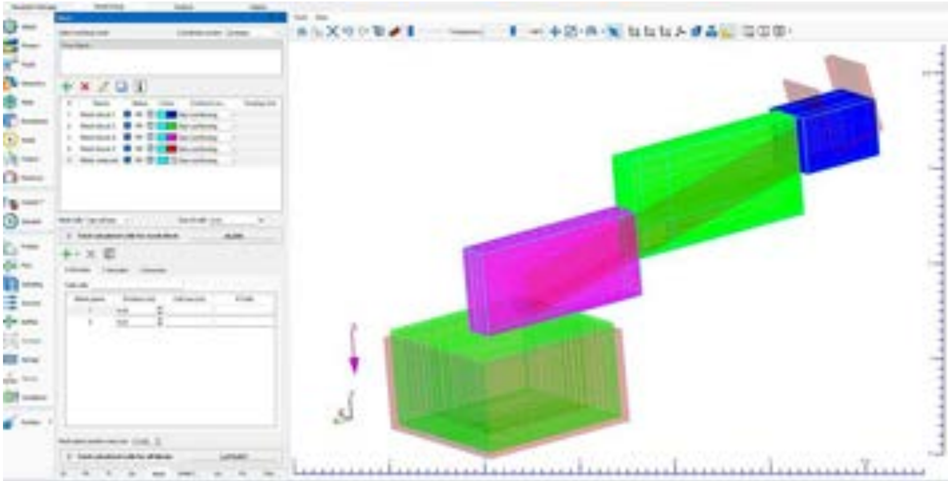

Fig. 5.17: Experimental setup – Block mesh of numerical Flow 3D model

Physics

In general, another fundamental aspect for accurate modeling in the field of Computational Fluid Dynamics (CFD) is the proper definition of the physical models.

The correct selection of the physical variables involved is essential to achieve a reliable physical interpretation of the phenomenon.

In the model under investigation, in addition to the debris flow which defines the type of fluid to be simulated and is implemented in Flow 3D by enabling the Tailings physics model the flow is characterized as a free-surface phenomenon, exposed to atmospheric pressure and occurring under turbulent conditions due to the low viscosity values.

As a result, laminar flow more suitable for highly viscous and homogeneous mud flows is excluded from consideration in this case.

Given the nature of the fluid, variable density effects were also taken into account.

Therefore, the following physics models were enabled:

- Gravity
- Tailings
- Turbulence and viscosity
- Variable density flow

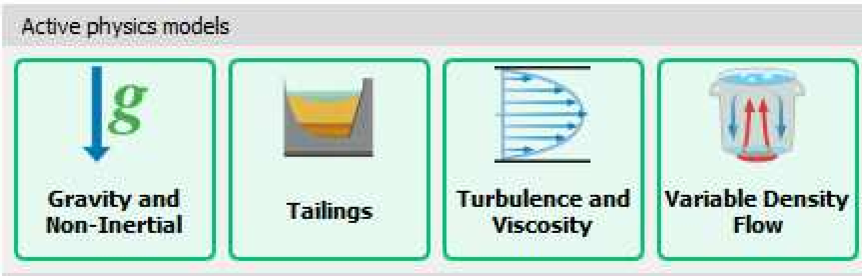

Fig. 5.18: Experimental setup – Physics considered in the numerical Flow 3D model

Initial Condition and Boundary conditions

o complete the development of the numerical model, it is necessary to define the initial and boundary conditions.

For a dambreak model, such as the flume case, the primary initial condition is the initial volume of the debris flow. As previously mentioned, the volume is 120 liters.

This volume was preliminarily created in 3D, consistent with the flume geometry, and then implemented in Flow 3D as an initial condition.

In addition to the volumetric element representing the debris flow, an initial water level was also defined at the location of the retention tank.

This contributes to improved numerical stability, as it also acts as an outlet boundary condition.

Furthermore, boundary conditions were specified. Unlike traditional numerical models, a CFD model requires boundary conditions to be defined for each face of the mesh blocks.

In this case, atmospheric pressure was assigned where appropriate, along with a symmetry condition a continuity condition that must be applied to the shared faces between adjacent mesh blocks.

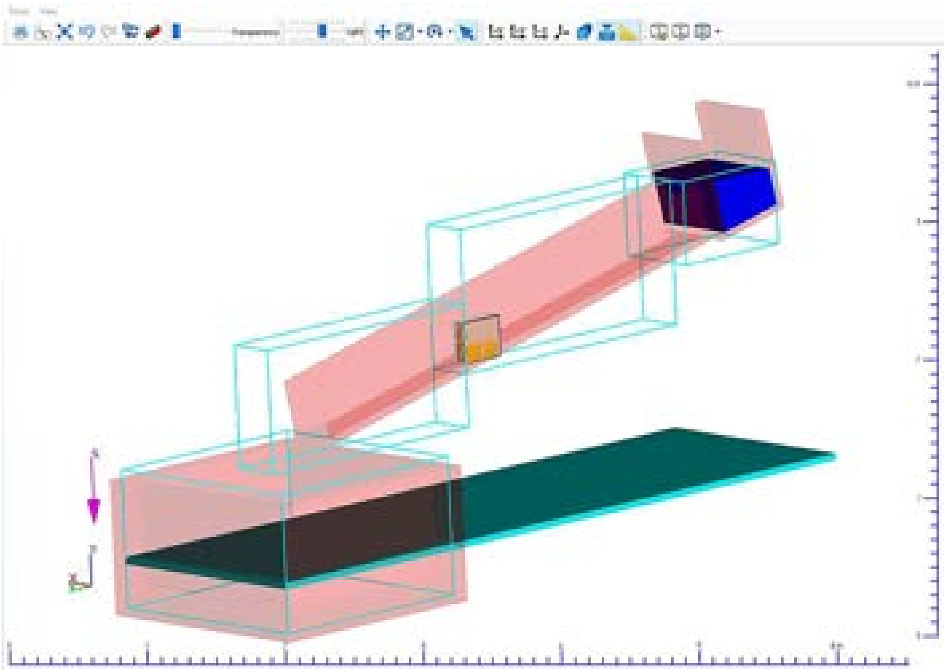

Fig. 5.19: Experimental setup – Flow 3d model initial condition

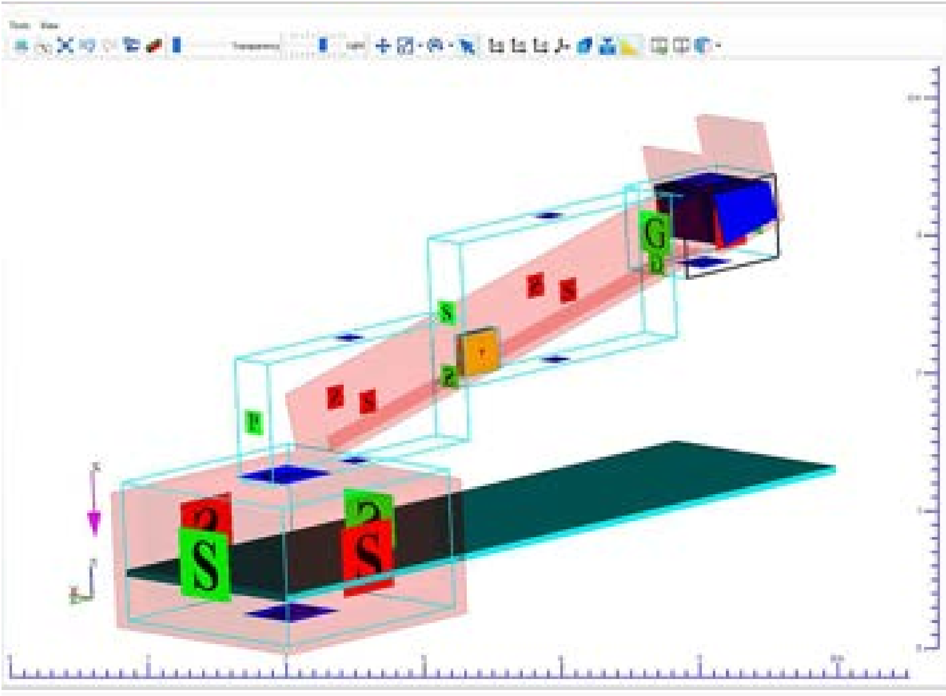

Fig. 5.20: Experimental setup – Flow 3d model boundary condition

In addition, for improved interpretation of the results and calibration of the model, two control sections were inserted within the numerical domain, located between the pier and the gate.

These sections allow for the analysis of key hydraulic parameters in order to verify compliance with the similarity principles adopted for scaling the model.

This aspect will be discussed in detail in the following chapter.

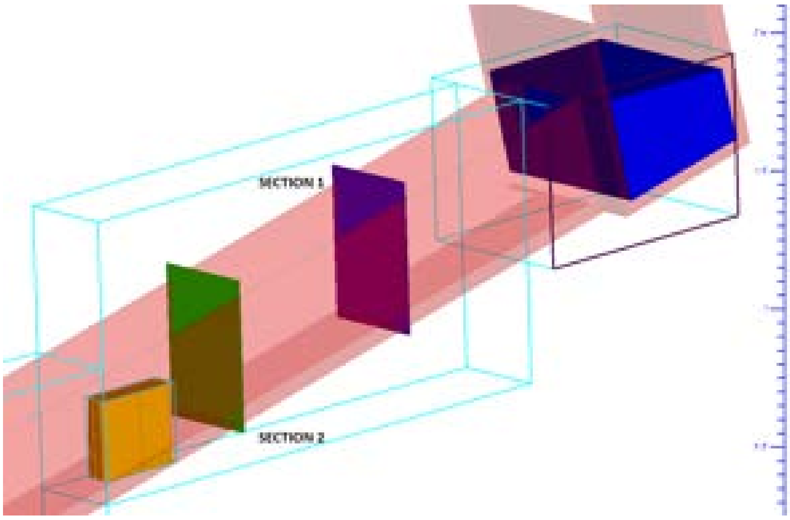

Fig. 5.21: Experimental setup – Flow 3D model control section location

5.2 Scale Modeling Framework and Dimensional Analysis

This section outlines the dimensional scaling approach adopted to investigate the debris flow impact on a bridge pier using FLOW-3D numerical simulations. The aim of this study is to perform a Class A prediction of a physical laboratory model and evaluate how scale effects influence the flow dynamics and impact forces when transitioning from small-scale models to real-world scenarios.

The base case is the experimental flume model described in the previous section, which is assigned a geometrical scale of 1:1. The three additional models represent progressively larger scenarios where the laboratory flume simulates a 1:10, 1:25, and 1:50 scaled down version of a real installation. The 1:50 case corresponds to the true scale of the real bridge pier, part of the high-speed railway viaduct "VI01" discussed in the previous sections.

To capture the governing flow dynamics across all scales, the analysis was framed around nondimensional group theory, particularly the Froude number and Bingham number, both of which characterize the behavior of free-surface flows and non-Newtonian fluids, respectively.

5.2.1 Scaling Methodology

The methodology employed is rooted in classical similitude theory and the Buckingham π theorem, which provides a systematic approach for identifying dimensionless parameters that govern the physical behavior of a system. In the context of debris flow impact modeling, the most relevant dimensionless numbers include:

- **Froude Number (Fr):** characterizing the ratio between inertial and gravitational forces,

$$Fr = \frac{V}{\sqrt{gH}}$$

- **Bingham Number (Bn):** describing the dominance of yield stress over viscous stress.

$$Bn = \frac{\tau_y H}{\mu_p V}$$

Where:

- V: characteristic flow velocity [m/s],
- H: flow depth [m],
- g: gravitational acceleration [m/s^2],
- τy: yield stress [Pa],
- μp: plastic viscosity [Pa· s].

Debris flows are governed by both inertial and rheological forces; however, for the purpose of studying impact forces, inertial forces dominate, making the Froude number the preferred scaling parameter.

Using Froude similarity allows for the correct replication of the dynamic behavior of the free-surface flow, even in the presence of complex rheology.

To derive the scaled parameters for the 1:10, 1:25, and 1:50 models, Froude similarity was adopted. This requires the Froude number to be invariant across all scales:

$$Fr_{model} = Fr_{prototype} \Rightarrow \frac{V_m}{\sqrt{gH_m}} = \frac{V_p}{\sqrt{gH_p}}$$

From which we derive the velocity relations:

$$\frac{V_m}{V_p} = \sqrt{\frac{H_m}{H_p}} = \sqrt{\lambda_L} \quad \Rightarrow \quad \lambda_V = \lambda_L^{0.5}$$

Where λL is the geometric scale factor (10, 25, 50).

Using these, all other parameters are scaled accordingly.

The yield stress and plastic viscosity of the Bingham model are rescaled using the condition of Froude similarity while acknowledging that this does not conserve the Bingham number.

With non-Newtonian behavior, one cannot preserve both Fr and Bn exactly. In this work we prioritize Fr to reproduce wave kinematics and impact timing. The rheological parameters adopted for upscaling are therefore pragmatically scaled from the laboratory values:

$$\tau_y(\lambda_L) = \tau_{y,lab}\,\lambda_L \qquad \mu_p(\lambda_L) = \mu_{p,lab}\,\sqrt{\lambda_L}$$

To further validate the respect of Froude similarity across the models, two control sections, Section 1 and Section 2 were introduced in each FLOW-3D model.

In order to maintain numerical consistency and computational efficiency, the total number of mesh cells was kept constant across the models. Consequently, the grid resolution was adjusted in proportion to the scale factor. This ensured that:

$$\Delta x_{model} = \lambda_L \cdot \Delta x_{lab}$$

However, coarsening the mesh implies that smaller-scale features (such as boundary layers and stress gradients) may not be fully resolved, requiring compensation through adjusted rheological parameters.

Thus, Froude-based parameter scaling was essential to balance this loss in resolution.

Parameter	**Prototype (Lab)**	**1:10 Scale**	**1:25 Scale**	**1:50 Scale (Real)**
Geometric Scale (λ_L)	1	10	25	50
Flow Depth H [m]	H_0	$10 \cdot H_0$	$25 \cdot H_0$	$50 \cdot H_0$
Velocity V [m/s]	V_0	$3.16 \cdot V_0$	$5.00 \cdot V_0$	$7.07 \cdot V_0$
Yield Stress τ_y [Pa]	6.8	68	170	340
Plastic Viscosity μ_p [Pa·s]	0.0039	0.039	0.098	0.196
Coarse Tailing Concentration [kg/m³]	1192.5	1192.5	1192.5	1192.5
Mesh Size [m]	0.01 / 0.02	0.1 / 0.2	0.25 / 0.5	0.5 / 1.0
Total Mesh Cells	≈ 1.2 million	≈ 1.2 million	≈ 1.2 million	≈ 1.2 million

Table 5.2 – Summary of Model Input Parameters

5.3 Results and Comparisons

After defining the laboratory-scale flume model and the three scaled models, as described in the previous chapters, simulations were carried out in Flow 3D using the following simulation times:

- Laboratory flume: 2.5 s
- 1:10 scale model: 5 s
- 1:25 scale model: 8 s
- 1:50 scale model: 10 s

The following sections present the results for each model, followed by a comparative analysis highlighting the effects of the scale ratio between the full-scale model and the laboratory model.

5.3.1 Laboratory flume model results

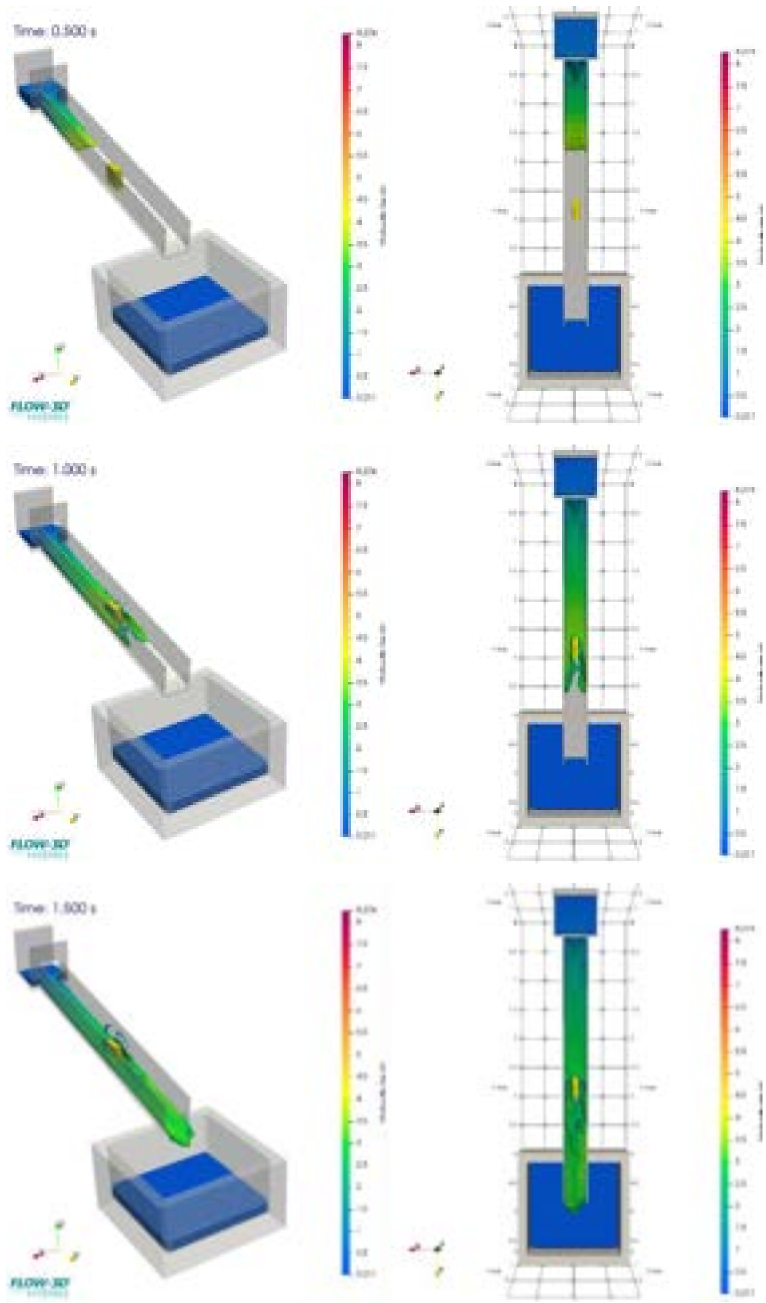

Fig. 5.22: Laboratory flume model velocity results – time 0.00 sec – 1.50 sec

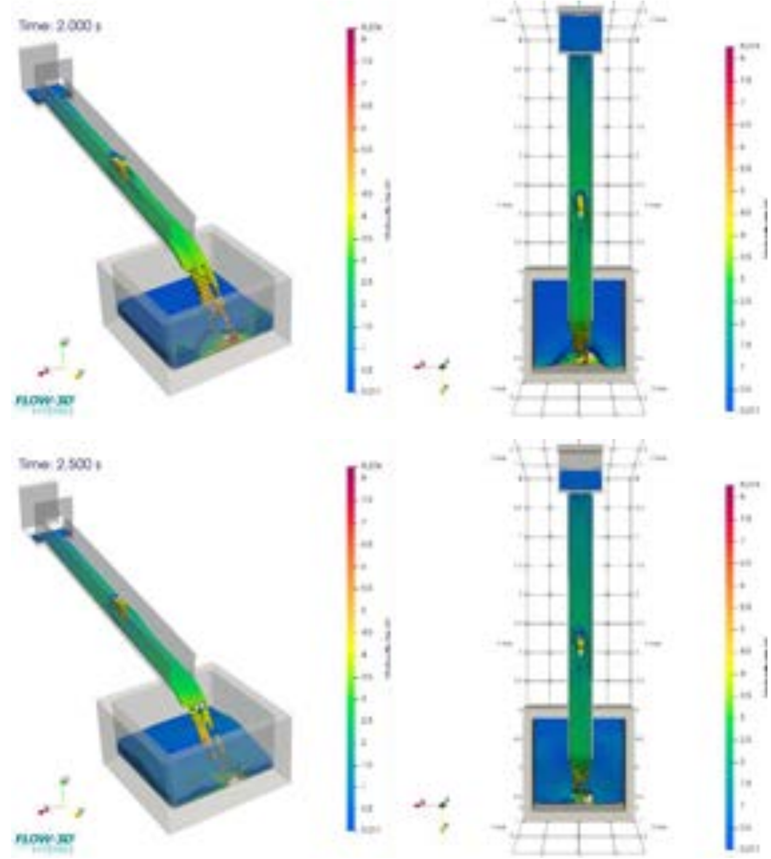

Fig. 5.23: Laboratory flume model velocity results – time 2.00 sec – 2.50 sec

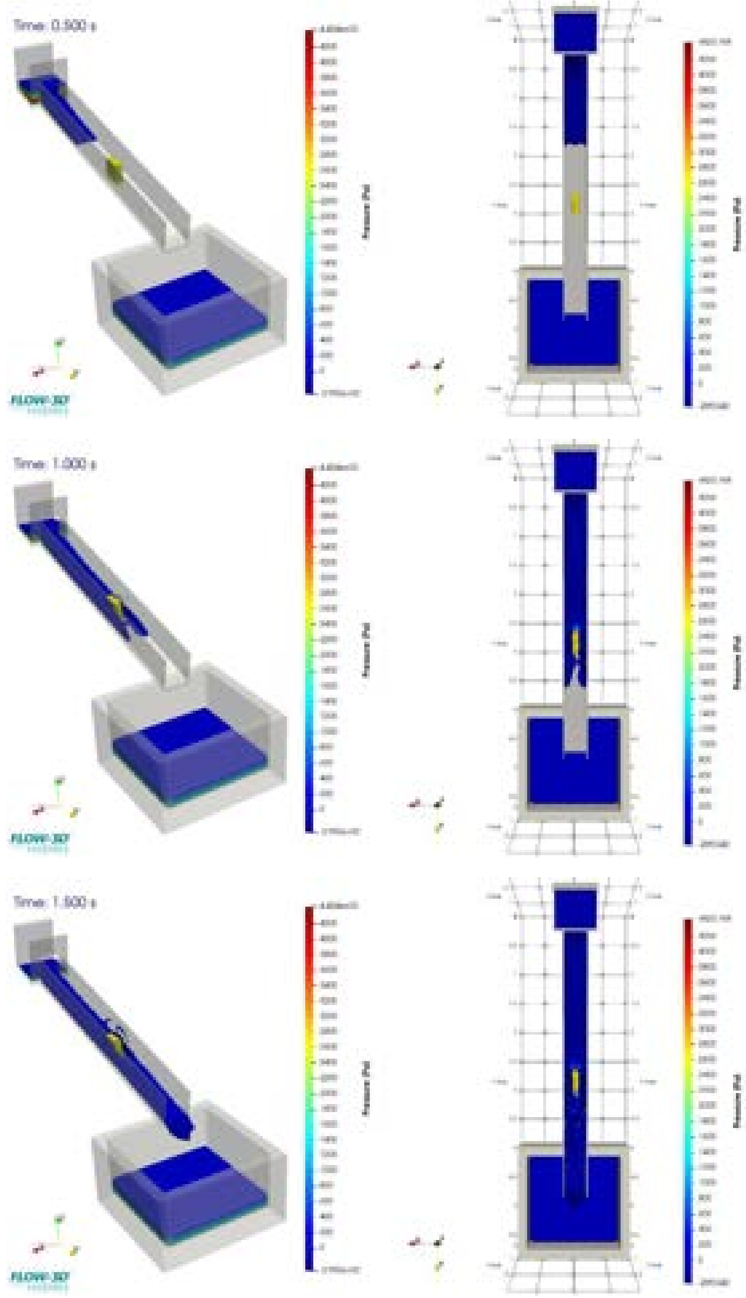

Fig. 5.24: Laboratory flume model pressure results – time 0.00 sec – 1.50 sec

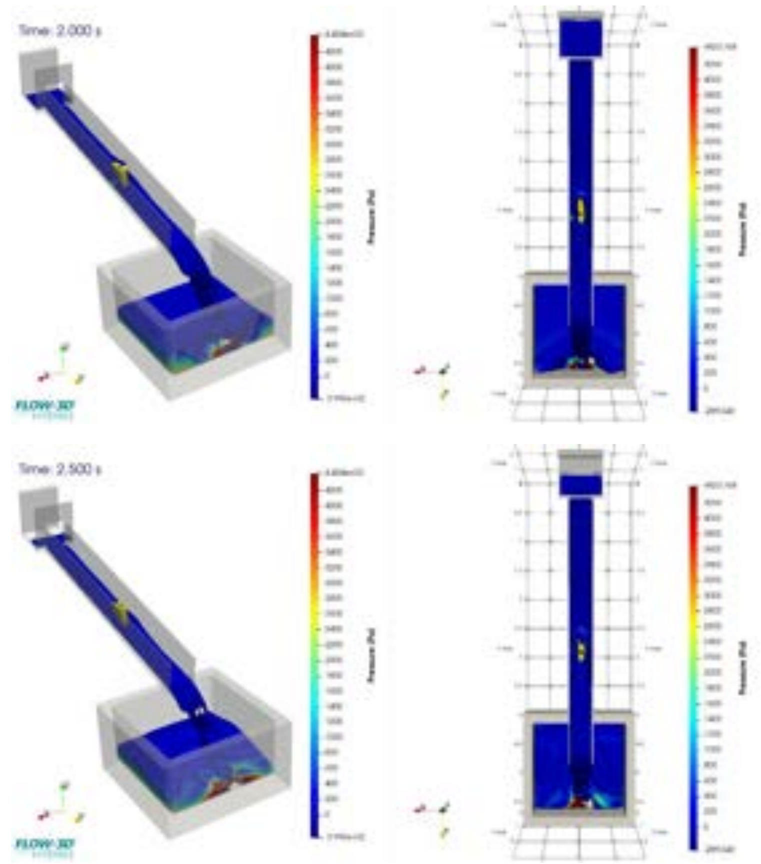

Fig. 5.25: Laboratory flume model pressure results – time 2.00 sec – 2.50 sec

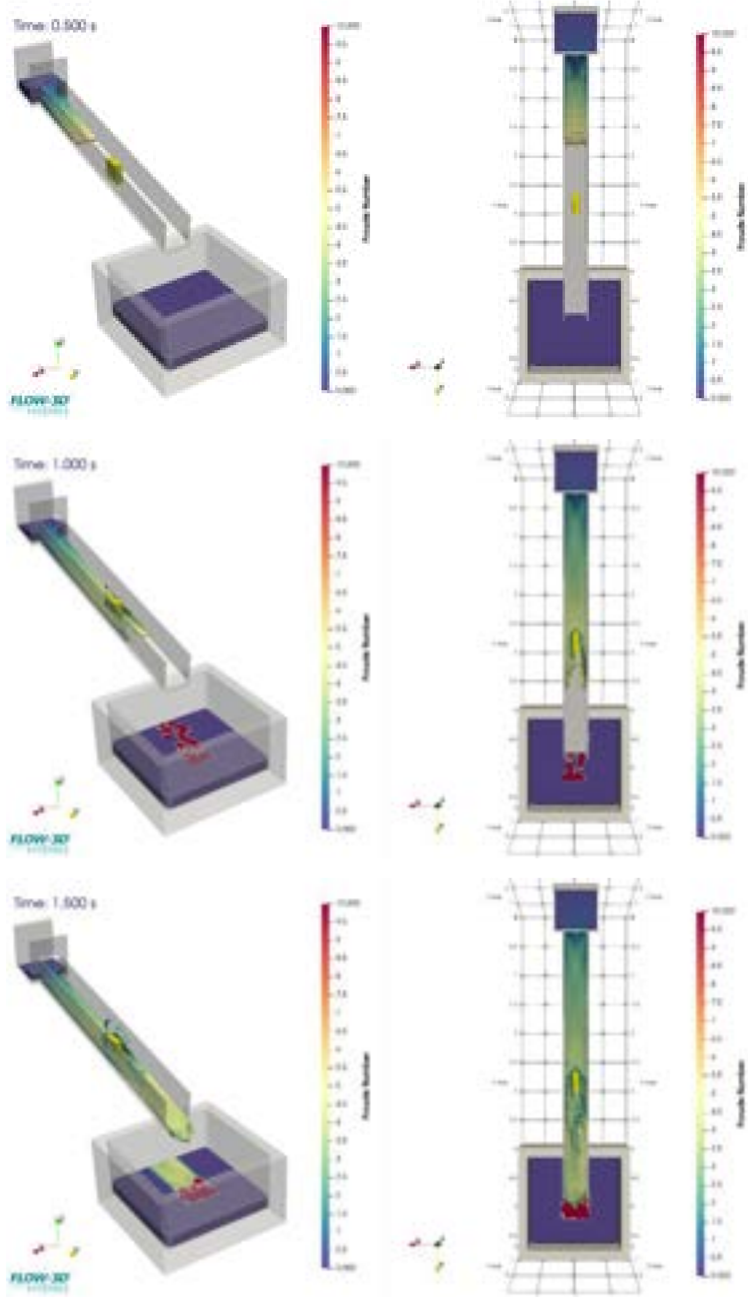

Fig. 5.26: Laboratory flume model Froude number results – time 0.00 sec – 1.50 sec

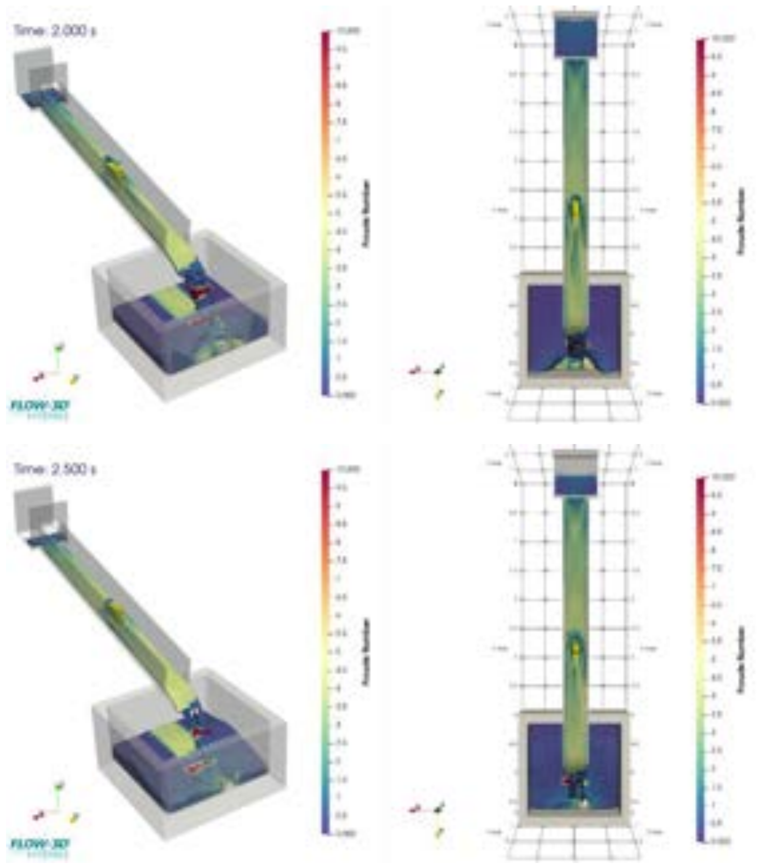

Fig. 5.27: Laboratory flume model Froude number results – time 2.00 sec– 2.50 sec

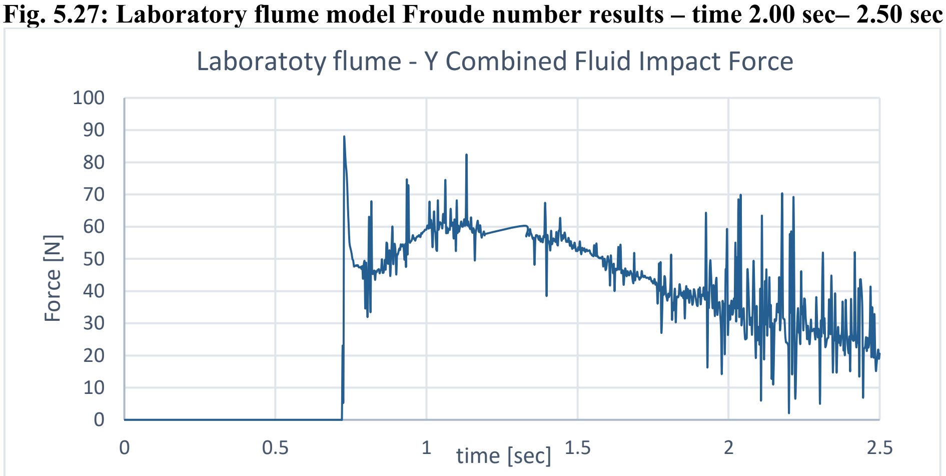

Fig. 5.28: Laboratory flume model Pier Impact Force

5.3.2 Scale 1:10 model results

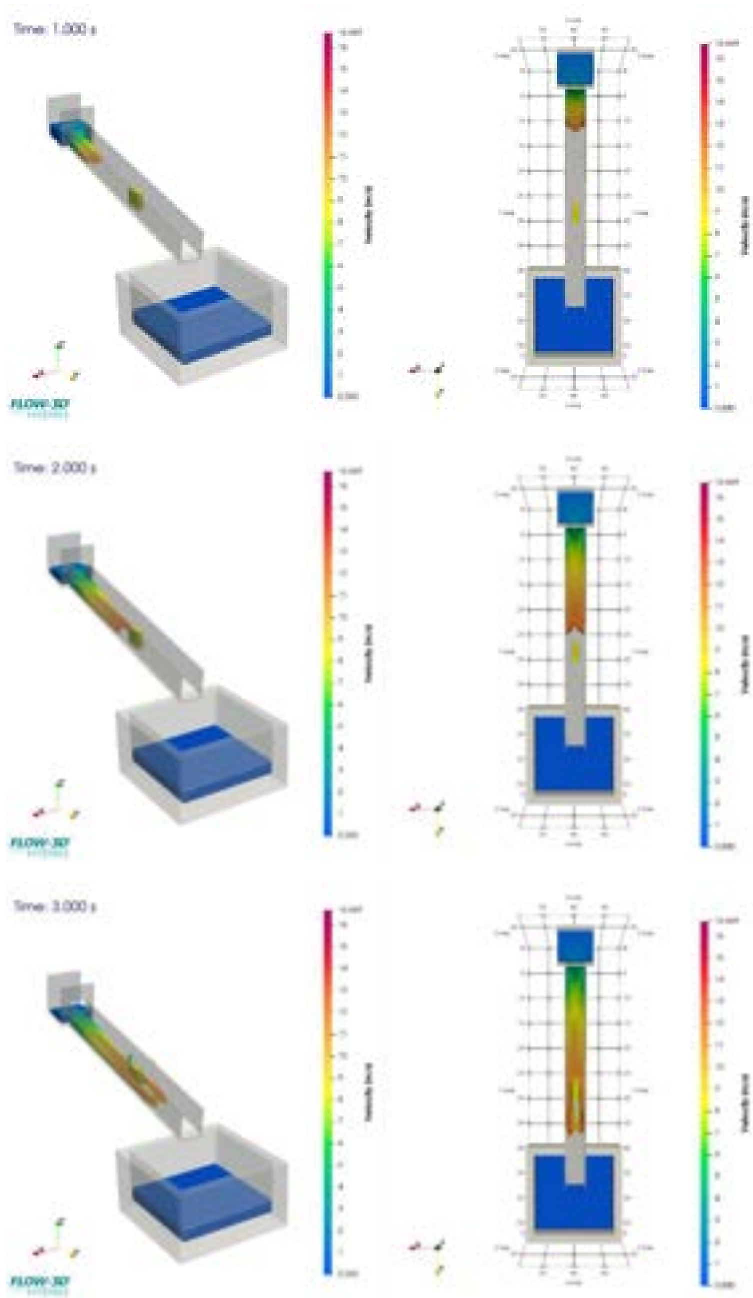

Fig. 5.29: Scale 1:10 model Velocity results – time 0.00 sec – 3.00 sec

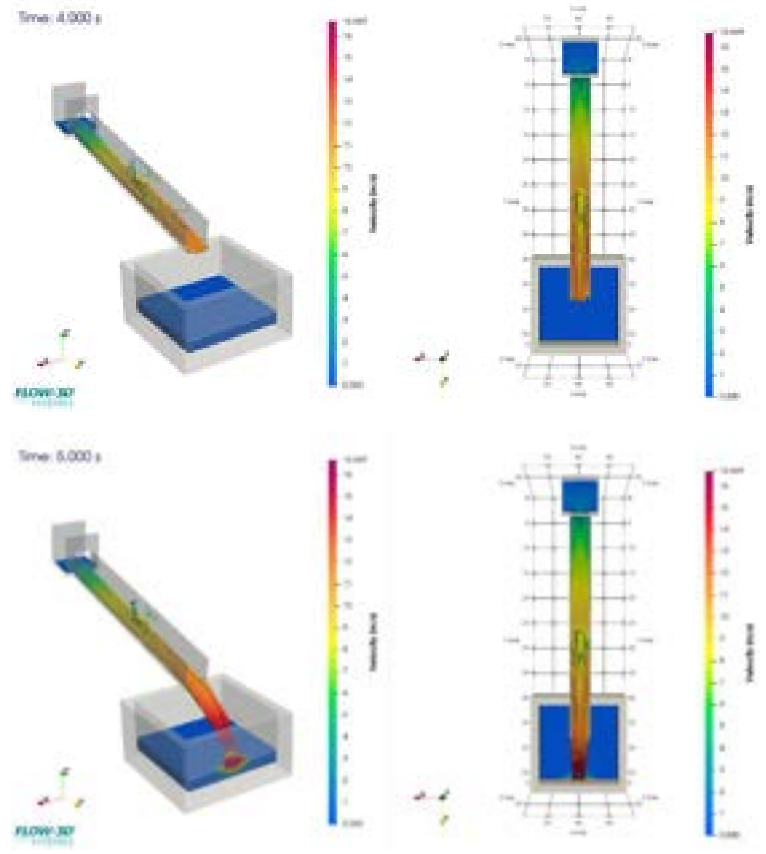

Fig. 5.30: Scale 1:10 model Velocity results – time 4.00 sec – 5.00 sec

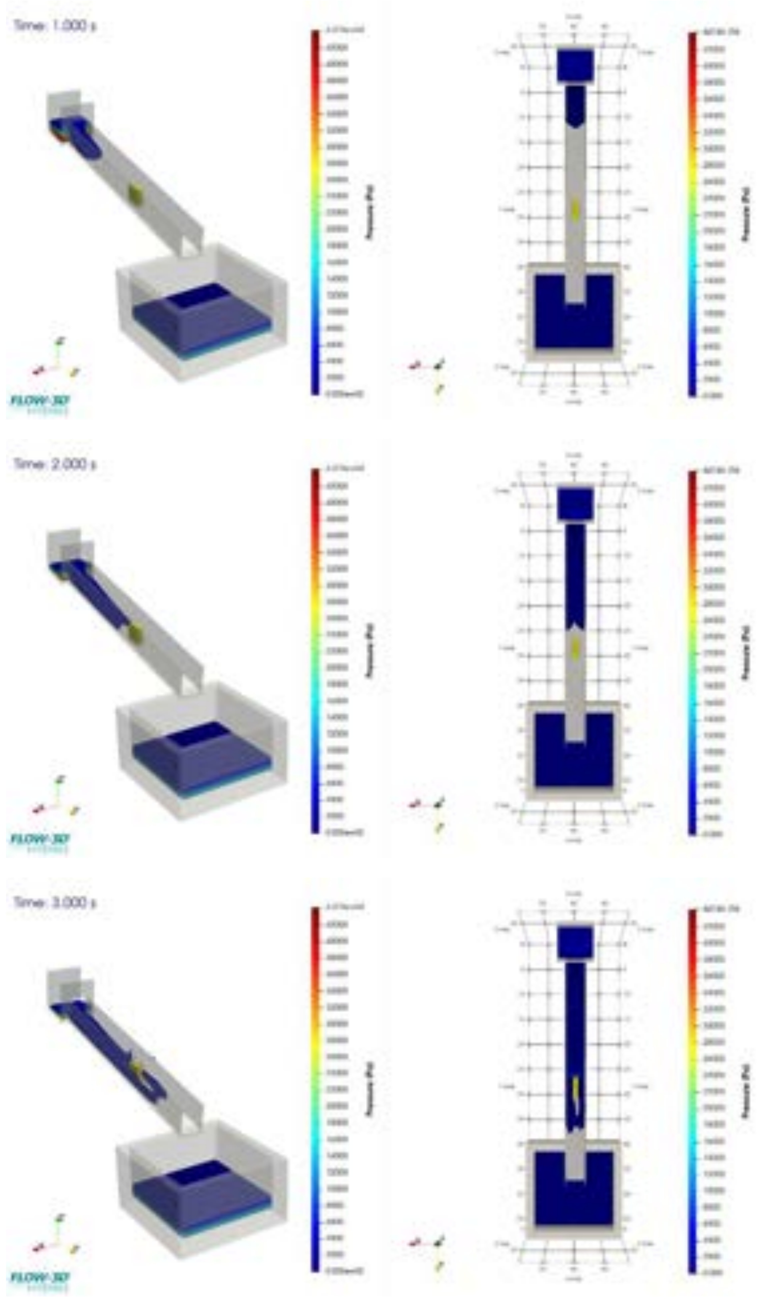

Fig. 5.31: Scale 1:10 model Pressure results – time 0.00 sec – 3.00 sec

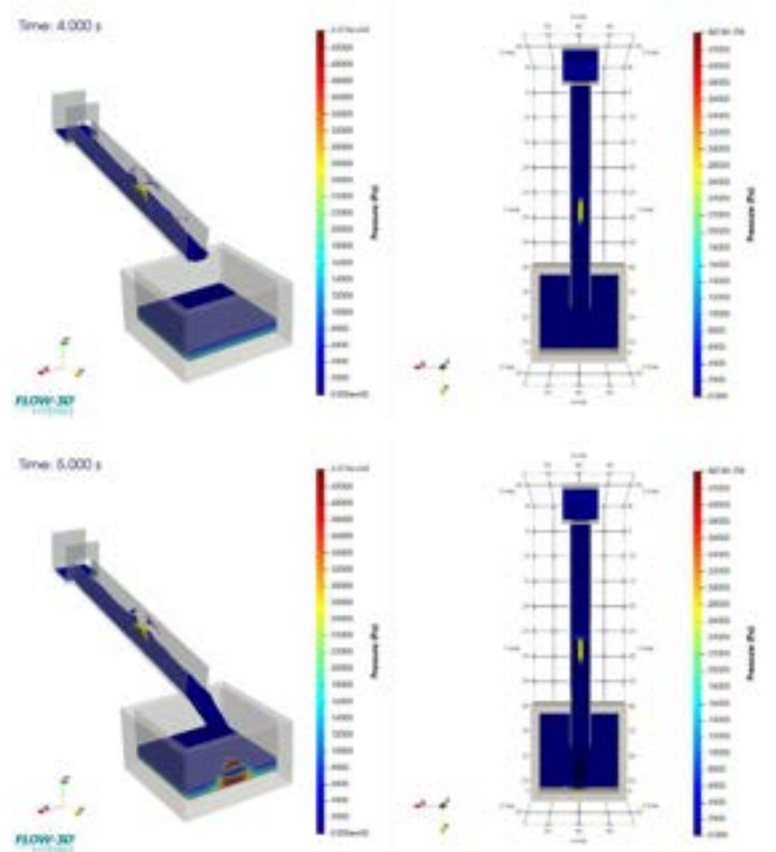

Fig. 5.32: Scale 1:10 model Pressure results – time 4.00 sec – 5.00 sec

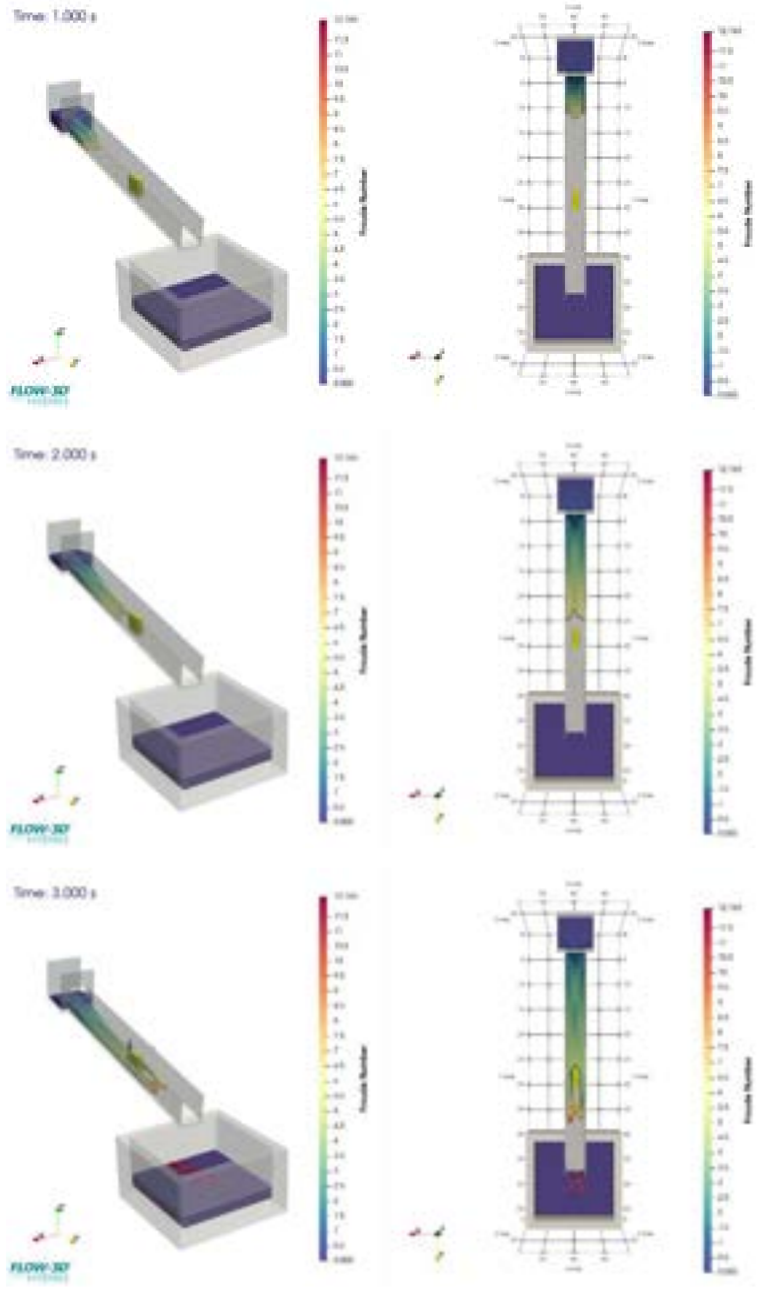

Fig. 5.33: Scale 1:10 model Froude Number results – time 0.00 sec – 3.00 sec

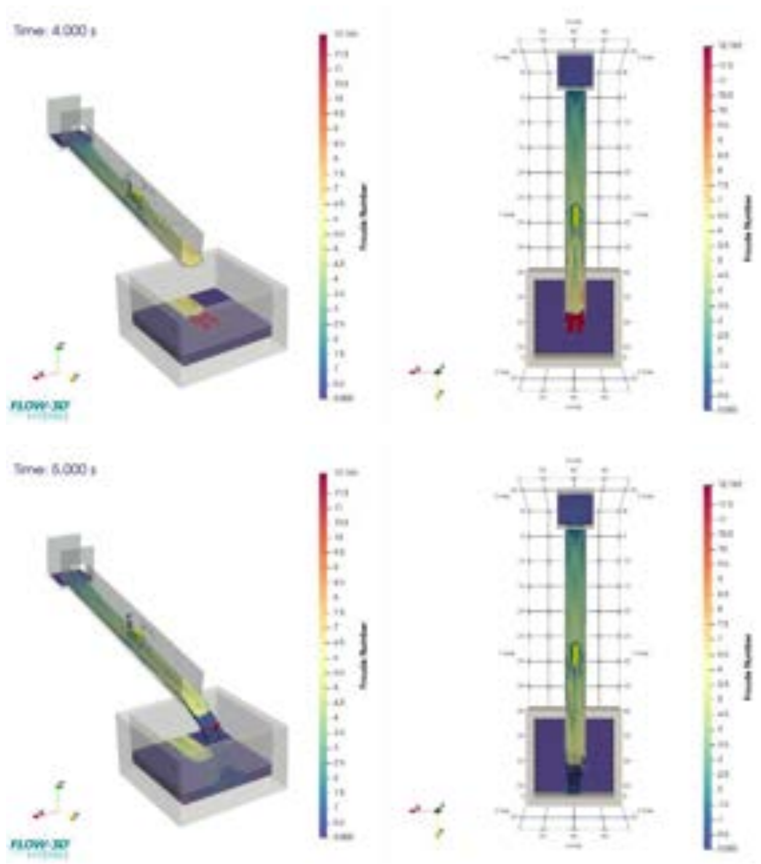

Fig. 5.34: Scale 1:10 model Froude Number results – time 4.00 sec – 5.00 sec

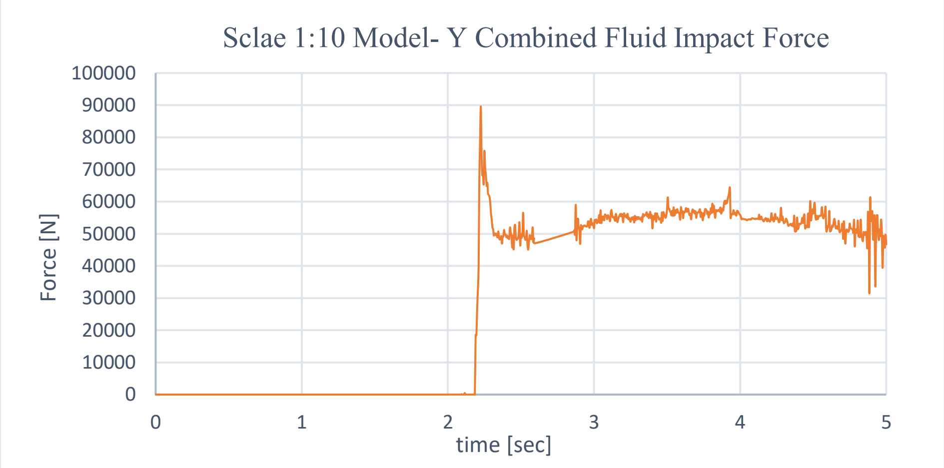

Fig. 5.35Scale 1:10 model Pier Impact Force

5.3.3 Scale 1:25 model results

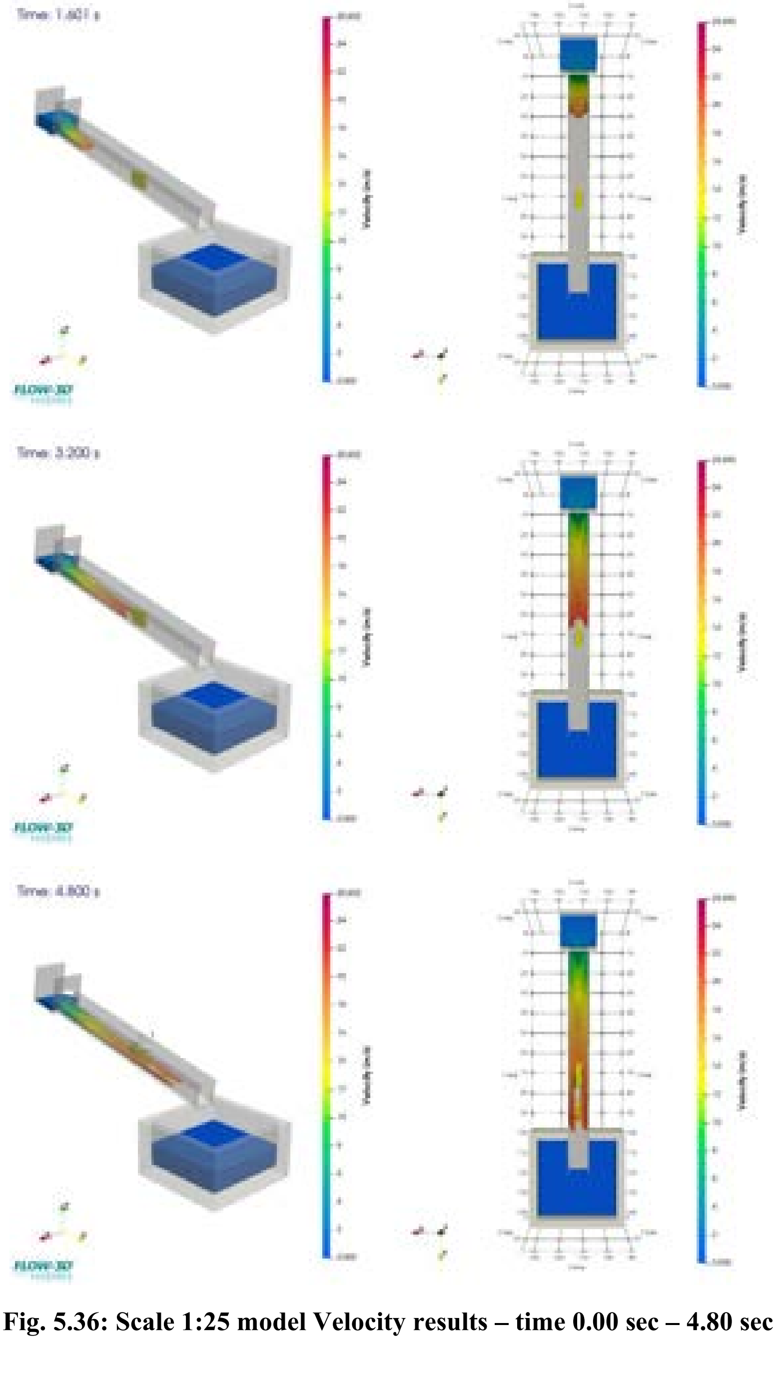

Fig. 5.36: Scale 1:25 model Velocity results – time 0.00 sec – 4.80 sec

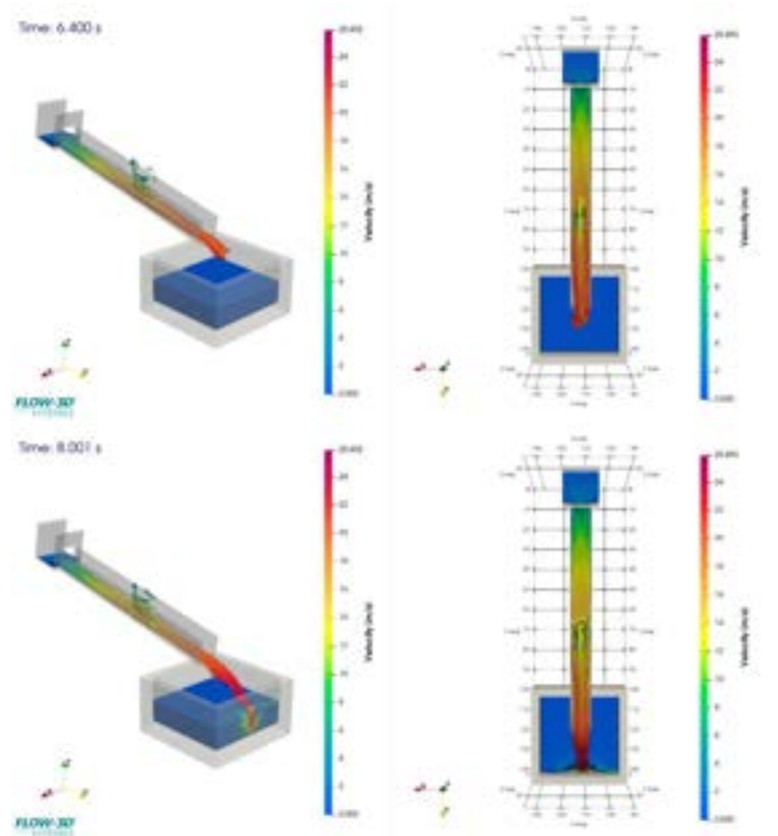

Fig. 5.37: Scale 1:25 model Velocity results – time 6.40 sec – 8.00 sec

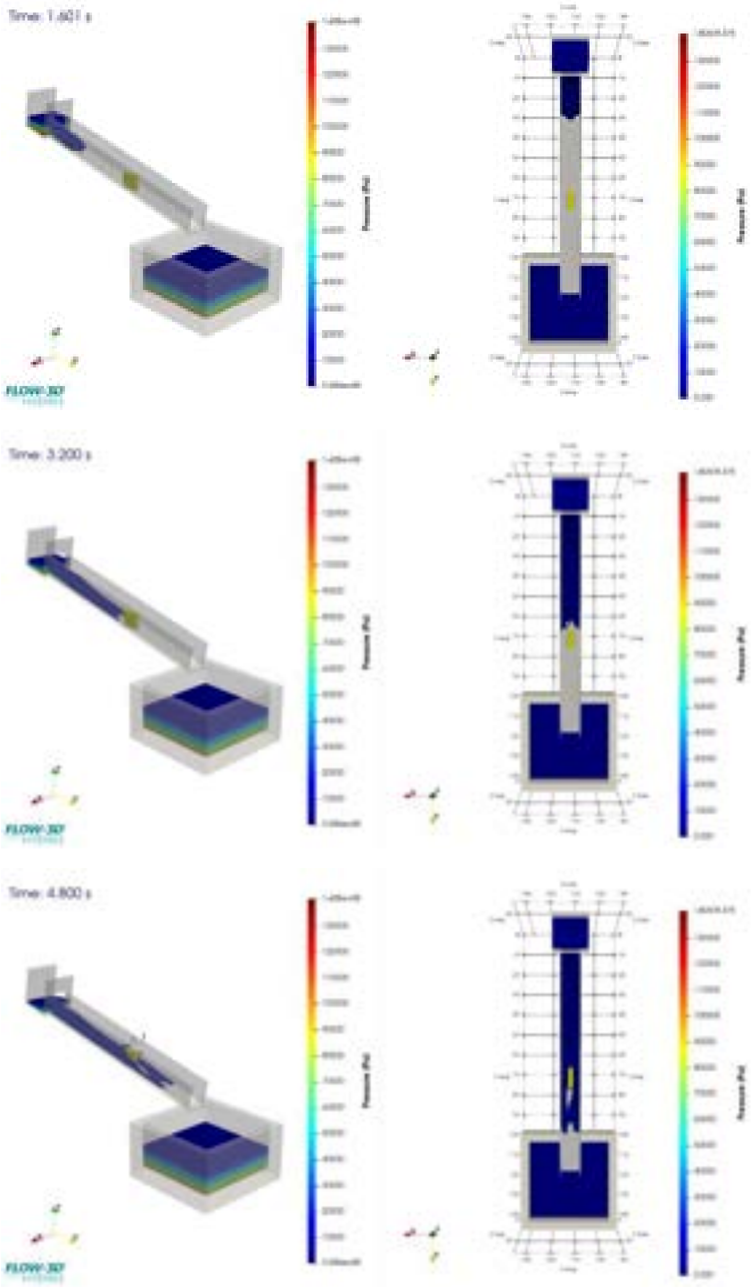

Fig. 5.38: Scale 1:25 model Pressure results – time 0.00 sec – 4.80 sec

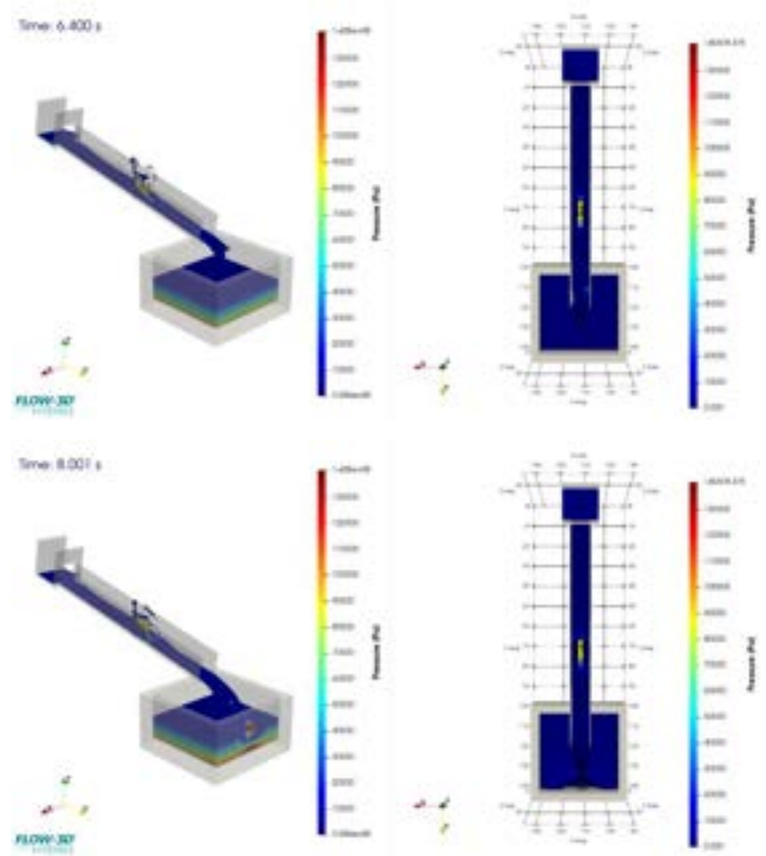

Fig. 5.39: Scale 1:25 model Pressure results – time 6.40 sec – 8.00 sec

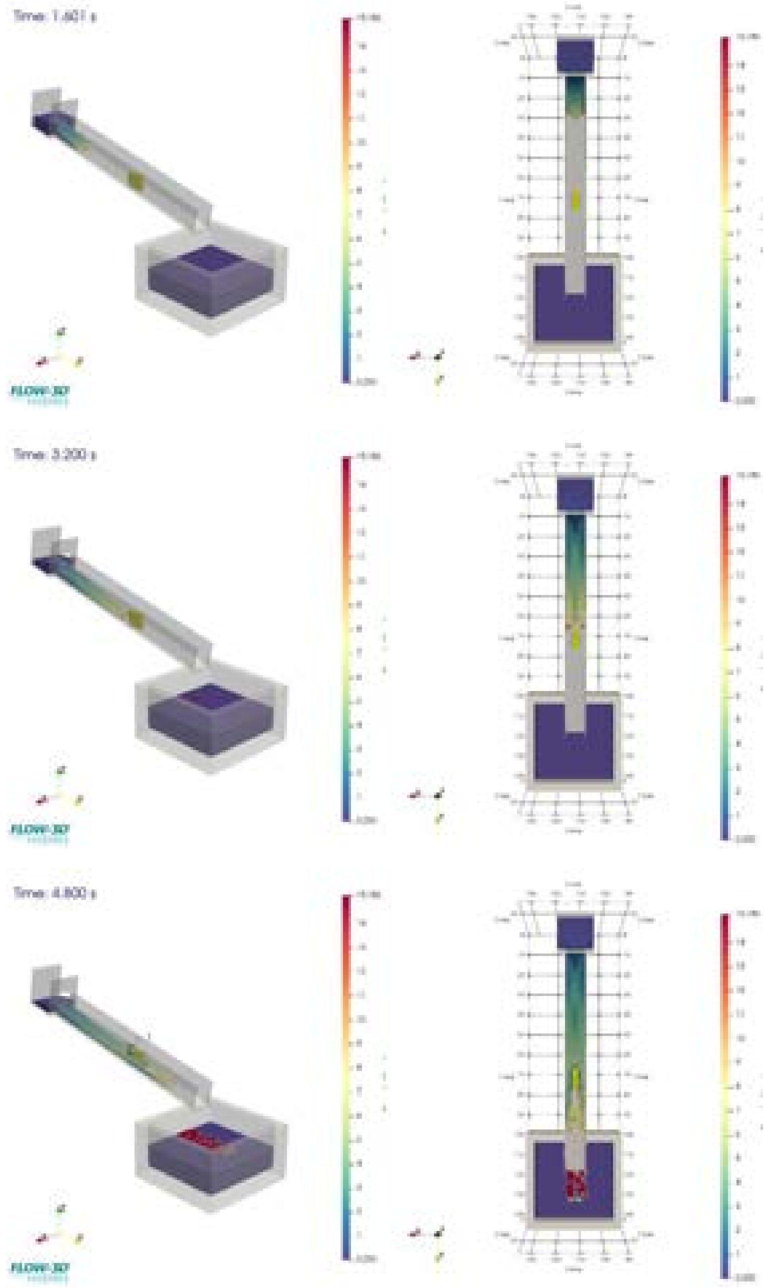

Fig. 5.40: Scale 1:25 model Froude Number results – time 0.00 sec – 4.80 sec

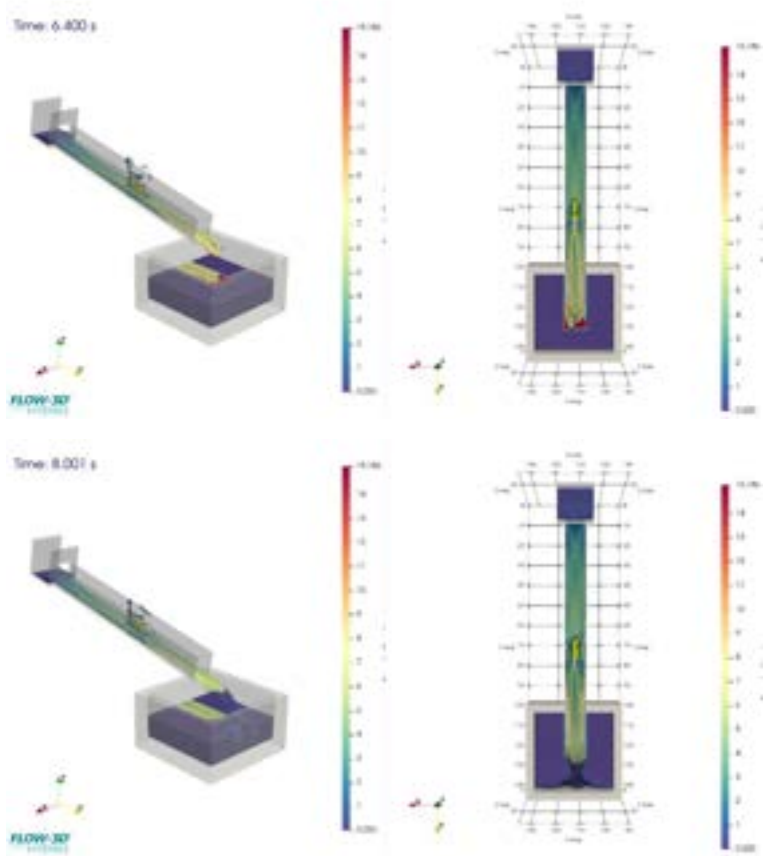

Fig. 5.41: Scale 1:25 model Froude Number results – time 6.40 sec – 8.00 sec

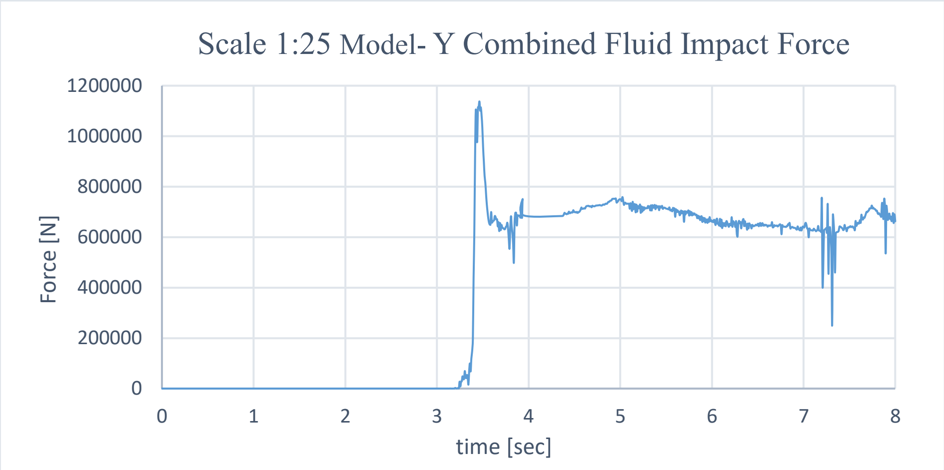

Fig. 5.42Scale 1:25 model Pier Impact Force

5.3.4 Scale 1:50 model results

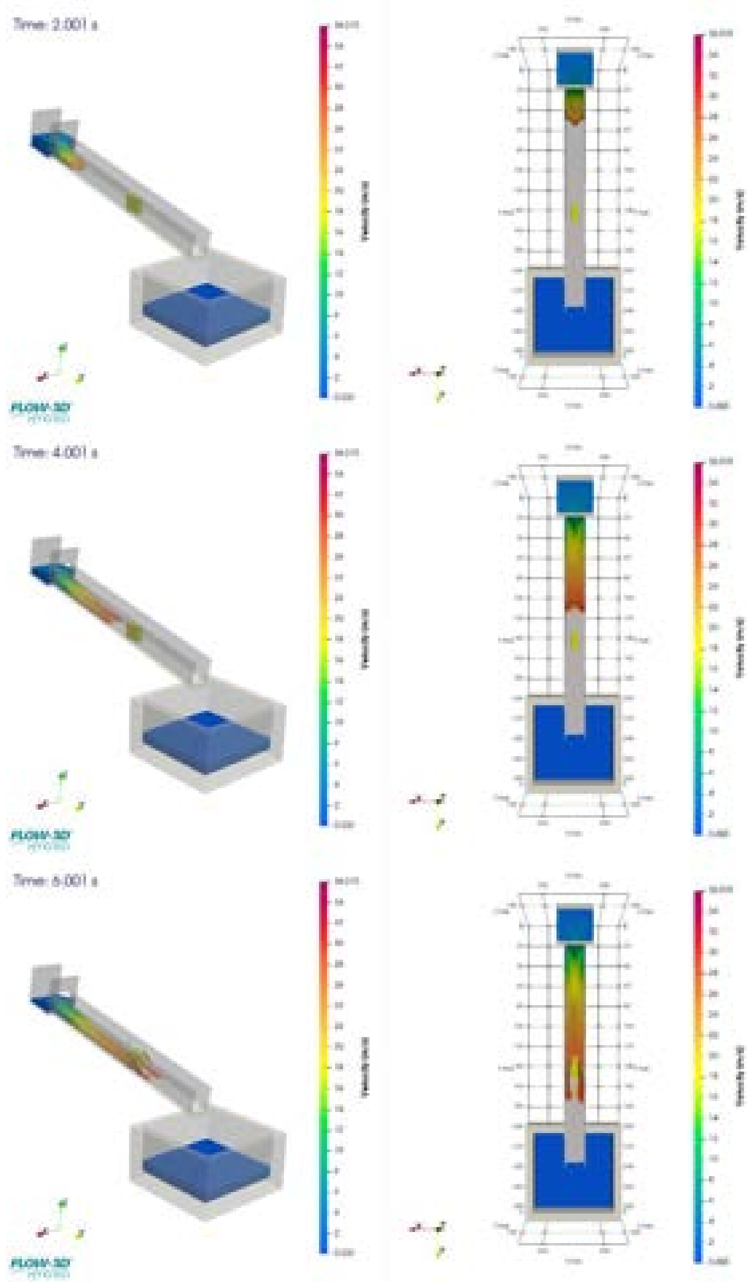

Fig. 5.43: Scale 1:50 model Velocity results – time 0.00 sec – 6.00 sec

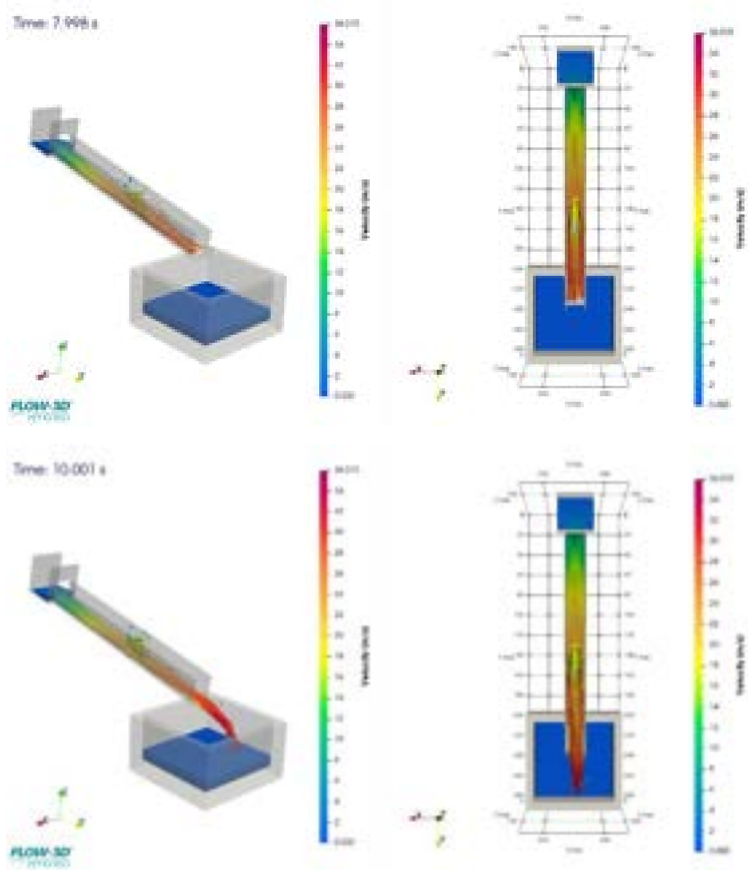

Fig. 5.44: Scale 1:50 model Velocity results – time 8.00 sec – 10.00 sec

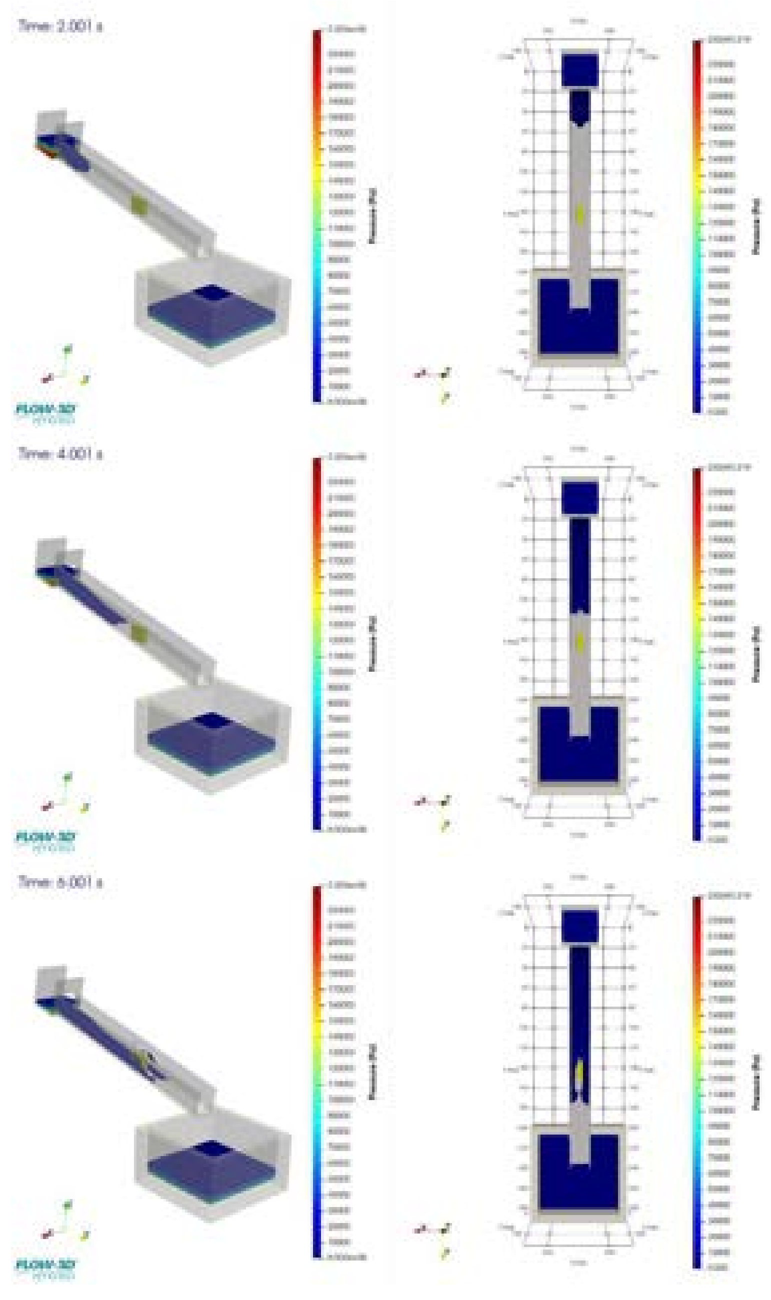

Fig. 5.45: Scale 1:50 model Pressure results – time 0.00 sec – 6.00 sec

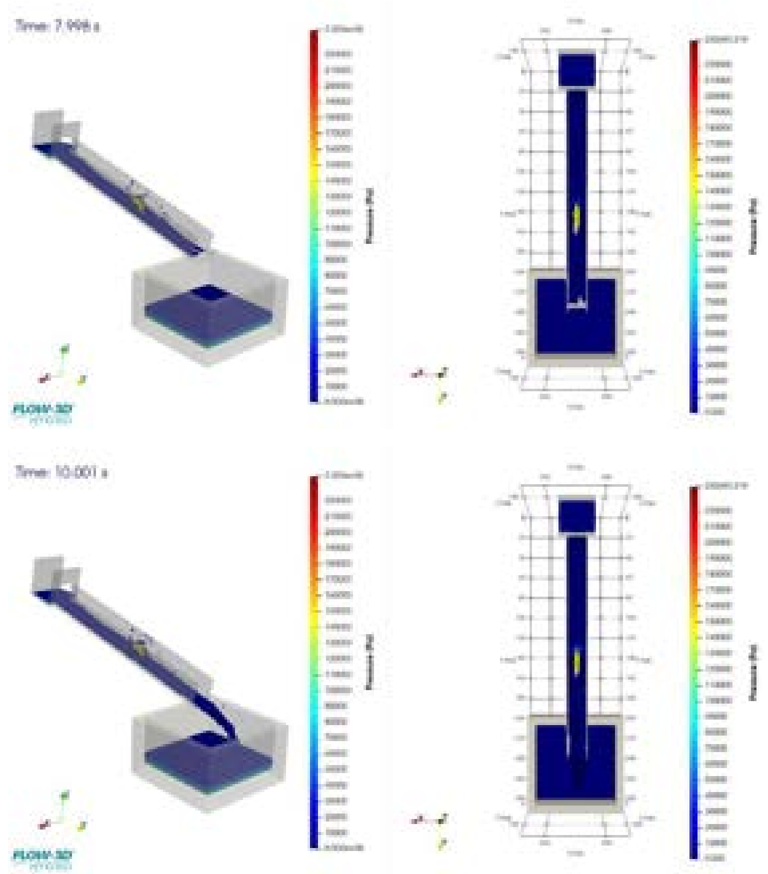

Fig. 5.46: Scale 1:50 model Pressure results – time 8.00 sec – 10.00 sec

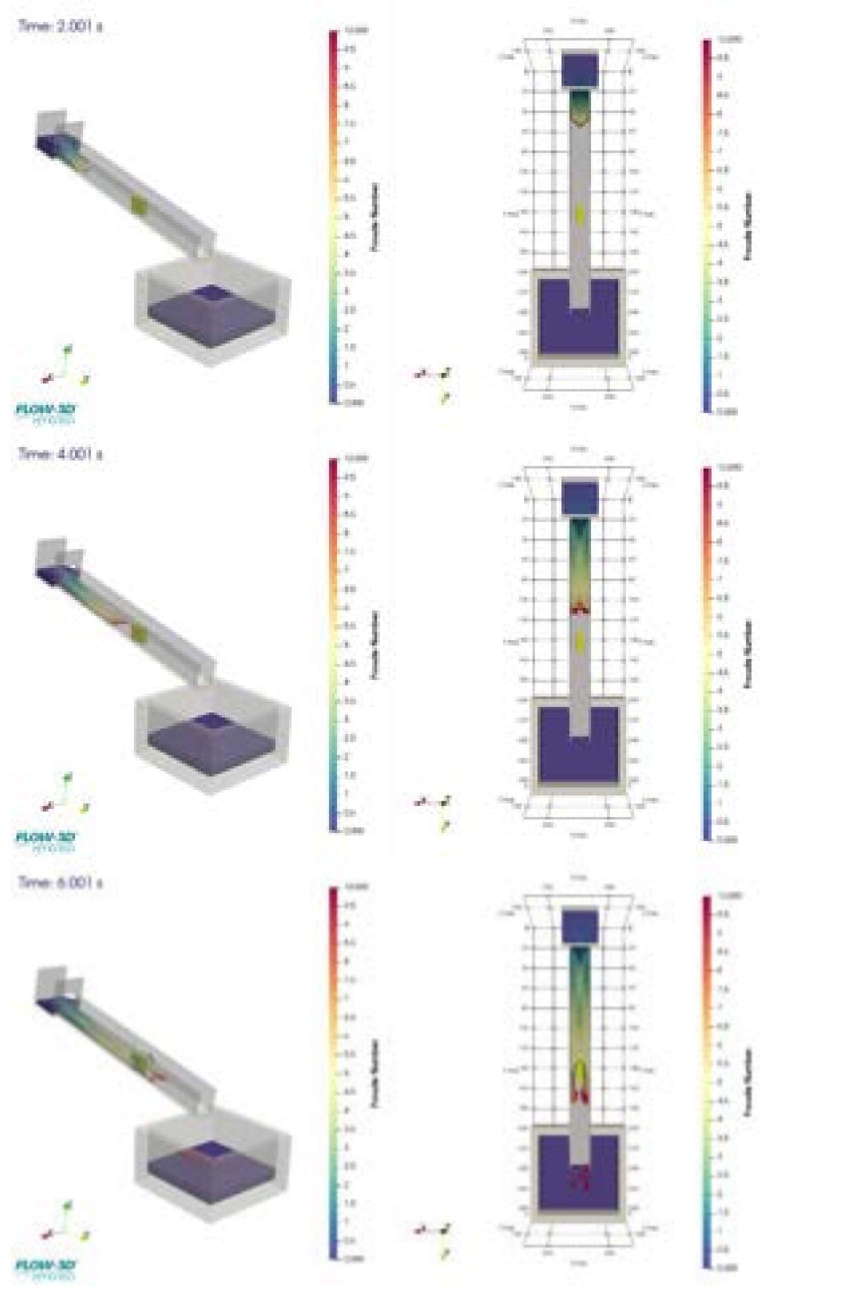

Fig. 5.47: Scale 1:50 model Froude Number results – time 0.00 sec – 6.00 sec

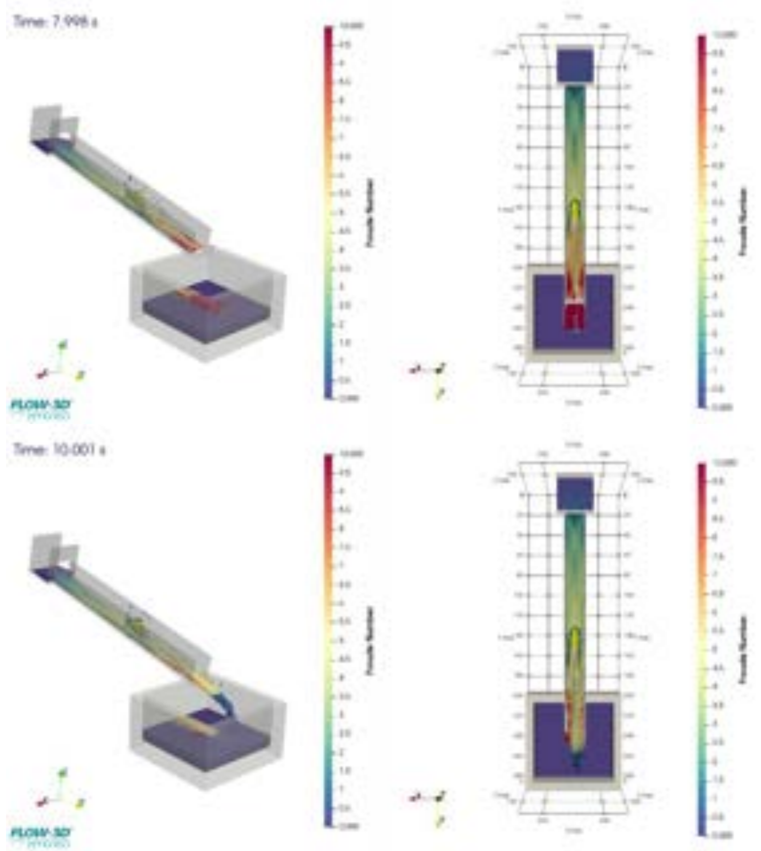

Fig. 5.48: Scale 1:50 model Froude Number results – time 8.00 sec – 10.00 sec

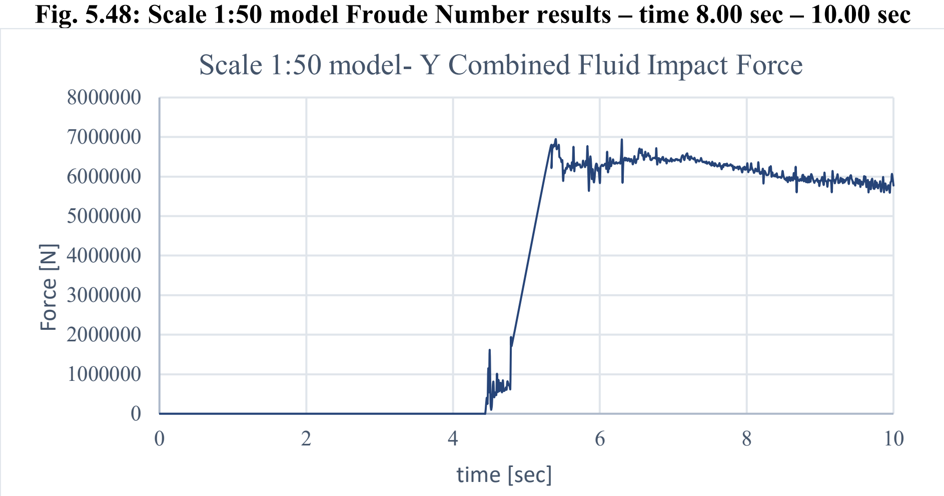

Fig. 5.49 Scale 1:50 model Pier Impact Force

5.3.5 Comparison of Results

This section synthesizes the outcomes of the four FLOW-3D simulations (Prototype 1:1, 1:10, 1:25, 1:50 real scale), focusing on (i) impact forces on the pier and their scale dependence, and (ii) dynamic similarity checks via the Froude number at the two control sections (Section 1 upstream and Section 2 downstream). Results are interpreted in the framework of Froude similitude, with rheology scaled as discussed in the previous chapter.

Impact Forces vs scale

Table 5.3 summarizes the initial impact peak forces extracted from the four simulations and compares them to the theoretical values expected from Froude scaling ($\propto \lambda\_L^3$). The measured growth factors are close to the theoretical ones; at the same time, the absolute error increases with scale. In particular, the segment of the curve between 1:25 and 1:50 shows a steeper slope than the preceding segments, indicating that the deviation from the ideal cubic law does not grow linearly with a constant slope. In practical terms: the smaller the laboratory scale relative to the real case, the smaller the scale-effect errors on the impact force.

Scale	Initial Impact Peak [N]	Expected (Froude) [N]	Error [%]	Growth vs Prototype (Model)	Growth vs Prototype (Theory)
1:1 (Prototype)	87.69	87.69	0.00	0.00	0
1:10	89,638.7	87,699.6	2.21	1,022.11	1,000
1:25	1,446,722	1,370,306	5.58	16,496.34	15,625
1:50 (Real scale)	13,026,900	10,962,450	18.83	148,539.98	125,000

Table 5.3 – Impact force comparison across scales

Two takeaways:

1. Near-cubic growth is captured: 1:10 and 1:25 closely follow λ_L^3 (+2.2% and +5.6% respectively).
2. Nonlinear departure at 1:50: the ~19% positive deviation is consistent with the increasing dominance of fully three-dimensional, transient free-surface effects and the material heterogeneity of a debris mixture. For a 3D flow governed by x–y–z interactions and a non-homogeneous slurry, an error of order 20% at 1:50 is acceptable for Class-A predictions centered on peak loads.

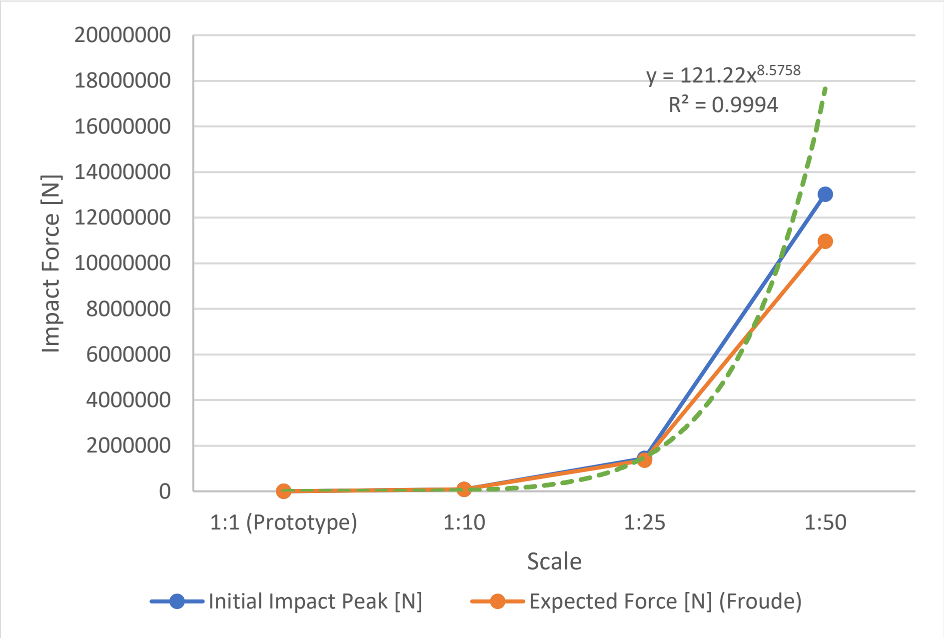

Fig. 5.50 Comparison of impact forces across scales

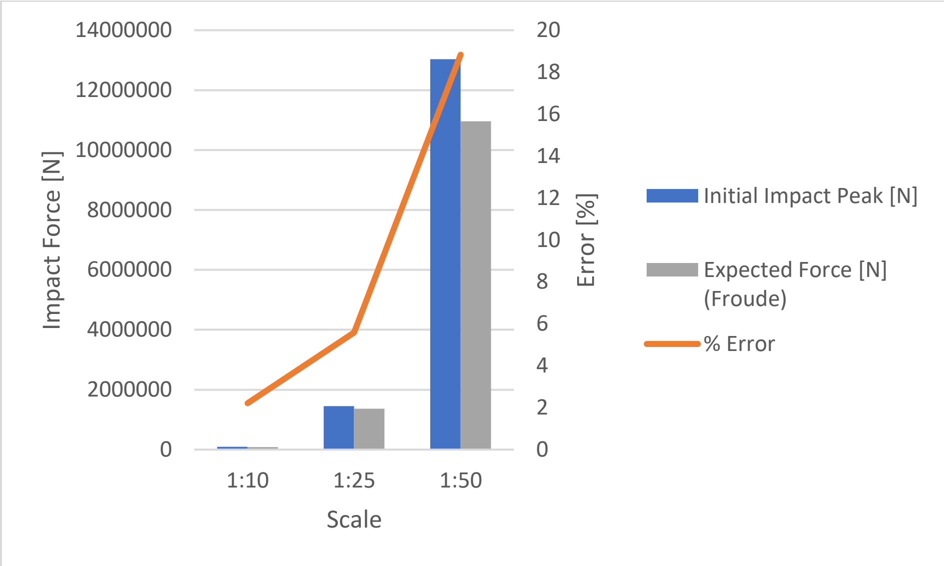

Fig. 5.51 Error between measured and Froude-expected forces

Besides the theoretical $F \propto \lambda_L^3$ growth implied by Froude similarity, the impact-force series can be described by an empirical trendline drawn on the points in Fig. 5.50.

$$y = 121.22\, x^{8.5758}, \qquad R^2 = 0.9994$$

This trendline captures remarkably well the non-linear increase of the force, especially the steeper rise from 1:25 to 1:50, and it is therefore a convenient descriptive law for the data shown in the figure.

For a physically meaningful scaling law directly tied to the geometric factor, it is useful to express the force as a power of the scale ratio $\lambda L \in \{1,10,25,50\}$. Fitting the same four points as $F_{peak} = a\, \lambda_L{}^b$:

$$F_{\text{peak}} \approx 87.7\, \lambda_L^{3.02}\ \text{N}, \qquad R^2 \approx 0.999$$

The exponent $b \approx 3.0$ confirms that the data follow nearly cubic growth as predicted by Froude scaling, while the visualization in Fig. 5.50 highlights that the deviation from the ideal curve increases with scale (the segment 1:25→1:50 is clearly steeper than the previous ones). In practical terms: the smaller the laboratory scale relative to the real case, the smaller the scale-effect errors on peak impact force. For the largest scale (1:50), an error of the order of ≈20% remains acceptable for a Class-A prediction in a fully three-dimensional, heterogeneous debris-flow impact.

Dynamic similarity: Froude number at control sections

Using the control sections the mean Froude number Fr was computed (with h=A/b, channel width b=0.35 m). The table below reports mean values between scaled model and prototype.

	Froude Number Section 1	Froude Number Section 2	Error Section 1	Error Section 2
Prototype	3.12	3.83	-	-
Scale 1:10	3.07	4.25	1%	11%
Scale 1:25	3.21	4.55	3%	19%
Scale 1:50	3.21	4.61	3%	20%

Table 5.4 – Froud Number Fr comparison across scales

The comparison of Froude numbers between the prototype and the full-scale models at Section 1 (upstream) shows that, with errors below 5%, Froude similarity is satisfied. At Section 2 (downstream), the increasing errors—up to a maximum of about 20% for the 1:50 real-scale model—highlight the influence of the pier on the debris flow. This corroborates the three-dimensional nature of the phenomenon and indicates that, as the scale ratio increases, additional turbulence effects arise that amplify scale effects.

5.4 Discussion and Conclusions

Aims and approach

This work set out to produce a **Class A prediction** of debris-flow impact on a bridge pier, using the Milano–Bicocca experimental flume as the 1:1 laboratory reference and three upscaled numerical models that represent real scenarios where the lab flume stands for **1:10**, **1:25**, and **1:50** scaled models of the field case (the **1:50** configuration corresponds to the real VI01 pier). The modeling framework was built on:

- **Froude similitude** to preserve the kinematics of a gravity-driven dambreak front;
- a **Bingham** rheology for the slurry, with fixed volumetric concentration Cv=0.45 and tailing concentration 1192.5 kg/m^3;
- pragmatic upscaling of rheology from the laboratory values:

  $$\tau_y(\lambda_L) = \tau_{y,lab}\,\lambda_L, \qquad \mu_p(\lambda_L) = \mu_{p,lab}\sqrt{\lambda_L},$$

  which keeps the flow resistance meaningful at larger scales while reproducing Froude similarity;
- two control sections (**Section 1** upstream and **Section 2** downstream) to monitor dynamic similarity via the **Froude number**.

Key findings

1) Impact forces scale nearly cubically with the geometric factor

Across the four models, the **initial impact peak** follows the expected **near-cubic** growth with geometric scale λ_L. Using the prototype force as reference, the measured growth factors are very close to the Froude-based prediction $F \propto \lambda_L^3$ at **1:10** (+2.2%) and **1:25** (+5.6%). At **1:50** the deviation rises to **~18.8%** (positive bias).

An **empirical trendline** drawn on the four points provides an excellent descriptive law,

$$y = 121.22\, x^{8.5758}, \qquad R^2 = 0.9994,$$

which captures the steeper rise from 1:25 to 1:50.

Expressed directly in terms of the geometric scale, a power-law fit yields

$$F_{\text{peak}} \;\approx\; 87.7\, \lambda_L^{3.02}\ \text{N} \quad (R^2 \approx 0.999),$$

confirming that the data are physically consistent with cubic scaling within the studied range.

Interpretation: the departure from the ideal curve increases with scale; the segment 1:25→1:50 shows a larger slope than the previous segments, indicating a nonlinear growth of scale effects as the real-scale limit is approached.

2) Dynamic similarity: Froude number at control sections

The Froude number Fr was evaluated at **Section 1** (upstream) and **Section 2** (downstream):

- **Section 1 (upstream):** the comparison between prototype and scaled models shows **errors below 5%**, indicating that **Froude similarity is satisfied** at the approaching front.
- **Section 2 (downstream):** the deviations increase with scale, reaching **~20%** at **1:50**. This highlights the **influence of the pier on the debris flow**, with stronger three-dimensional wake processes and turbulence generation as scale grows. The finding

consolidates the view that, as the **scale ratio increases**, additional **3D and turbulent interactions** intensify and amplify **scale effects** in the near-wake.

Overall, the **global impact metrics** (initial peaks) remain consistent with Froude scaling, while **section-wise Froude numbers** reveal the expected spatial variability: excellent agreement at the upstream approach and controlled, non-linear departures in the downstream wake.

<u>Scientific and engineering implications</u>

1. **Scaling of peak loads.** For dambreak-type debris impacts on rigid piers, **use $F_{peak} \propto \lambda_L^3$** as a first-order law. Within $1 \le \lambda_L \le 50$ the calibrated relation $F_{peak} \approx 87.7\, \lambda_L^{3.02}$ provides an accurate descriptor for interpolation and scenario building.
2. **Verification via sections.** Embedding two control sections and monitoring **Froude numbers** is an effective, low-cost way to check dynamic similarity: **Section 1** validates the approaching front; **Section 2** quantifies wake-induced departures that naturally grow with scale.
3. **Rheology at fixed concentration.** Keeping C_v and tailing concentration fixed and scaling τ_y, μ_p as above gives consistent, conservative predictions for peak impacts; it also avoids the underestimation associated with Bn-invariant approaches.
4. **Use in design.** The present **Class A** predictions can be used to set **target envelopes** for peak force and section-wise Fr in future laboratory campaigns or for preliminary screening in hazard and structural checks on debris-prone sites.

Chapter 6

6 Conclusions and Future Perspectives

This doctoral research focused on the assessment and quantification of debris flow impact forces on protective structures using a coupled approach of laboratory validation and numerical simulation with the CFD model Flow-3D. The overarching aim was to bridge the gap between theoretical models and real-world applications by validating numerical methodologies against benchmark experimental data and subsequently applying these validated tools to simulate a real-case debris flow event in the La Valletta catchment (Aosta Valley, Italy). Furthermore this thesis developed a Class A prediction for debris-flow impact on a bridge pier using FLOW-3D, with the Milano-Bicocca experimental flume as 1:1 laboratory reference and three up-scaled numerical scenarios in which the same flume represents field cases at 1:10, 1:25, and 1:50 (the latter corresponding to the real VI01 pier).

1) <u>**Summary of Key Findings**</u>

- **Initial Literature Review and Methodological Analysis:**
  At the outset of this research, an extensive literature review was conducted to frame the state of the art on debris flow dynamics, impact mechanisms, and protective structure design. This included a critical analysis of existing **empirical formulas** used to estimate impact forces, their applicability limits, and their theoretical

foundations. Furthermore, all major **computational codes and modelling strategies** were examined—both simplified models and advanced CFD approaches—to identify the most suitable tools for simulating debris flow processes with high physical fidelity.

- **Model Validation:**
  The Flow-3D model was successfully validated using the experimental campaign described by Zhao et al. (2018), reproducing the flume geometry, rheological parameters, and boundary conditions. A precise calibration of the Bingham parameters (yield stress and plastic viscosity) allowed an accurate match between simulated and experimental impact forces, demonstrating the model's capacity to replicate key dynamic interactions in a debris flow event.
- **Real-Case Application – "La Valletta" Basin:**
  A detailed hydrological and geological analysis of the La Valletta basin provided the basis for defining input parameters such as a 42% volumetric concentration and a debris density of 1700 kg/m³. Based on this, three simulation scenarios were developed:
  - **Scenario A:** Tailings with large blocks (Dmax = 30 cm),
  - **Scenario B:** Tailings with smaller sediment size (Dmax = 1.5 cm),
  - **Scenario C:** No tailings, constant density Bingham model.

  These simulations highlighted substantial differences in impact forces and temporal evolution, emphasizing the importance of sediment size and rheological properties.

- **Comparison with Empirical Formulas:**
  Impact forces computed via CFD simulations were compared with those derived from the empirical formula proposed by Zhao et al. Good agreement was found in terms of peak force and temporal trends, particularly for the scenario matching the experimental setup (Scenario B). However, discrepancies emerged when applying the formula to scenarios outside its empirical calibration range, underscoring the advantage of using CFD models for more complex or large-scale cases.
- **Class A Prediction of University of Milano Bicocca Experimental flume installation**
  The results of Chapter 5 demonstrate that impact forces follow a near-cubic law in the geometric scale and that departures from the ideal trend increase non-linearly with scale, particularly between 1:25 and 1:50. Froude numbers confirm dynamic similarity upstream, while downstream differences up to ~20% reflect enhanced three-dimensional wake dynamics. These outcomes validate the choice of Froude similitude for impact-driven problems and support the use of FLOW-3D as a Class A prediction tool. When the laboratory setup corresponds to field scales larger than 1:25, the scale-effect deviations on peak impact grow non-linearly (up to ~20% at 1:50). In such cases, full-scale CFD simulations provide a reliable alternative to direct extrapolation, preserving Froude kinematics and capturing 3D wake dynamics around the pier.

2) **Implications for Engineering Design**

- **Parameter Sensitivity:**
  The study demonstrated how varying sediment sizes and concentrations significantly alter flow behavior and resulting forces. This reinforces the need for accurate field characterization before selecting design parameters.
- **Design Optimization:** By replicating the impact force distribution and not just the peak values, CFD models enable more refined design of protective structures, minimizing oversizing and material waste.
- **Limitations of Empirical Models:**
  While empirical models provide quick estimates, they may not fully capture the physical complexity of debris flows in real terrain configurations. CFD-based approaches offer a more robust alternative, especially when calibrated with reliable experimental or field data.

3) **<u>Future Research Directions</u>**

- **Field Validation:**

  Future studies should aim to collect in-situ measurements during real debris flow events to further validate and refine simulation models under natural conditions.

- **Advanced Rheological Models:**

  The use of more sophisticated rheological models (e.g., Herschel–Bulkley, two-phase models) could be investigated to better capture the behavior of highly heterogeneous debris mixtures.

- **Coupled Multi-Physics Simulations:**

  Integration of CFD models with structural response models could allow simultaneous simulation of debris flow impact and structural deformation, enhancing the predictive capability for barrier design.

- **Scenario Expansion:**

  Additional simulations exploring variable inflow conditions, rainfall scenarios, or dam-break dynamics would enrich the understanding of debris flow behavior under diverse circumstances.

- **Future research prospective for Bicocca Laboratory flume setup**

  The present Chapter 5 provides calibrated targets for upcoming laboratory campaigns at the University of Milano-Bicocca. By testing multiple rheologies and concentrations and by monitoring Froude numbers at Section 1 and Section 2, the experimental program will enable a focused calibration of the numerical model and the refinement of design-oriented guidelines for debris-flow impacts on bridge piers.

Bibliography

- Armanini, A., & Scotton, P. (1992). Experimental analysis on the dynamic impact of debris flows. *Journal of Hydraulic Research*, 30(4), 437–458. https://doi.org/10.1080/00221689209498768

- Bingham, E. C. (1922). *Fluidity and Plasticity: Mathematical Theory of Plasticity and Methods of Measuring Viscosity and Plasticity*. McGraw-Hill.

- Bird, R. B., Armstrong, R. C., & Hassager, O. (1987). *Dynamics of Polymeric Liquids. Vol. 1: Fluid Mechanics*. Wiley.

- Carreau, P. J. (1972). Rheological equations from molecular network theories. *Transactions of the Society of Rheology*, 16(1), 99–127.

- Chhabra, R. P., & Richardson, J. F. (2011). *Non-Newtonian Flow and Applied Rheology: Engineering Applications*. Butterworth-Heinemann.

- Coussot, P. (2000). Direct determination of rheological characteristics of debris flow. *Journal of Hydraulic Engineering*, 126(2), 158–161. https://doi.org/10.1061/(ASCE)0733-9429(2000)126:2(158)

- Coussot, P., & Meunier, M. (1996). Recognition, classification and mechanical description of debris flows. *Earth-Science Reviews*, 40(3–4), 209–227. https://doi.org/10.1016/0012-8252(95)00065-8

- Cruden, D. M., & Varnes, D. J. (1996). Landslide types and processes. In *Landslides: Investigation and Mitigation* (pp. 36–75). National Research Council, Transportation Research Board.

- Einstein, A. (1906). Eine neue Bestimmung der Moleküldimensionen. *Annalen der Physik*, 324(2), 289–306.

- Einstein, H. H. (1988). Landslide risk assessment procedure. In *Proceedings of the 5th International Symposium on Landslides*.

- Faug, T. (2013). Analytical model for debris flow impact.

- Faug, T. (2021). Granular flow impact forces: A unified view from dry to immersed conditions. *Journal of Fluid Mechanics*, 928, A3. https://doi.org/10.1017/jfm.2021.721

- Herschel, W. H., & Bulkley, R. (1926). Konsistenzmessungen von Gummi-Benzollösungen. *Kolloid-Zeitschrift*, 39(4), 291–300.

- Hungr, O., Evans, S. G., Bovis, M. J., & Hutchinson, J. N. (1984). Quantitative analysis of debris torrent hazards for design of remedial measures. *Canadian Geotechnical Journal*, 21(4), 663–677. https://doi.org/10.1139/t84-073

- Iverson, R. M. (1997). The physics of debris flows. *Reviews of Geophysics*, 35(3), 245–296. https://doi.org/10.1029/97RG00426

- Julien, P. Y., & O'Brien, J. S. (1993). Recent developments on debris flows. In *Proceedings of the International Symposium on Erosion Control* (pp. 153–162).

- Krieger, I. M., & Dougherty, T. J. (1959). A mechanism for non-Newtonian flow in suspensions of rigid spheres. *Journal of Rheology*, 3(1), 137–152.

- Major, J. J., & Pierson, T. C. (1992). Debris flow rheology: Experimental analysis of fine-grained slurries. *Water Resources Research*, 28(3), 841–857. https://doi.org/10.1029/91WR02834

- Mizuyama, T. (1979). Dynamic pressure of avalanche. *Natural Disaster Science*, 1(1), 43–54.

- ONR 24800. (2009). *Technical guideline for the design of protective structures against torrential hazards*. Austrian Standards Institute.

- Ostwald, W. (1925). Über die scheinbare Viskosität disperser Systeme. *Kolloid-Zeitschrift*, 36, 99–117.

- O'Brien, J. S., & Julien, P. Y. (1988). Laboratory analysis of mudflow properties. *Journal of Hydraulic Engineering*, 114(8), 877–887. https://doi.org/10.1061/(ASCE)0733-9429(1988)114:8(877)

- Pierson, T. C. (1986). Flow behavior of channelized debris flows, Mount St. Helens, Washington. *Geological Society of America Bulletin*, 97(8), 1054–1061.

- Proske, D., Suda, J., & Hübl, J. (2011). Debris flow impact estimation for breakers. *Georisk*, 5(2), 115–126. https://doi.org/10.1080/17499518.2010.516227

- Rickenmann, D. (1999). Empirical relationships for debris flows. *Natural Hazards*, 19(1), 47–77. https://doi.org/10.1023/A:1008003622785

- Roberto Savi. (2020). *Sviluppo e validazione di sistemi di monitoraggio per il controllo remoto delle opere passive a protezione del territorio*. Tesi di Dottorato, Università degli Studi di Parma.

- Scheidl, C., Rickenmann, D., & Hübl, J. (2013). Empirical assessment of dynamic pressures in debris flows. *Natural Hazards and Earth System Sciences*, 13(5), 1221–1230. https://doi.org/10.5194/nhess-13-1221-2013

- Scheidl, C., Friedl, C., Reider, L., et al. (2023). Impact dynamics of granular debris flows based on a small-scale physical model. *Acta Geotechnica*, 19, 3979–3997. https://doi.org/10.1007/s11440-023-02116-8

- Shen, W., Zhao, T., & Zhang, L. M. (2018). A novel dynamic impact pressure model of debris flows and its application to flexible barriers. *Engineering Geology*, 241, 86–96. https://doi.org/10.1016/j.enggeo.2018.05.011

- Sonoda, T., & Sawada, Y. (2024). Flume model tests on debris flow impact.

- Sosio, R., Crosta, G. B., & Frattini, P. (2007). Field observations, rheological testing and numerical modelling of a debris-flow event. *Earth Surface Processes and Landforms*, 32(2), 290–306. https://doi.org/10.1002/esp.1416

- Takahashi, T. (2008). *Debris Flow: Mechanics, Prediction and Countermeasures*. Taylor & Francis.

- Tanner, R. I. (2000). *Engineering Rheology*. Oxford University Press.

- Varnes, D. J. (1978). Slope movement types and processes. In *Landslides: Analysis and Control* (pp. 11–33). National Academy of Sciences.

- Zhao, T., Shen, W., Zhang, L. M., & Wang, Y. (2018). Quantifying the impact of dry debris flow against a rigid barrier by DEM. *Engineering Geology*, 241, 86–96. https://doi.org/10.1016/j.enggeo.2018.05.011

- Zeng, C. (2014). Experimental analysis on the impact force of viscous debris flow. *Earth Surface Processes and Landforms*, 39(6), 774–786. https://doi.org/10.1002/esp.3744